LAPPEENRANTA UNIVERSITY OF TECHNOLOGY
LUT School of Energy Systems
LUT Mechanical Engineering

Antti Ahomäki

DEVELOPMENT OF A COORDINATE-BASED CONTROL STRATEGY FOR A MATERIAL HANDLING MACHINE UTILIZING A REAL-TIME SIMULATION

Examiner(s): Professor Heikki Handroos
D. Sc. (Tech.) Hamid Roozbahani

TIIVISTELMÄ

Lappeenrannan teknillinen yliopisto
LUT School of Energy Systems
LUT Kone

Antti Ahomäki

Koordinaatti pohjaisen ohjausstrategian kehittäminen materiaalinkäsittelijälle käyttäen reaaliaikasimulaatiota

Diplomityö

2018

86 sivua, 55 kuvaa, 7 taulukkoa ja 2 liitettä

Tarkastajat: Professori Heikki Handroos
TkT Hamid Roozbahani

Hakusanat: Koordinaattiohjaus, suljettu-säätöpiiri, hydrauliikka, reaaliaika-simulaatio, avoin-säätöpiiri

Tässä työssä käydään lävitse kehittyneen hydraulisen manipulaattorin kehitystä ja asetetaan tavoitteet mahdollisimman hyvän koordinaattiohjauksen kehittämiseksi, jonka lisäksi tehtiin kirjallisuusselvitys, jossa käytiin lävitse operaattoreiden merkitystä koneen suorituskyvylle ja millaisilla tekniikoilla sitä voitaisiin parantaa. Matemaattiset yhtälöt luotiin koneelle, jotta koordinaattiohjaus voitaisiin toteuttaa kahdella eri tavalla ja koneen tekniset tiedot esiteltiin samalla. Simulaatioympäristö ja kahden eri mallin toiminta ympäristössä käytiin lävitse. Suljetun säätöpiirin toiminta oli tarkempaa kuin avoimen, mutta molemmat ohjausjärjestelmät osoittivat sen, että jatkokehitykselle on tarvetta ja näitä kehityskohteita pohditaan työn lopussa.

ABSTRACT

Lappeenranta University of Technology
LUT School of Energy Systems
LUT Mechanical Engineering

Antti Ahomäki

Development of a coordinate-based control strategy for a material handling machine utilizing a real-time simulation

Master's thesis

2018

86 pages, 55 figures, 7 tables and 2 appendixes

Examiners: Professor Heikki Handroos
D. Sc. (Tech.) Hamid Roozbahani

Keywords: Coordinate control, real-time simulation, closed-loop, hydraulics, open-loop

This work discusses the background of more intelligent hydraulic manipulator control, sets goals to make a suitable coordinate control system and provides a literature research on the importance of the machine operator and its value to the machine performance with other promising control methods. The mathematical equations to make a coordinate control were derived and the machine properties with the operating principle of the two different developed methods were introduced. The simulation environment and the operating principle of the created models was shown in detail. In the results part the two created systems were tested and the accuracy of these two methods were shown. The closed loop system performed better however both control methods were found to have problems in them that further research and development could address to improve the accuracy of the boom tip control.

ACKNOWLEDGEMENTS

This thesis was done for the DigiPro project in Lappeenranta University of Technology.

I would like to thank Professor Heikki Handroos for this topic and all of his assistance to finish this thesis and Hamid Roozbahani with all the help he gave me to finish this work. I would also like to thank Mantsinen Ltd Oy for giving me this opportunity work with them and Simo Huttunen from Mantsinen for the endless patience and motivation to answers the millions of questions I had about the project.

Antti Ahomäki

Antti Ahomäki
Lappeenranta
Monday 30th of October 2018

TABLE OF CONTENTS

LIST OF SYMBOLS AND ABBREVIATIONS

a	Triangle side
a_i	Link length
a_1	Boom length
a_2	Stick length
b	Triangle side
BC	distance between two points [m]
BD	distance between two points [m]
BTC	Boom Tip Control
c	Triangle side
CAN	Controller area network
CBC	Conventional boom control
CD	distance between two points [m]
c_i	cos(θi)
c_{12}	cos(θ1) * cos(θ2) - sin(θ1) * sin(θ2)
DH	Denavit-Hartenberg
DOF	Degree of freedom
EJ	distance between two points [m]
FG	distance between two points [m]
FJ	distance between two points [m]
HE	distance between two points [m]
HJ	distance between two points [m]
ISO	International Organization for Standardization
J	Jacobin matrix
JG	distance between two points [m]
Kcr	Proportional gain where steady state error occurs
K_p	Proportional element
K_i	Integral element
K_d	Derivative element
${}^{i}p$	Position vector in i frame
Pcr	Sustained period of oscillation
p_i	i axle direction position vector

PI	proportional integral
PID	proportional integral derivative
PSO	particle swarm optimization
${}^{i}_{j}R$	Rotation matrix from frame j to frame i
s_i	sin(θi)
s_{12}	cos(θ1) * sin(θ2) + sin(θ1) * cos(θ2)
${}^{i}_{j}T$	Transformation matrix from frame j to frame i
VDC	subsystem-dynamics-based-virtual decomposition control
${}^{i}v_j$	Link j linear velocity according to frame i
${}^{i}\hat{X}_j$	Frame j x-direction unit vector written in frame i
${}^{i}\hat{Y}_j$	Frame j y-direction unit vector written in frame i
${}^{i}\hat{Z}_j$	Frame j z-direction unit vector written in frame i
δ	Differentials time element
ε_i	Angle i
θ_i	Joint i angle
$\dot{\theta}_I$	Joint i angular velocity
${}^{i}\omega_j$	Link j angular velocity according to frame i

1 INTRODUCTION

The traditional way to operate heavy hydraulic machinery such as excavator, forest harvesters, forest loaders and cranes, is to control each of the hydraulic actuators with joystick input. It means that one direction of joystick input would represent one-actuator movement in the machine. In order to control the machine smoothly and achieve desired movement, the operator needs to control all the hydraulic actuators required for the process at the same time. This type of eye-hand coordination is complicated and require bountiful sessions of training to master and perform effectively.

The solution for this problem is to implement coordinate control also known as tip control. In this method the machine's joysticks will directly control the tip of the of machines hydraulic manipulator by commanding all the actuators simultaneously with one general input instead of controlling each actuator with separate input. There are multiple different methods to apply coordinate control to a heavy hydraulic machinery and some of these methods are listed in the second chapter of this thesis.

In the past couple of years, several manufacturers have developed different types of coordinate control methodologies to their products; companies such as Ponsse which offers forest harvesters machines equipped with tip control, John Deere with intelligent boom control for forest harvesters and Technion Oy with xCrane Techion control for hydraulic crane arm.

1.1 Background

Academics have developed theoretical approaches to coordinate control of hydraulic working machines since 90s however these proposed methods have not become popular as it would have required additional mechanical components. In addition, with the development in technology, nowadays, complete electrical solutions have become available and manufacturers of different types of hydraulic machinery are investing on development of coordinate-controlled machinery as it will also provide opportunities for further development of machines towards semi or full-automation.

This work is done as a part of the Digital Product Processes through Physics Based Real-Time Simulation – DigiPro project in Lappeeranta University of Technology for Mantsinen Group Ltd Oy. Mantsinen is a Finnish corporation with headquarter in Joensuu, Finland. Mantsinen business was founded in 1974 as a logistic company and later during the late 90s the company transformed into a machine manufacturer. Mantsinen is a family owned and operated, and their material handlers are one of the largest hydraulic material handlers in the world.

1.2 Research problem, objectives and delimitations

The goal of this thesis work is to develop satisfying coordinate control system for the Mantsinen 200 material handler without installing any additional equipment or sensors to the machine and only using the sensors that Mantsinen has already installed on their machine. Another objective is to examine which of the two proposed control systems would work better and would it make any significant differences in the machines performance.

The focus of the work is to keep the design of the coordinate control system as simple as possible as it needs to be suitable for the wide range of material handlers available in the fleet of Mantsinen and transforming the control software to another machine size would not require too many modifications in the code created.

To keep the work as simple as possible the amount of degrees of freedom for the hydraulic manipulator is delimited to two rather than the three that the system has. The control of the third link which is swing link is different than the rest of the hydraulic components and would not provide any relevant data for the tests. Also, the singularity points of the manipulator where one or more degree of freedom is lost are not discussed in this work as Mantsinen has already implemented a dead zone compensator for their machinery.

2 COMPARISON OF DIFFERENT CONTROL METHODS IN MANIPULATOR CONTROL

The common modern method of controlling heavy-duty machinery is a one-to-one mapping between the joystick movement and corresponding link motions. Traditionally these types of system would have a lever that would be directly connected to the spool of the hydraulic actuator and the operator could easily sense the feedback from the lever when the system load would increase or decrease. Nowadays modern heavy-duty machine has been equipped with joysticks, so called pilot control, which reduces the fatigue of the machine operator and improves their quality of work during the long run as moving the manual levers is physically a much more demanding task.

2.1 Operators influence on machine performance

Joysticks provide more comfortable operation conditions for the machine operator and are relatively easy to implement, the pure skill and experience required to operate a heavy-duty machine effectively is tremendous. The required accurate coordinate-motion is necessary for routine operations and requires certain amount of training and effort, increasing the running costs of the machine. The operator needs to learn what joint speeds are necessary at each instant for the desired end-effector speed and direction. (Mu, B., 1996).

In a study concluded by Purfürst it was found out that the operator of the machine has a decisive influence on the machine performance and the performance of the operator could be doubled within 8 months. It was identified that differences between human operators are large and training phase can be expensive however, the operators are valuable assets for the successful operation of the business. (Purfürst, F.T., 2010).

2.2 Machine control

With the implementation of joysticks, the further possibilities of developing manipulator control lead towards the implementation of the Cartesian coordinate control also known as boom tip control (BTC). This control method resolves the motions in Cartesian space commands or trajectories instead of individual actuator commands which means that in the

traditional control, the operator adjust every hydraulic actuator with his joystick inputs to obtain the desired boom tip to the location while in BTC the operator directly controls the tip of the boom. The main claim of the Cartesian control is to make it easier for new comers to start using the equipment and learning the control of the machine.

When Manner et al. conducted a study with upper-secondary school students with John Deere's new BTC harvester to examine if the BTC is easier for rookies to learn than the conventional boom control (CBC). It was found out that the BTC did not generate a steeper learning curve and that the total time for the BTC was consistently lower than for the CBC. (Manner et al., 2017).

Yoon et al. found in their study that the suggested BTC increases the overall excavating performance without constraining the motion while allowing the operators to use their full set of acquired skills to perform divergent tasks in diverse environments. (Yoon et al. 2010).

A study conducted by Rudolfsen et al. focused on the Cartesian trajectory tracking of a loader crane where the studied system was equipped with a feed-forward and feedback control architecture with a dead zone compensator. The maximum deviation from the measured path was 12.6 mm and standard deviation was found to be 3.64 mm. The system was evaluated with hardware in loop method and later with experiments where the system was found to be reliable and constant with its results. (Rudolfsen et al., 2017).

One of the further development possibilities that are obtained with the BTC is the possibility to semi-automate the operating process of the heavy-duty machinery for instance, when unloading raw material from a vessel, the swinging movement and boom position could be automated that the operator would only have to load and unload the machine with the raw material. The load and unload points could be saved into the memory of the machine which would then allow the rotation of the machine with the press of a button however, this type of system requires high accuracy to work safely and properly. (Lindroos et al., 2015).

In order to achieve the required accuracy and location of the boom tip, the machine must be equipped with additional sensors increasing the manufacturing costs of the machine, however it allows the machine to gather data which opens further machine development

opportunities. Different type of sensors and their capabilities to fit this type of purposes were studied by Lindoors et al. and their results give a satisfactory understanding for suitable options. The sensors must be relatively economical, rugged enough to withstand the harsh environmental conditions and provide high accuracy data for the system. (Lindroos et al., 2015).

Shen et al. compared three different control methods while running the same working cycle to examine which of the three studied setups has the best fuel effectiveness while providing satisfactory hydraulic actuator performance on a hybrid excavator. (Shen et al., 2015).

Lee et al. developed a contour control-based control algorithm for hydraulic excavator where the goal was to reduce contour error rather than focus on position tracking. While applying the contour tracking method on surfaces with three different inclinations, it was found out that the contour performance was improved while slightly decreasing the tracking performance. The suggested control method was found to be useful when the machine process requires the operator to follow a certain contour level. (Lee et al., 2013).

Wang et al. study shows how to improve the performance of the boom control of a hybrid excavator by designing an energy recovery controller instead of direct speed control as it is prone to oscillations. Their proposed control system method includes composite control strategy, leakage compensation and load torque observations, which would recover energy effectively while keeping the boom control performance at acceptable levels.
(Wang et al., 2012).

2.3 Implementation methods

The world of automated excavator control with diverse different methods used is a hot topic in the academic field which results in copious new studies in the field. The main problem of finding a stable and reliable solution for the control of excavators and other large hydraulic equipment relays on the highly complex nonlinear control behavior of hydraulic systems which has caused the development of multiple different control methods that have been developed by both industry and academy however, the industrial ones have focused on either

improving the economic aspects of the machine such as fuel and energy consumption while the academic ones have been focusing on the trajectory control performance.

Multiple different ideas have been proposed to implement advanced boom tip control for hydraulic systems and some of these methods that could be used are briefly mentioned below and other that have more potential are introduced more broadly later on. Methods of implementing nonlinear control that have been studied are Fourier series approximation based adaptive control (Yao et al., 2015), quantitative feedback control (Karpenko et al., 2010), particle swarm optimization (PSO) which is used to improve PID performance (Ye et al., 2017) and fuzzy logic controller to enhance the performance of a traditional PID controller (Wonohadidjojo et al., 2013). The main reason for lack of potential comes from the uncertainty of the control during the whole operating region.

One of the biggest challenges with automation lies with the closed-loop systems as it can cause large instability in hydraulic systems due to the amplifications of the control signals. Koivumäki & Mattila proposed a novel impedance control method in the Cartesian space by using a subsystem-dynamics-based-virtual decomposition control (VDC) approach where high-bandwidth closed-loop is acquired for the system and VDC feature virtual power flow was used to analyze the results from where a method was developed that the parameters for the impedance control could be applied to the hydraulic actuator. It was found out that the stability for both free space and constrained motion control was guaranteed and this method could be expanded further to cover other items. (Koivumäki & Mattila., 2017).

Construction environment can be crowded and many tasks are occurring at the same time and the level of automation in construction sites is increasing which why the need for automatic excavators exists. Automatic excavators are already being tested by different sources however their usage requires many of sensors, controllers, remote communication systems and real-time modeling of the environment. (Kim J., et al., 2018).

Kim S., et al have developed a robust controller to handle the hydraulic excavators digging process by providing robust performance and stability while not having explicit knowledge of the actuator dynamics. Their solution was μ-synthesis controller which works as balancing factor between the outer and inner loop controllers which was validated with test

done with a 21-ton excavator and the study found out that the µ-controller can balance the unknown load disturbances which are occurring during the digging process. (Kim S., et al. 2018).

Excavator digging automation was studied by Haga et al. who created a system where a coordinate system was introduced to aid the driver by correcting the digging depth of the excavator bucket. The reference for the digging was produced by an external laser sensor and only 10 cm inaccuracy was found during the 16-meter digging process. (Haga et al., 2001).

In the future possible control methods for the heavy-duty machine could be teleoperation which means that machine is remotely controlled from anywhere in the world without any presence from the machine operator. The benefits of this type of design would allow the machine development to move away from the operator centered design which prioritizes in the operators' safety and comfort in the cabin and focus on making the actual machines better. An example of this is the well-known drone program of the United States which is one the largest teleoperated systems in the world. Nevertheless, teleoperation would require more visual aids to be installed into the machine however, with the rapid development of self-driving cars and other sensor-based technologies such as machine vision the implementation of this type of technology to heavy-duty machinery is not that far in the future. (Westerberg, S., 2014).

3 MANIPULATOR KINEMATICS

Manipulator kinematics are used to observe the position, velocity and acceleration of the end effector which are critical in order to successfully transform the control system of the material handler into coordinate-based control. Kinematics are considered to be the science of motion that treats its subjects without the regard to the initial force and hence it can be utilized to setup fundamental equations for controlling the system. (Craig, 2005, p. 19).

3.1 Position, orientation and frame

It is possible to locate any point in the universe with a 3x1 position vector shown in equation 3.1 once a coordinate system is established.

$$ {}^{A}P = \begin{vmatrix} p_x \\ p_y \\ p_z \end{vmatrix} \tag{3.1} $$

where, p_x, p_y and p_z are individual components of each representing x, y, z axle direction of position vector P. Some situations also require the description of the orientation of the body as the mere position is suitable for only points in coordinate space. Figure 3.1 describes the orientation of the position vector ${}^{A}P$.

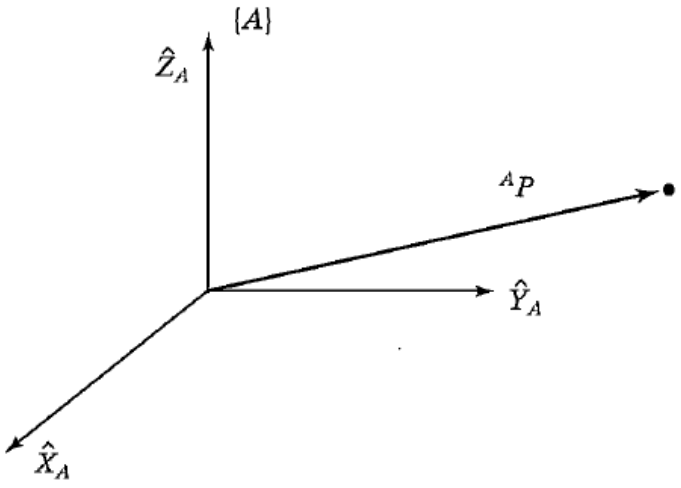

Figure 3.1. Vectors relativity to the base frame (Craig, 2005, p. 20).

Coordinate system B has been attached to the body shown in figure 3.2 and because the way of its attachment is known regarding the orientation of coordinate system A. One way to describe the body B this is to write three-unit vectors with principle axes that are written in terms of the body A. This matrix formed is a 3x3 matrix which is called rotation matrix and when it describes the relation of B to A it is named ${}^{A}_{B}R$ shown in equation 3.2.

$$ {}^{A}_{B}R = \begin{bmatrix} {}^{A}\widehat{X_B} & {}^{A}\widehat{Y_B} & {}^{A}\widehat{Z_B} \end{bmatrix} = \begin{bmatrix} r_{11} & r_{12} & r_{13} \\ r_{21} & r_{22} & r_{23} \\ r_{31} & r_{32} & r_{33} \end{bmatrix} \tag{3.2} $$

Where, ${}^{A}\widehat{X_B}$, ${}^{A}\widehat{Y_B}$ and ${}^{A}\widehat{Z_B}$ are coordinate system B unit vectors written in coordinate system A. (Craig, 2005, p. 21).

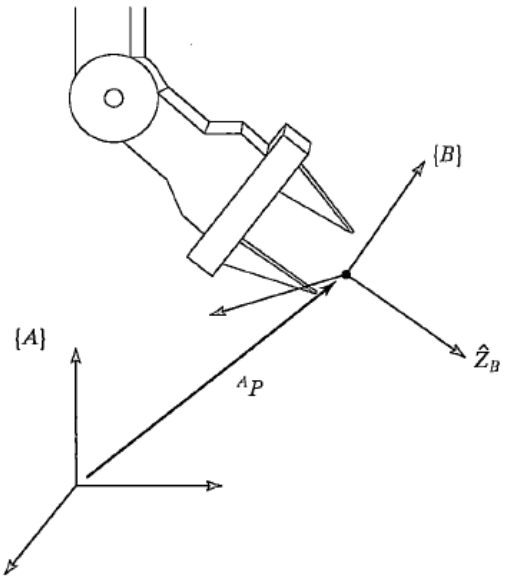

Figure 3.2. Local coordinate system connected to global coordinate system (Craig, 2005, p. 21).

Position and orientation pair are a common occurrence that it is called a frame which is set of vectors giving position and orientation information. In figure 3.3 coordinate frame B has translated to different offset from frame A, however it can be located with ${}^{A}P_{B_{ORG}}$ vector. B has also rotated and the rotation can be described with ${}^{A}_{B}R$ and the location of point A can be calculated with equation 3.3. (Craig, 2005, p. 23).

$$ {}^{A}P = {}^{A}_{B}R \ {}^{B}P + {}^{A}P_{B_{ORG}} \tag{3.3} $$

Equation 3.3 has a more conceptual form shown in equation 3.4.

$$ {}^{A}P = {}^{A}_{B}T \ {}^{B}P \tag{3.4} $$

where ${}^{A}_{B}T$ is called a homogeneous transform matrix which consist of a 4x4 matrix described in equation 3.5.

$$ \begin{bmatrix} {}^{A}P \\ 1 \end{bmatrix} = \begin{bmatrix} & {}^{A}_{B}R & & {}^{A}P_{B_{ORG}} \\ 0 & 0 & 0 & 1 \end{bmatrix} \begin{bmatrix} {}^{A}P \\ 1 \end{bmatrix} \tag{3.5} $$

where the rotation matrix ${}^{A}_{B}R$ is combined with the origin vector ${}^{A}P_{B_{ORG}}$. Where 1 is added to the last element of the 4x1 vectors and a row of [0 0 0 1] is added as the last row of the 4x4 matrix. In other fields of study, the last row can be used as a scaling element, however for this purpose it is kept as it is. Transformation matrices of each link can be formed and link parameters calculated with the combination of transformation matrices where the frame N relates to the base frame 0 shown in equation 3.6. (Craig, 2005, p. 28).

$$ {}^{0}_{N}T = {}^{0}_{1}T \ {}^{1}_{2}T {}^{2}_{3}T \cdots {}^{N-1}_{N}T \tag{3.6} $$

Where the following coordinate frames are merged with the initial base coordinate frame. (Craig, 2005, p. 36).

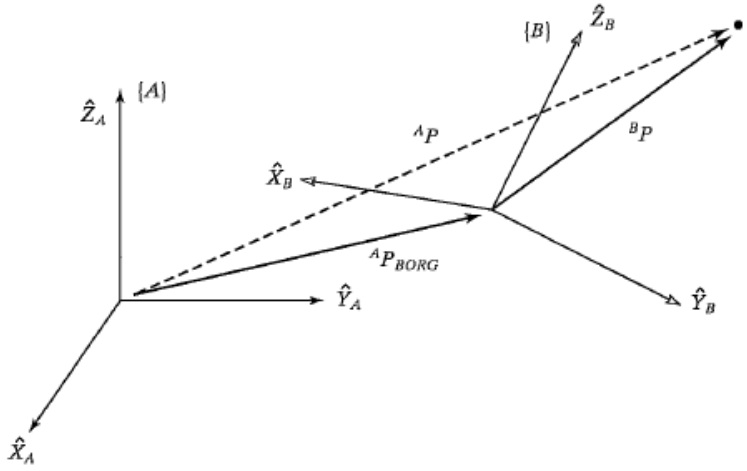

Figure 3.3. General transformation of a vector (Craig, 2005, p. 27)

3.2 Denavit-Hartenberg Notation

A manipulator is formed with pairing joints and links together and the manipulator with n joints will have n+1 links and the numbering start from the base link which is immobile and numbering of joints starts from the first moveable link connected to the base link. This process is illustrated in figure 3.4 and will continue until the end effector of the system is reached. In order to compile the information of each link component into one kinematic solution, the local coordinate frame is attached in to each link i at join i+1. This method is called Denavit-Hartenberg (DH) method which is the standard method with relating components of a manipulator. (Jazar, R.N., 2010, p. 233)

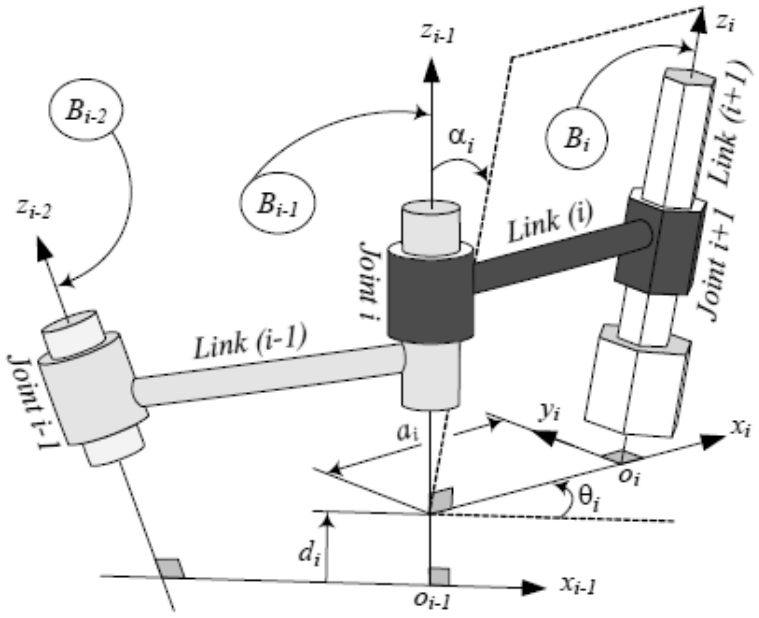

Figure 3.4. Link kinematics with DH parameters (Jazar, R.N., 2010, p. 235)

In the figure above, certain parameters related DH method are used which are, a_i is the kinematic length of a link, α_i is the link twist, d_i is joint distance and θ_i is the joint angle. These parameters are used to also describe the type of joints the manipulator has. (Jazar, R.N., 2010, p. 235)

3.3 Forward kinematics

Forward kinematics are used to determine the coordinate frame configuration of every frame and every link attached to it. The parameters of the system can be easily formed with the DH method which then allows the use of equation 3.6 to form the trigonometric transformation matrix between the joint coordinates which then makes it possible to solve the end effector position.

In this work the forward kinematics are used to track the position of the end effector. The absolute angle data is provided from the angle sensors that are located in the machine. There are joints that are relevant to the forward kinematic model of this material handler.

Using the equation 3.5 the following transformation matrices were formed:

$$ {}^{0}_{1}T = \begin{bmatrix} \cos(\theta_1) & -\sin(\theta_1) & 0 \\ \sin(\theta_1) & \cos(\theta_1) & 0 \\ 0 & 0 & 1 \end{bmatrix} \tag{3.7} $$

$$ {}^{1}_{2}T = \begin{bmatrix} \cos(\theta_2) & -\sin(\theta_2) & a_1 \\ \sin(\theta_2) & \cos(\theta_2) & 0 \\ 0 & 0 & 1 \end{bmatrix} \tag{3.8} $$

$$ {}^{2}_{3}T = \begin{bmatrix} 0 & 0 & a_2 \\ 0 & 0 & 0 \\ 0 & 0 & 1 \end{bmatrix} \tag{3.9} $$

Where a_1 and a_2 are link lengths and θ_1 and θ_2 are joint angles. When the above matrices are multiplied according to equation 3.6:

$$ {}^{0}_{3}T = \begin{bmatrix} 0 & 0 & a_1\cos(\theta_1) + a_2\cos(\theta_1 + \theta_2) \\ 0 & 0 & a_1\sin(\theta_1) + a_2\sin(\theta_1 + \theta_2) \\ 0 & 0 & 1 \end{bmatrix} \tag{3.10} $$

Where the third term of the first row is the x- coordinate of the and third term of the second row is the y- coordinate of the end effector in global coordinates as the function of manipulator joint absolute angles. As the slew link is also known as rotation link, the actual center point of the machine, the distance from that point must be added to the obtained x- and y- coordinate values in order to obtain the real global coordinate values.

3.4 Inverse kinematics

In inverse kinematics the problem is to solve the joint angles when the end effector position is known. There are no standard methods for solving the inverse kinematic problem and in this case the joint angles are solved with trigonometry. The cosine rule also known as law of cosines is used to solve the real angles of the triangle formed with the boom structure. Equation 3.11 displays the basic cosine rule from where the angles A and B can be solved and figure 3.5 shows the triangle formed from the manipulator arms. Where A is the boom and machine body link and B is the boom and stick link.

$$a^2 = b^2 + c^2 - 2bc\cos(A) \tag{3.11}$$
$$b^2 = a^2 + c^2 - 2ac\cos(B)$$

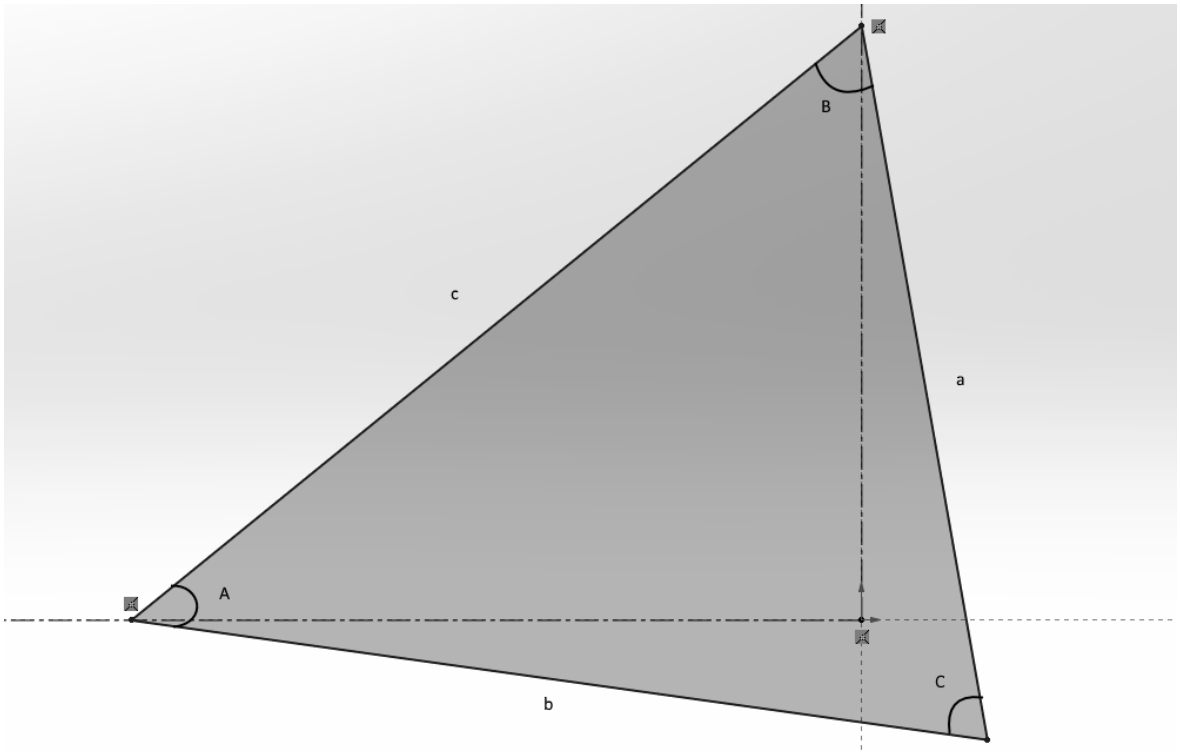

Figure 3.5. Manipulator arm configuration as a triangle

3.5 Velocity kinematics

As described previously in chapter 3.2 a manipulator consists of links and joints that are related to each other to form one moving mechanism and because of this, same structure the DH method of link combinations can be applied to velocity kinematics too. Each link is a rigid body with linear and angular velocities describing its motion where vectors v_i and ω_i which describe the link velocity and angular velocity regarding a specific frame. The angular velocity can be then combined with i+1 frames angular velocity vector and written respect to the same frame i as shown in equation 3.12 and notation for the equation is shown in 3.13. (Craig, 2005, p. 145)

$$ {}^{i}\omega_{i+1} = {}^{i}\omega_{i} + {}^{i}_{i+1}\mathrm{R}\,\dot{\theta}_{i+1}\,{}^{i+1}\hat{Z}_{i+1} \tag{3.12} $$

$$ \dot{\theta}_{i+1}\,{}^{i+1}\hat{Z}_{i+1} = {}^{i+1}\begin{bmatrix} 0 \\ 0 \\ \dot{\theta}_{i+1} \end{bmatrix} \tag{3.13} $$

When multiplying both sides of equation 3.12 with rotation matrix ${}^{i+1}_{i}\mathrm{R}$ the angular velocity of link i+1 with respect to the frame i+1 is shown in equation 3.14.

$$ {}^{i+1}\omega_{i+1} = {}^{i+1}_{i}\mathrm{R}\;\; {}^{i}\omega_{i} + \dot{\theta}_{i+1}\,{}^{i+1}\hat{Z}_{i+1} \tag{3.14} $$

The linear velocity of the manipulator frame i+1 is the same as i added with link i angular velocity component. Because ${}^{i}\mathrm{P}_{i+1}$ is constant in frame i it vanishes.

$$ {}^{i}v_{i+1} = {}^{i}v_{i} + {}^{i}\omega_{i} \times {}^{i}\mathrm{P}_{i+1} \tag{3.15} $$

When multiplying both sides with ${}^{i+1}_{i}\mathrm{R}$ equation 3.16 is obtained.

$$ {}^{i+1}v_{i+1} = {}^{i+1}_{i}\mathrm{R}\;\left({}^{i}v_{i} + {}^{i}\omega_{i} \times {}^{i}\mathrm{P}_{i+1}\right) \tag{3.16} $$

When applying equations 3.14 and 3.16 to all the links of the manipulator can be computed ${}^{N}\mathrm{v}_{N}$ and ${}^{N}\omega_{N}$, which are the linear and angular velocity of the end effector. (Craig, 2005, p. 146)

The manipulators x- and y- direction velocity components are presented in equation 3.17 as function of joint angles in the local coordinate system of the end effector. This type of system has two degrees of freedom (DOF) and figure 3.6 illustrates this type of system which similar to the system modeled in this work.

$$ {}^{3}v = \begin{bmatrix} a_1 \sin(\theta_2)\dot{\theta}_1 \\ a_1 \sin(\theta_2)\,\dot{\theta}_1 + a_2(\dot{\theta}_1 + \dot{\theta}_2) \\ 0 \end{bmatrix} \tag{3.17} $$

When combining the rotation matrix with equation 3.17, the end effect velocities in the global coordinate frame are obtained and shown in equation 3.18.

$$ {}^{0}v = \begin{bmatrix} -a_1 \sin(\theta_1)\,\dot{\theta}_1 - a_2\,(\sin(\theta_1)\cos(\theta_2) + \cos(\theta_1)\sin(\theta_2))(\dot{\theta}_1 + \dot{\theta}_2) \\ a_1 \cos(\theta_1)\,\dot{\theta}_1 - a_2\,(\cos(\theta_1)\cos(\theta_2) - \sin(\theta_1)\sin(\theta_2))(\dot{\theta}_1 + \dot{\theta}_2) \\ 0 \end{bmatrix} \tag{3.18} $$

(Craig, 2005, p. 148)

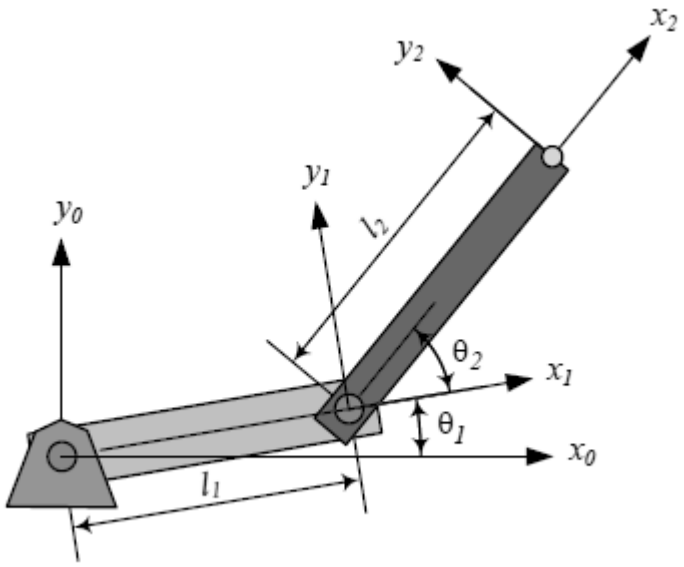

Figure 3.6. 2-DOF manipulator (Jazar, R.N., 2010, p. 448)

3.6 Jacobian matrices

Jacobian matrix is a linear transformation, mapping joint speeds to Cartesian speeds. It is a multidimensional form of derivative which has six functions with each having 6 independent variables. The Jacobian can be presented in vector mode shown in equation 3.19.

$$Y = F(X) \tag{3.19}$$

Next step is to calculate the differentials of X which is shown in equation 3.20.

$$\delta Y = \frac{\partial F}{\partial X}\delta X \tag{3.20}$$

When dividing both sides of the equation 3.18 with the time element δ, equation 3.21 is obtained. (Craig, 2005, p. 149)

$$\dot{Y} = J(X)\dot{X} \tag{3.21}$$

In robotics the Jacobians are used to relate joint velocities with Cartesian velocities of the hydraulic manipulators arm tip. This relation is described in equation 3.22

$$^{0}v = {}^{0}J(\theta)\dot{\theta} \tag{3.22}$$

, where θ is the vector of joint angles of the manipulator and v is the vector of Cartesian velocities regarding the base frame. (Craig, 2005, p. 150)

Size of the Jacobian matrix is dependent on the amount of DOFs in the system under observation. For instance, a 6 DOF manipulator would require a 6x6 Jacobian matrix which would consist of a 6x1 $\dot{\theta}$ joint angle vector and 6x1 ${}^{0}v$ Cartesian velocity vector. The Cartesian velocity vector on the other hand consist of 3x1 linear velocity and 3x1 rotational velocity vectors stacked together shown in equation 3.23.

$$ {}^{0}v = \begin{bmatrix} {}^{0}v \\ {}^{0}\omega \end{bmatrix} \tag{3.23} $$

(Craig, 2005, p. 150)

This application has a two-link arm and by using equation 3.17 a 2x2 Jacobian can be written that relates to the end effector velocity to joint rates in the third frame shown in 3.24.

$$ {}^{3}J(\theta) = \begin{bmatrix} a_1 s_2 & 0 \\ a_1 c_2 + a_2 & a_2 \end{bmatrix} \tag{3.24} $$

And according to equation 3.22 the Jacobian can be written according to the base frame shown in equation 3.26.

$$ {}^{0}J(\theta) = \begin{bmatrix} -a_1 s_1 - a_2 s_{12} & -a_2 s_{12} \\ a_1 c_1 + a_2 c_{12} & a_2 c_{12} \end{bmatrix} \tag{3.25} $$

, where s_i and c_i are sine and cosine for the respective link angles, s_{12} equals to $c_1s_2+s_1c_2$ and c_{12} equals to $c_1c_2-s_1s_2$. (Craig, 2005, p. 150).

For this work the main purpose is to use the inverted Jacobian matrix to calculate the joint rates. The only way that the Jacobian matrix has an inversion is that the matrix is not singular. In equation 3.26 the Jacobian matrix is inverted according to equation 3.22 and the joint rates for each joint are obtained. (Craig, 2005, p. 151)

$$ \dot{\theta} = J^{-1}(\theta)v \tag{3.26} $$

When operating the material handler, the joystick inputs acts as velocity input guide for the boom tip x and y directions. In order to give the right type of command signals for the

actuator the velocity of the joints must be known and when that velocity is computed, the required hydraulic actuator velocities can be then calculated.

3.7 Actuator piston velocities in terms of joint speeds

With the real angles of the joints solved with inverse kinematics, the actuator lengths can be computed and used with the results of equation 3.33 to form the actual actuator piston speeds required for the desired input. In this work the obtained actuator piston speeds are used to compute the required guidance voltage for the hydraulic control valves.

Ultimately the lengths of the piston rods determine the joint angles of the respective links. There is a direct relation between the joint angles and rod lengths and in this work the lengths of the piston rods are determined by the line segment joining two actuator's attachment points.

To solve the velocity of the piston rods one must first solve the geometrics of the piston rod actuators and then form the equations where when the length of the piston rod actuator is known then the angle of said joint which the piston is working around can be solved. This process is shown in equations 3.33 to 3.35 where equation 3.33 is regarding the boom lift actuator and equation 3.34 regarding the lower tilt actuator and equation 3.35 the upper tilt actuator whereas figures 3.7 and 3.8 show the geometry of the pistons. Table 3.1 shows the values used for the variables used in the calculations. The geometry relations are solved in equations 3.27 to 3.29.

The known values are the locations of actuator attachment points C and D and the joint location at B. Also angles θ_1 (robot) and ε_1 (absolute) are known. BC length can be calculated from the locations of B and C and the angle ε_5 when a right triangle is formed between the two points. Angle ε_5 can be solved and angle ε_6 can also be solved as follows:

$$\varepsilon_6 = \frac{\pi}{2} - \varepsilon_1 \tag{3.27}$$

Which then makes it possible to solve ε_2 and the length of CD.

$$\varepsilon_2 = 2\pi - \varepsilon_6 - \varepsilon_5 \tag{3.28}$$

$$CD = \sqrt{BC^2 + BD^2 - 2 \times BC \times BD \times \cos(\varepsilon_2)} \tag{3.29}$$

In figure 3.8 coordinate locations of E, F, G, J and H are known and the angle θ_2 is also known from the inverse kinematic solution. Actuator lengths HE and FG need to be solved and also angle ε_{10}.

$$\varepsilon_{10} = \pi - \theta_2 \tag{3.30}$$

$$HE = \sqrt{EJ^2 + HJ^2 - 2 \times EJ \times HJ \times \cos(\varepsilon_{10})} \tag{3.31}$$

$$FG = \sqrt{JG^2 + FJ^2 - 2 \times JG \times FJ \times \cos(\theta_2)} \tag{3.32}$$

$$\theta_1 = 2\pi - \varepsilon_6 - \varepsilon_5 - \tan^{-1}\left[\frac{\left\{4\,BC^2\,BD^2 - \left[BC^2 + BD^2 - CD^2\right]^2\right\}^{\frac{1}{2}}}{(BC^2 + BD^2 - CD^2)}\right] \tag{3.33}$$

$$\theta_2 = -\tan^{-1}\left[\frac{\left\{4\,JG^2\,FJ^2 - \left[JG^2 + FJ^2 - FG\right]^2\right\}^{\frac{1}{2}}}{(JG^2 + FJ^2 - FG^2)}\right] \tag{3.34}$$

$$\theta_2 = \pi - \varepsilon_{10} - \tan^{-1}\left[\frac{\left\{4\,EJ^2\,HJ^2 - \left[EJ^2 + HJ^2 - HE^2\right]^2\right\}^{\frac{1}{2}}}{(EJ^2 + HJ^2 - HE^2)}\right] \tag{3.35}$$

Equations 3.36 to 3.38 are then differentiated with respect to time which yields the velocity of the actuator piston in terms of the joint angle velocity. Equations 3.30 to 3.32 give out the velocity for each piston rod.

$$v_{CD} = \frac{\{-BD \times BC \times \sin(\epsilon_2)\}}{CD} \times \dot{\theta}_1 \tag{3.36}$$

$$v_{FG} = \frac{\{-FJ \times JG \times \sin(\theta_2)\}}{FG} \times \dot{\theta}_2 \tag{3.37}$$

$$v_{HE} = \frac{\{-EJ \times HJ \times \sin(\epsilon_{10})\}}{EH} \times \dot{\theta}_2 \tag{3.38}$$

(Patel, B.P. and Prajapati, J.M., 2013)

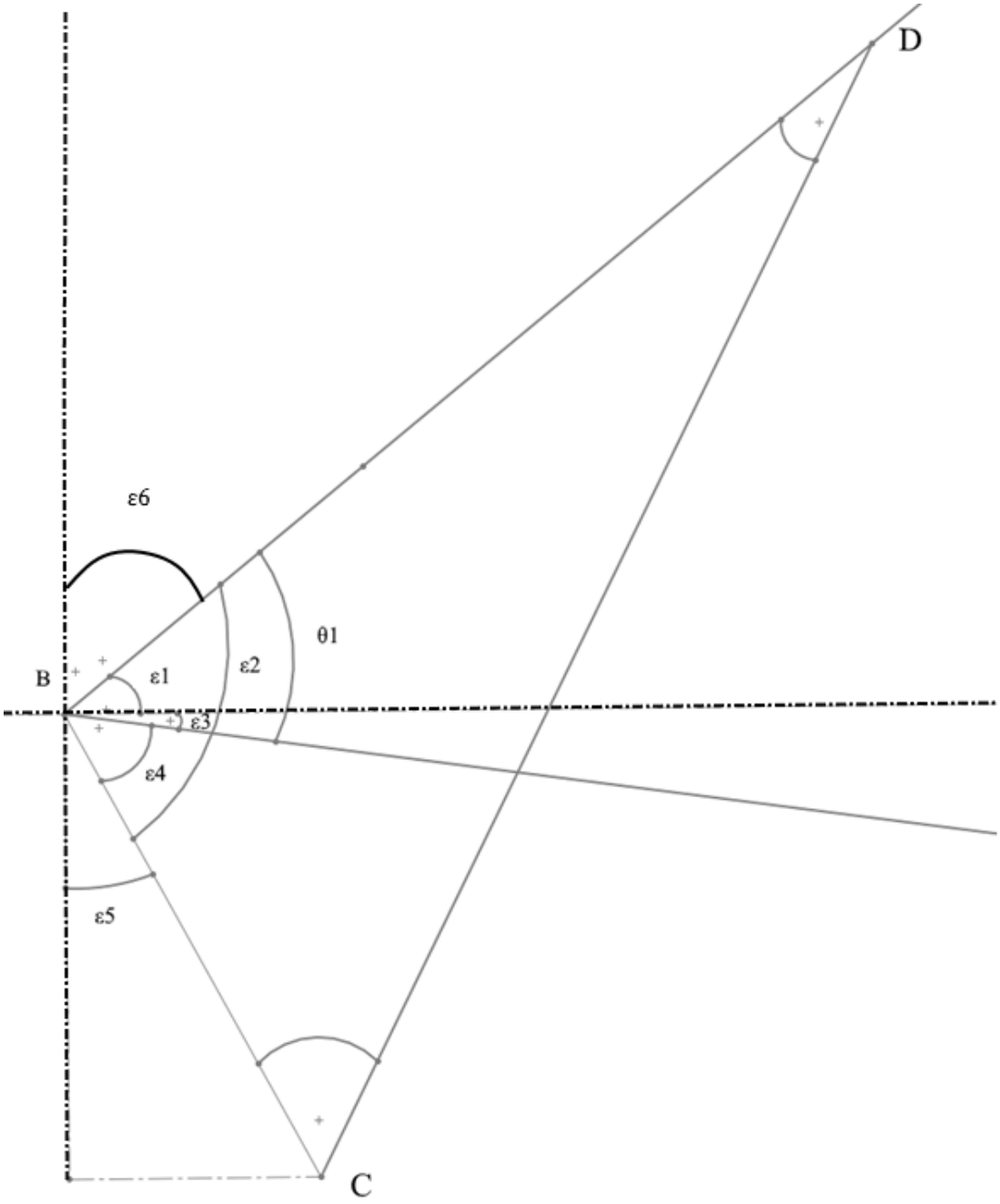

Figure 3.7. Lift actuator geometry

Table 3.1 Model parameters

Parameter	Definition	Value (units)
C	Actuator 1 lower attachment point coordinates	(2.68; 0.835)
D	Actuator 1 upper attachment point coordinates	(4.774; 1.082)
E	Actuator 2 central lower attachment point coordinates	(11.82; 1.548)
H	Actuator 2 central upper attachment point coordinates	(15.506; -1.2)
F	Actuator 2 side lower attachment point coordinates	(11.517; 0.599)
G	Actuator 2 side upper attachment point coordinates	(15.3680; 1.192)
a1	Boom length	15.506 m
a2	Stick length	12 m
a3	Boom start to stick end	(initial)
d1	Origin to boom start x-direction	1.4 m
d2	Origin to boom start y-direction	2.309 m
θ_1	Absolute angle boom link	rad
θ_2	Absolute angle stick link	rad

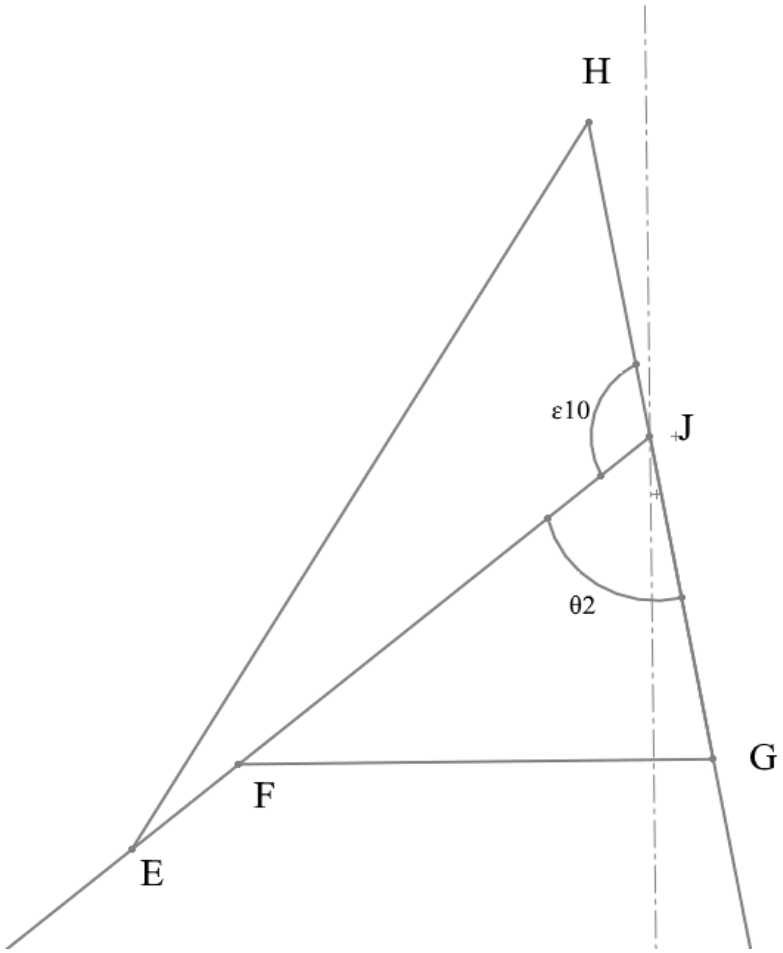

Figure 3.8. Tilt actuator geometry

4 MATERIAL HANDLER PROPERTIES

Material handling is a process that is a part of the manufacturing and logistics process of all products and it is a critical part of the total logistics and manufacturing costs of products. Material handling involves short-distance movement of material between two points which can be buildings and/or vehicles whereas, the actual process can be done manually or it can be automated depending on the application. The size of the material handling industry is large which can be seen from the United States Bureau of Labor Statistics as in 2016 there were 682,000 people working with the title material moving machine operator. (Bureau of Labor Statistics, 2018). The importance of well-engineered material handling machinery is vital for the successful day to day operations in the manufacturing and logistics process and driver aiding systems such as boom tip control are essential to improve the quality, accuracy and speed of such processes.

4.1 Machine description

This work was done by utilizing a material handler provided by Mantsinen which manufactures a wide range of material handlers from small to large depending on the customers' needs however this work is based on the Mantsinen 200 machine which is described as a mobile harbor crane and comes with either fixed, wheels, tracks or rails as its desired undercarriage structure. The Mantsinen 200 is shown in figure 4.1 with the tracks as undercarriage structure. The Mantsinen 200 is designed to handle bulk materials such as coal and logs, however it can also handle standard size shipping containers and also general cargo for instance, steel coils which makes suitable for many different types of situations. (Mantsinen Group Ltd Oy, 2018).

Figure 4.1. Mantsinen 200 with tracks moving shipping containers. (Mantsinen Group Ltd Oy, 2018).

The Mantsinen 200 is based on the same principle idea behind an excavator and its structure consists of the undercarriage, upper structure, cabin, boom, stick and tool however, depending on the undercarriage structure configuration the material handler can be self-driven into the desired operation position and provides more flexibility to the day to day operations. The body is equipped with service walk ways in order to access the engine compartment and cabin which position is adjustable with its own hydraulic boom and stick in order to give the operator the satisfactory visibility however also a static cabin system is available. (Mantsinen Group Ltd Oy, 2018).

The upper structure is connected with a rotational body to the lower structure which allows the 360-degree rotation and improves the machines operating range. Mantsinen provides a quick coupling method for tool attachment and 9 different tool types for the material handler and the possibility to have your own customized tool head for specific needs however, in this work the material handler is only equipped with the clamshell bucket tool. (Mantsinen Group Ltd Oy, 2018).

Mantisinen has developed HybriLift technology which allows up to 35% energy efficiency in normal operations and the 200 has been equipped with this technology. HybriLift stores hydraulic energy from the boom movement to a hydraulic accumulator which then can be released to assist the boom lifting process where two of the three actuators are operated as normal hydraulic actuators while the third one is only used for the HybriLift energy recovery process. For the stick there are three hydraulic actuators which are configured in a way that the central actuator is moving to the reverse direction compared to the other two parallel actuators. The hydraulic control pattern of the material handler follows the ISO 10968:2017 standard where left hand joystick controls the swing direction by moving left or right and the sticks directional movement by moving forwards and backwards while the right-hand joystick controls the tool opening and closing by left or right and lifting or lowering of the boom by going up or down with the right joystick as shown in figure 4.2. (Mantsinen Group Ltd Oy, 2018).

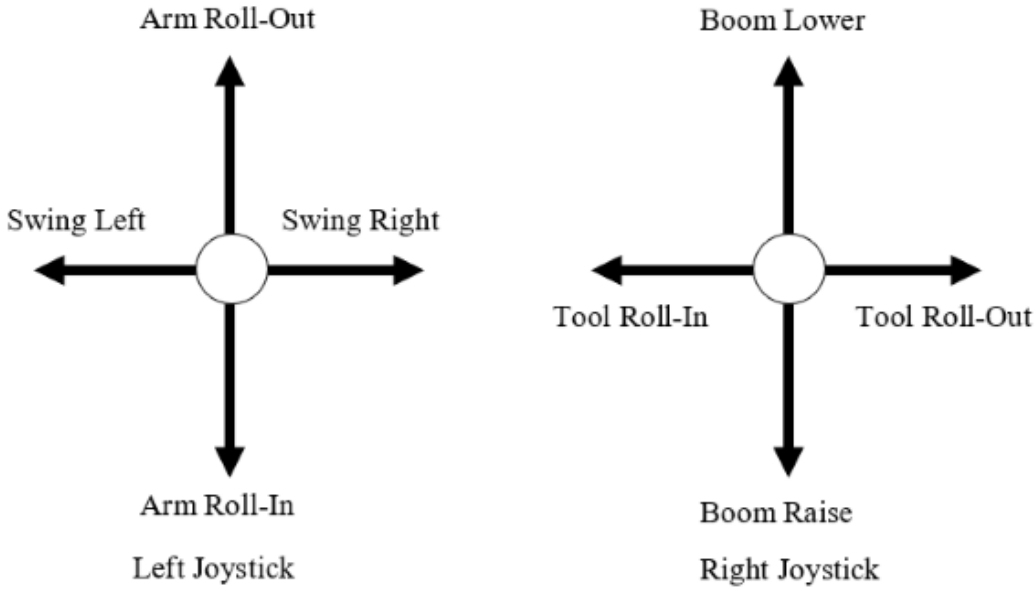

Figure 4.2. Joystick control pattern based on ISO 10968:2017 standard

4.2 Key values

Mantsinen 200 can be equipped with a boom that's length varies from 10.5 meters up to 21.5 meters while the sticks length varies from 9 meters to 18 meters providing the machine with a 37-meter horizontal reach. This is illustrated in figure 4.3 with the y-axis having the vertical lifting range and x-axis having the horizontal lifting range with the middle part demonstrating masses the machine can transport at specified heights and lengths. Mantsinen 200 can also be configured for heavy lifting mode which then limits the machines reach however allows it to lift much more weight as shown in figure 4.4 where the y-axis is for the vertical and x-axis for the horizontal reach and middle part of the figure displays the masses that the machine is capable of handling. (Mantsinen Group Ltd Oy, 2018).

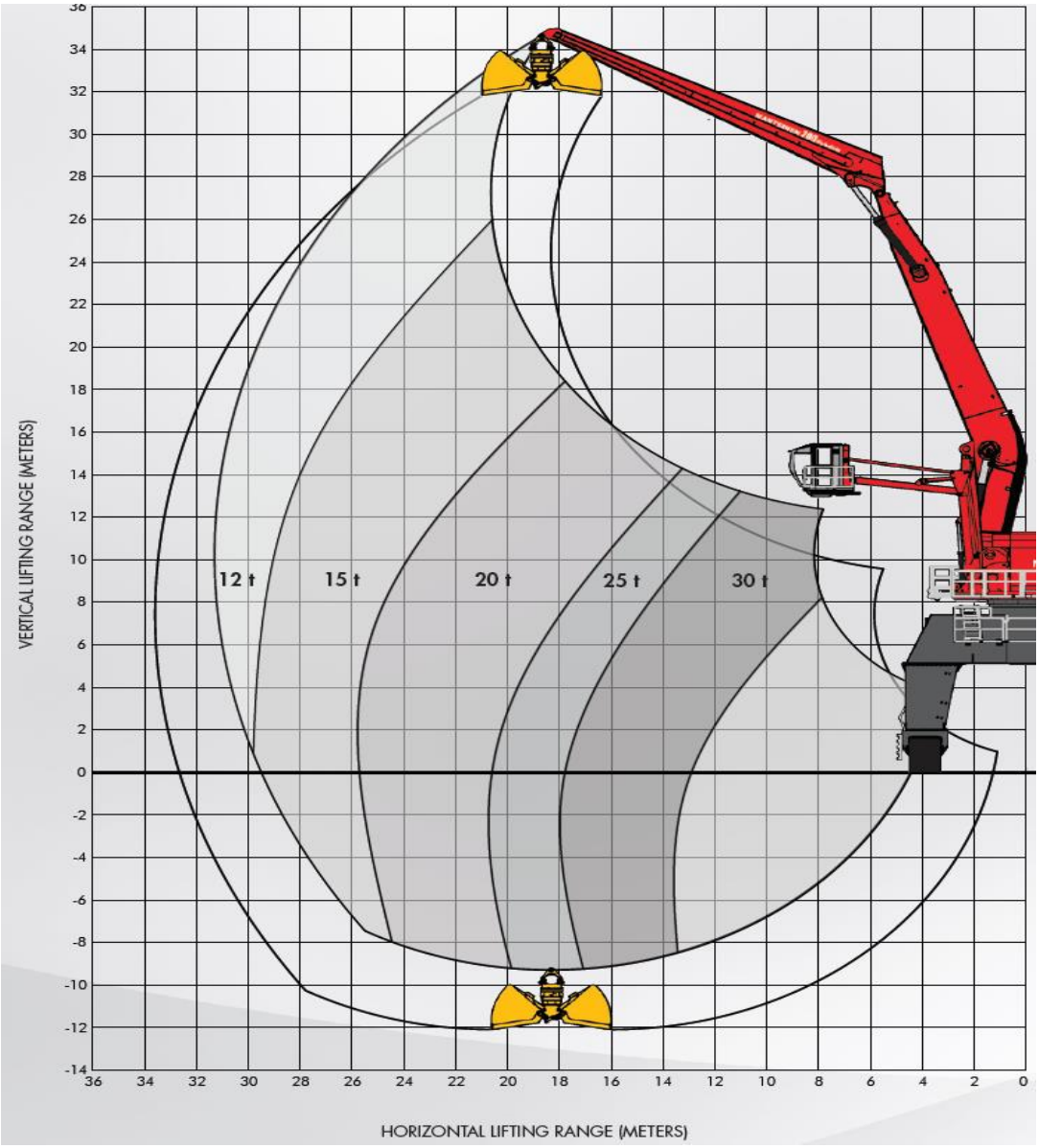

Figure 4.3. Lifting capacity and range of Mantsinen 200 with 17.5m boom and 15m stick (Mantsinen Group Ltd Oy, 2018).

The hydraulic system of Mantsinen 200 has been designed to fit this purpose by having 4 x 420 liters per minute hydraulic oil flow available with the operating pressure 330 bars and while in heavy lifting mode up to 360 bars. The swing system has its independent oil flow system providing up to 540 liters per minute oil flow and 300 bar pressure. All of this is powered with Volvo TAD1643VE diesel engine providing 565 kilowatts (kW) of power at 1800 revolutions per minute and the total weight of the machine is between 230 to 280 tons depending on the configuration. (Mantsinen Group Ltd Oy, 2018).

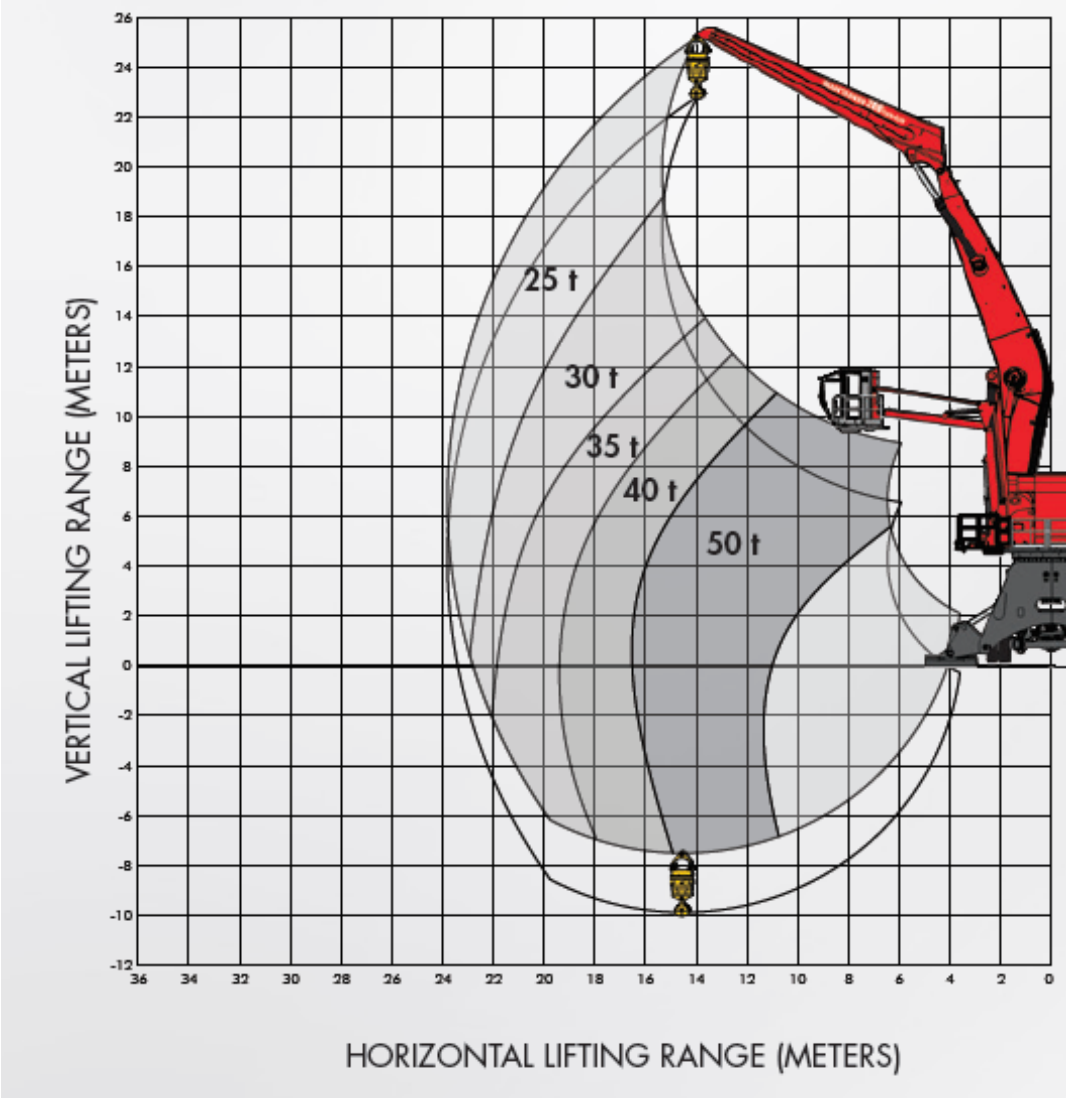

Figure 4.4. Mantsinen 200 in heavy lifting mode with a 13.5m boom and 11m stick (Mantsinen Group Ltd Oy, 2018).

Alternatively, the Mantsinen 200 can also be equipped with an electric motor to replace the diesel motor where the electric motor is a 355 kW IEC cast iron motor working at 1500 rpm and operating voltage varies between 400 and 690 volts. Mantsinen provides an additional power pack feature that allows the machine to run some hydraulic features while relocating with its own power. (Mantsinen Group Ltd Oy, 2018).

5 PRINCIPLES OF COORDINATE CONTROL

This chapter will describe the basic principles of implementing coordinate control and the two methods used in this work are open loop and closed loop in which the first method has an open loop control system which acts purely with provided input signals and the output has no effect on the system whereas the second system is based on looping back the output of the system. Comparing the output with the desired input and then adjusting the system to have zero difference between the two. Figure 5.1 illustrates the operating principle of the open control system and figure 5.2 illustrates the operating principle of the closed loop system.

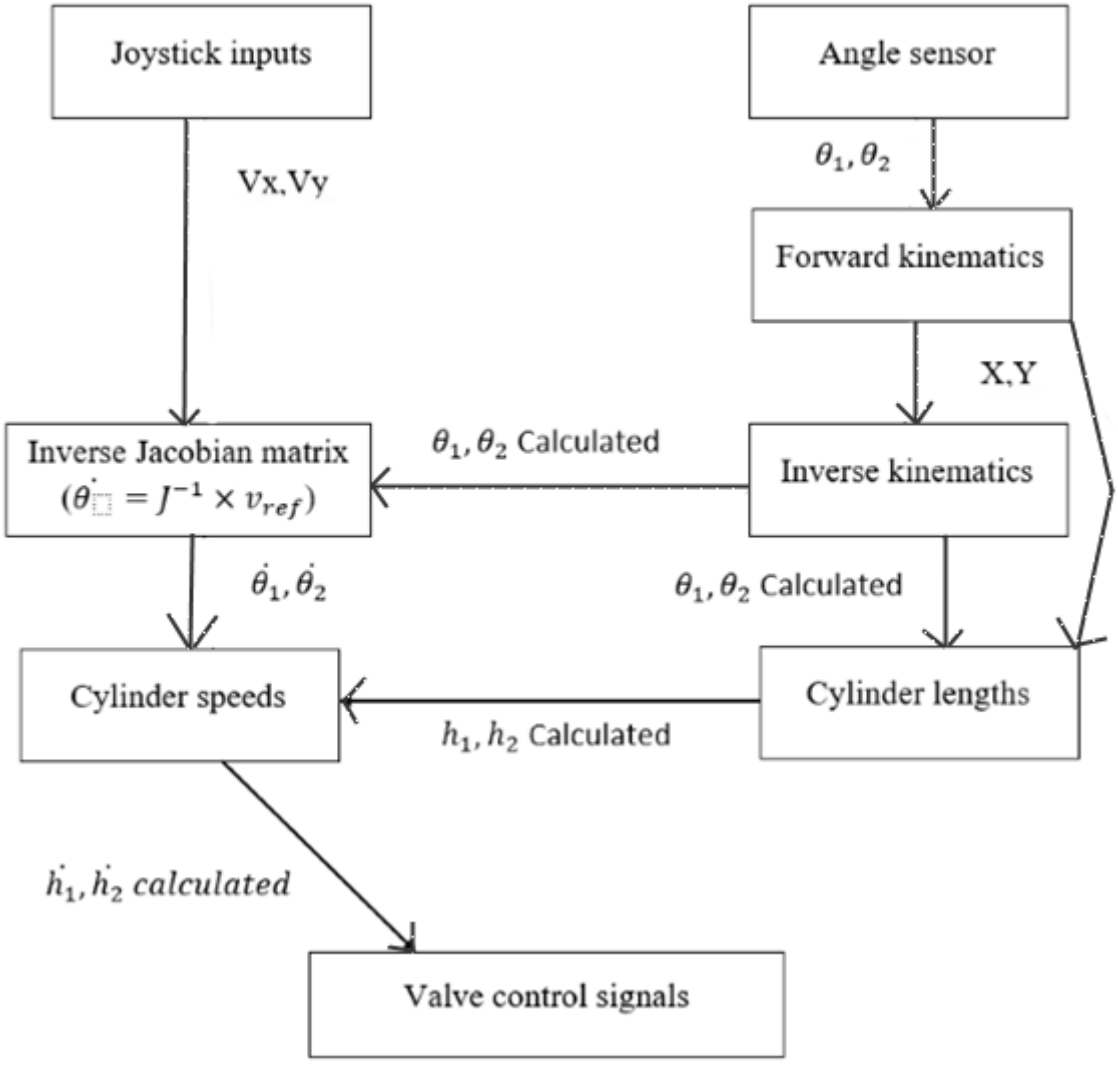

Figure 5.1. Open loop control system operating principle

In the open and closed system, the joystick gives the x- and y- direction linear boom tip velocities and the angle data obtained from the sensors of the system is used to calculate the boom tip x and y locations. After that it is transformed into robot angles which is used to calculate the lengths of the actuators and the robot angles are inserted to a Jacobian matrix with the desired linear velocity inputs of the arm structure. The angular velocities are formed in the Jacobian matrix which are then used to calculate the actuator velocities to form valve guidance signals.

The closed loop system uses the angular velocity sensors to provide the feedback for the system and the joysticks function the same way as in open control system, however the angle sensors are fed directly into the Jacobian matrix with the linear velocity inputs. The Jacobian matrix gives out the angular velocities that are then compared to the angular velocities of the angular velocity sensors which in this model are the same sensors as the angle sensors. When these two angular velocity signals are added together as the input being positive and sensor data being negative, difference between them is calculated and inserted to the PI controller, which starts to adjust the signal which is then directly inserted to the valves.

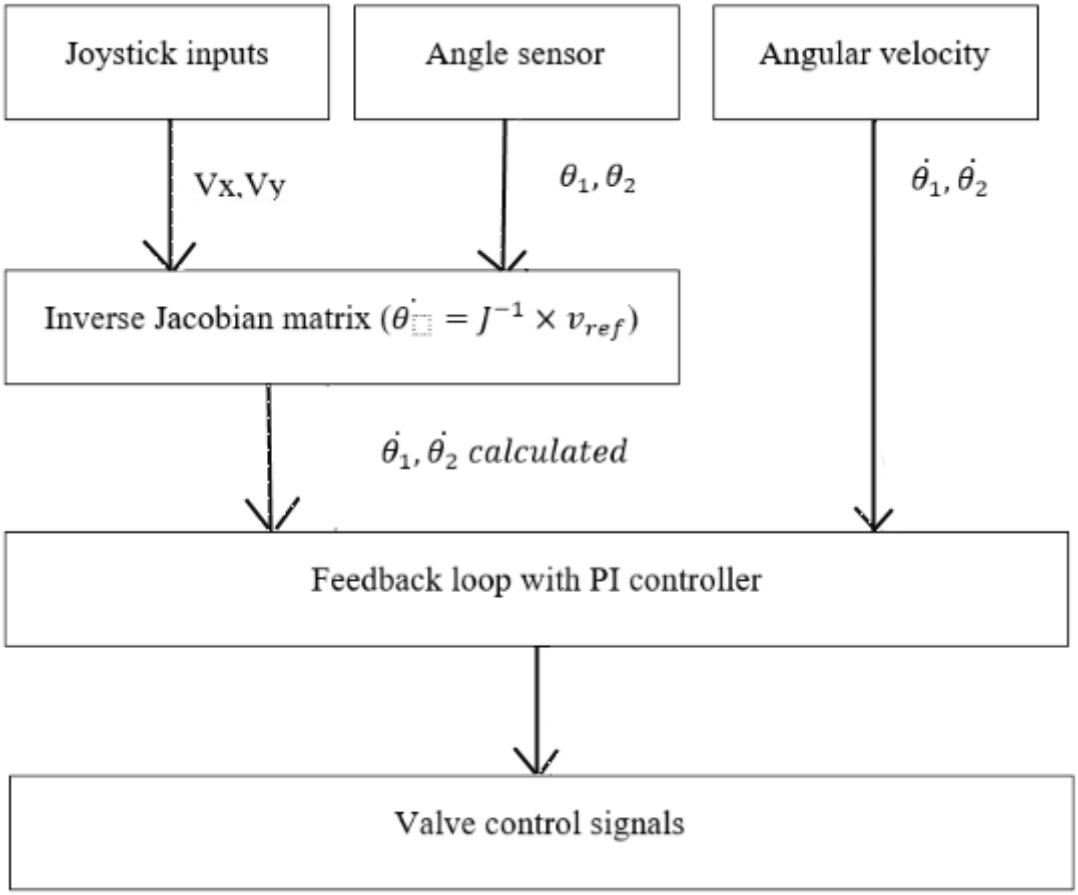

Figure 5.2. Closed loop control system operating principle

6 SIMULATION ENVIRONMENT

The main simulation program used for this work is Mevea industrial simulator which allows the user to accurately create real world problems that occur in with the hydraulic systems such as a material handler and it consist of three elements which are Modeller, I/O toolbox and Solver. The modeler is used to construct the model of the system with all of its constraints and functionalities whereas the solver is used to simulate the model whereas the simulator can simulate the movement of hydraulic actuators and motors of mechanical model and taking into consideration structural flexibility.

Mevea simulator is based on Mevea Ltds own physics engine which allows the users to model mechanics, hydraulics, transmission and operating environments. The simulator has many different applications however the most common ones are to use it to train new machine operators and product development before making physical products which significantly decreases costs and provides accurate data for the original equipment manufacturers. The version of the simulator software used for this work was v2.3.704 build 7.70.2677. (Mevea Ltd. 2018).

In this work the material handler model was provided by Mantsinen and it is the same as their equipment in the real-world and all the data values used here can be used when implementing this system into their real material handlers. The composition of the material handler is shown in figure 6.1 and 6.2, where the first one is the over view of the simulation environment where the testing would be done and the later one is the side view showing the arm configuration and actuator positioning. The front side actuators have a pair operating on the other side of the arm structure which is not visible in the figure. Two changes were done to the model which were the addition of the socket interface and its signals that allow the Mevea simulator to import and export data to Matlab Simulink which is the other program used in this work. Also, the position of the arm was modified to touch the ground in order to avoid initial velocity spikes of the swinging bucket due to gravity.

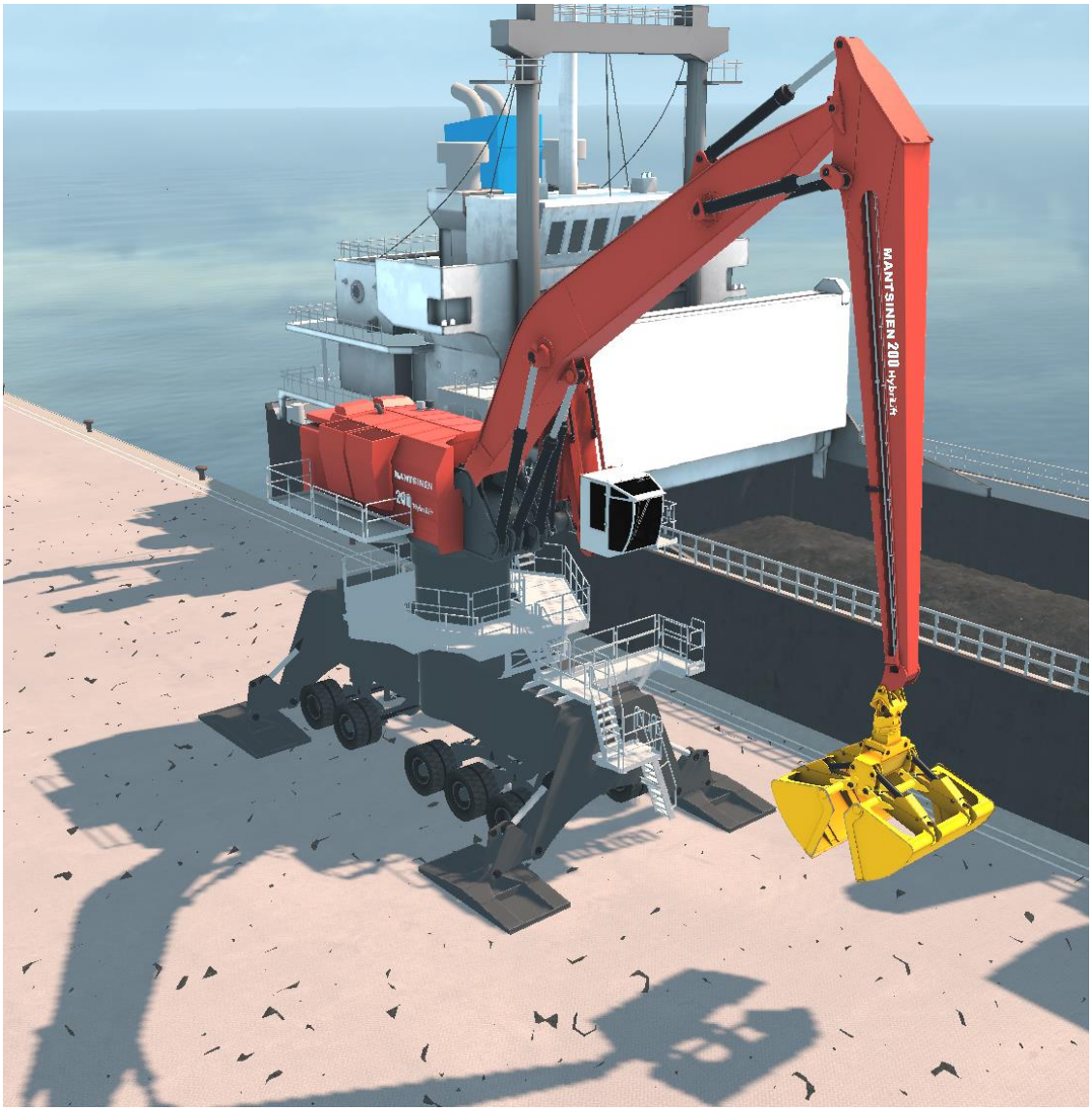

Figure 6.1. Mantsinen 200M in Mevea simulation environment

Matlab is developed by Mathworks and it is a multi-paradigm numerical computing environment whereas, Simulink is an addon inside the Matlab program that can be used to create graphical programming of mathematical models. The version 2017b was used for both software while doing this work.

Figure 6.2. Side view of the Mantsinen 200M with the arm structure clearly visible

6.1 Model description and parameters

The solver choices are made with empirical testing as which would work the fastest with the made model. The Simulink solver was set to run in with a fixed step size with Ode3 (Bogacki-Shampine) solver for infinite amount of time to allow the simulation of the system. Step size was set to 0.0012 Simulink and 0.001 for Mevea and also Ode4 (Range-Kutta) solver was used for Mevea environment.

A premade interface block that was provided by the university was added as function block to act as a communication hub between the Simulink code and the Mevea Solver in order for the required data to be extracted from the model and calculations shown in chapter 3 of this work could be performed, after which the necessary signals were added to the Mevea Modeller I/O socket interface. The angle values from the sensors are in degrees however, Simulink operates better with radians and these values were converted from degrees to radians also, the Mantsinen model had multiple different locking mechanisms in place that would have to be controlled manually in the I/O fault control which was found out to be demanding. The machine has pilot and Hybrilift valves that need to be manually controlled

every time the arm is driven. The solution for these problems was solved by inserting these signals to Simulink and automating their control based on the actuator control signals.

In the Mevea socket interface several pre-existing signals were added to the output directory of the socket interface in order to obtain the input values from joysticks given by the operator. These joystick values contain the direction of each joystick and the input value the operator is giving to each joystick where the scale goes from 0 to 250 and initial touch is compensated to give a smoother input feeling however otherwise joystick inputs follow a linear path for spool position. The joysticks values are used to create the desired actuator speeds what the operator is requesting from the system. As the system is pressure compensated the area of the actuators can be reduced into one area that receives the maximum flow rate that the system can provide and with the relation shown in equation 6.1 the maximum speed of the hydraulic actuator can be calculated and table 6.1 shows the results of the calculations for each direction.

$$v_{max} = \frac{Q_{max}}{A_p} \tag{6.1}$$

Where v_{max} is the maximum velocity of the hydraulic piston, Q_{max} is the maximum flow rate and A_p is the combined piston area. The formula is used to calculate the lifting and lowering speeds for the actuator as when the direction of the flow changes the area affected by the flow is opposite side of the hydraulic actuators' piston. (Rabie, 2009. p. 31).

Table 6.1. Actuator speeds

Parameter	Definition	Value (units)
Yref_pos	x-direction max speed up	0.1883 m/s
Yref_neg	x-direction max speed down	2.598 m/s
Xref_pos	y-direction max speed forwards	0.1474 m/s
Xref_neg	y-direction max speed backwards	0.7958 m/s

The simplification of the joystick directions was made in order to keep the model as simple as possible and maintain the basic operating principle. Depending on the joystick direction the control algorithm creates a different input signal value varying from 0 to 10 where the signal is formed by direction one being away from operator and two towards the operator while left side is four and right side eight while the center is zero. When the joystick is moved to one of the four corners, the signal formed is the sum of the surrounding directions for instance top-left corner is surrounded by one and four so the corner is five and when the process is repeated to all corners we obtain nine for top-right, ten for bottom-right and six for bottom-left displayed in figure 6.3. This design for the coordinate control model was altered in a way that only allows one direction input at any time. Figure 4.2 displayed the function of each direction so the limit made with this model prevents the same time operation of the bucket and arm y-direction movement or swing and arm x-direction movement and figure 6.4 shows the limitation method made in the Simulink model.

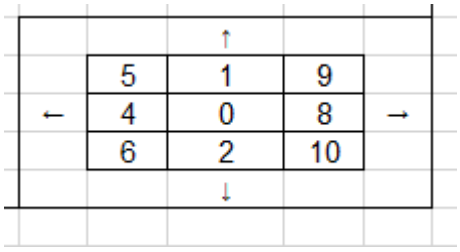

Figure 6.3. Joystick control pattern signal forming for Mantsinen 200M

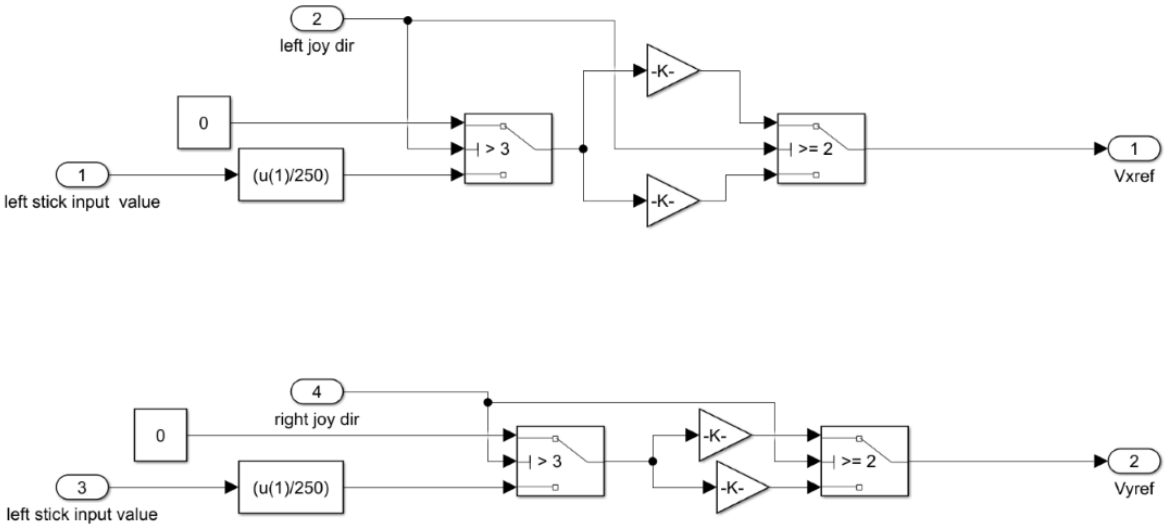

Figure 6.4. Reference speed creation block with direction limiter

Both boom and stick are equipped with their individual sensors and the angles measured are absolute angles meaning that angles provided by the booms and the sticks sensor are relative to angle of Earth however, the machine already has the end effector location as a CAN (Controller area network) bus value that can be extracted directly into the Simulink model and when using the equation 3.11 along with the known parameters listed in table 3.1 the robot angles that are between each link of the hydraulic manipulator structure can be calculated.

6.2 Open and closed loop differences in model parameters

When the robot angles are known the process shown in chapter 3 can be performed to calculate the length of each actuator and using desired velocity input from the operator the robotic angular velocities can be calculated as shown in equation 3.33 and this data is further processed into actual actuator speeds as shown in equations 3.36 to 3.38. The last step in the model is to convert the obtained actuator speeds into actual control valve voltages which done by taking the actuator speed and dividing it by the maximum speed of each joint based on the direction of movement. This percentage that is obtained is then scaled to the maximum value of the control voltage of the control valve. The system has a total of 8 control valves which control the stick and boom and 2 load control valves which are operated at the same time as the normal control valves and the operating values are listed below in table 6.2 including the joystick input value ranges.

Table 6.2. Valve and joystick control values

Parameter	Definition	Value (units)
J_{left}	Joystick direction left	1-2
J_{right}	Joystick direction right	1-2
Jvalue	Joystick input value	0-250
U_{bspool}	LUDV valve control boom	0-800 mV
U_{sspool}	LUDV valve control stick	-800 to +800 mV
U_{blc}	Load control valve control voltage boom	100 to 670 mV
U_{slc}	Load control valve control voltage stick	100 to 670 mV
V_1	Valve 1 guidance compensation	370 mV
V_2	Valve 2 guidance compensation	350 mV
V_3	Valve 3 guidance compensation	330 mV
V_4	Valve 4 guidance compensation	310 mV

When lowering the boom, the machine opens the load control valve to let the boom come down and recharge the Hybrilift energy storage system. The sticks' load control valve is used simultaneously with three of the control valves when bringing it towards the cockpit. The initial input of the joystick opens the valve to a preset value defined by the manufacturer however after that the valve opening is linear compared to the joystick input. The valve control block is shown in figure 6.5 which is the same for all the 8 LUDV valves and 2 load control valves which each having its own specific set of rules shown in table 6.3 which explains how each valve operates when positive or negative direction control signal is given.

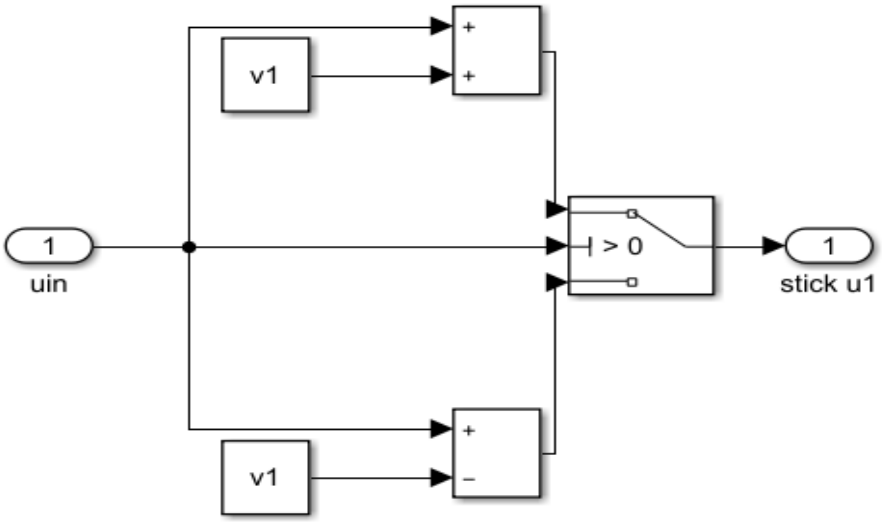

Figure 6.5. Valve control block with direction control

Table 6.3. Valve guidance rules

Valve	Direction positive Valve control values	Direction negative Valve control values
Boom 1 to 4	0…800	0
Stick 1 to 3	0…800	-800…0
Stick 4	0…800	0
Boom LC	0	0…670
Stick LC	0	0…670

In the closed loop system, the total amount of parameters is much less than in open control system making the system more straightforward and a comparison picture is shown in Appendix I to demonstrate to major differences between the two different control methods. In the actual model, the signal from the linear velocity guide is inserted to the block with the absolute angles and out comes the angular velocities and the angular velocities are then summed up with the angular velocity sensor data and sent to a PI controller which then gives out directly the desired signals for the 8 valves that are controlled for the boom and stick control.

6.3 Controller design and tuning

In this work a PID-controller was used to control the valve signals for the hydraulic actuators. PID which stands for Positive, Integral, Derivative and it is used in a great diverse of different industrial fields, from mechanics to electronics (Åström, K.J. & Hägglund, T., 1995). Block diagram of PID-controlled plant is presented in figure 6.6 and in equation 6.2 is the mathematical form of a PID controller whereas figure 6.7 has the PID controller used in the model which is same for both link valve controls.

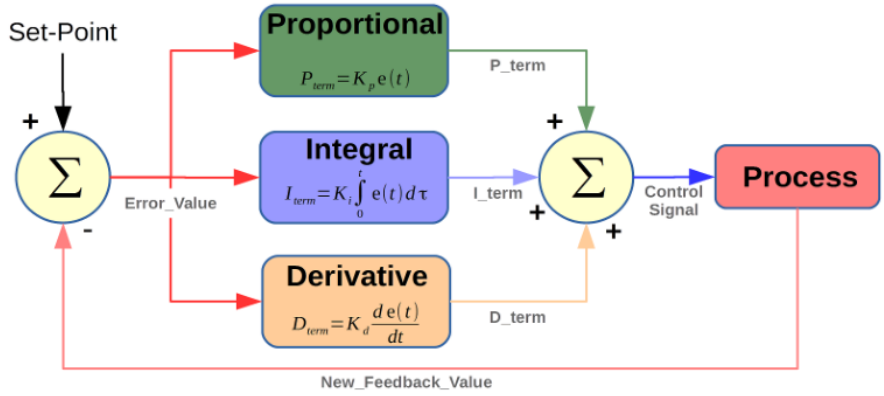

Figure 6.6. Block diagram of PID-controller (MathWorks 2018).

Transfer function for PID-controller can be written as:

$$u = K_p e + K_i \int e\, dt + K_d \frac{de}{dt} \tag{6.2}$$

Where K_p is the proportional gain, e is the error which is a subtraction of set point value and output value, K_i is the integral gain and K_d is the derivative gain. There are other mathematical expressions of PID-controller however in this work the mentioned one is used. The gains K_p, K_i and K_d have different effect on the system dynamics. For instance, K_p and K_i decrease the rise time whereas K_d will not have effect to it. K_d, however, has an effect to the overshoot and settling time. The relation of each component of the PID controller to the control signal changes are shown in table 6.4.

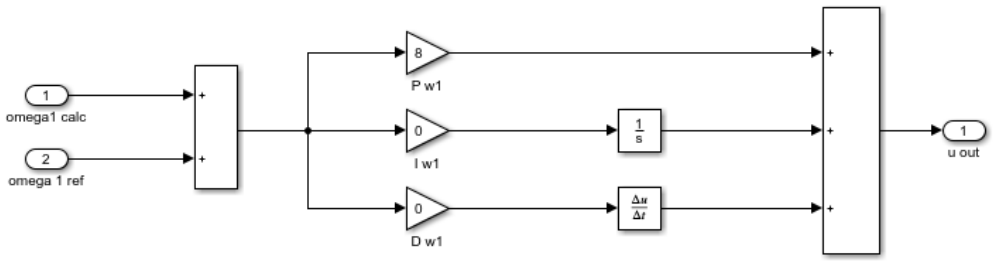

Figure 6.7. PID controller in the Simulink model

Table 6.4. Effects of controller components to control signal (Jenkins, H.E., 2014).

Response	Rise Time	Overshoot	Settling Time	S-S Error*
K_p	Decrease	Increase	NT**	Decrease
K_i	Decrease	Increase	Increase	Eliminate
K_d	NT**	Decrease	Decrease	NT**

*S-S stands for Steady State
** NT stands for No definite trend

The tuning of the controller was done by using Ziegler-Nichols tuning method which is a heuristic method for controller tuning where the principle idea is to set K_i and K_p to zero and then slowly increase the value of K_p until the signal reaches a state where steady state oscillation occurs. This gain is called K_{cr} and the period of time between each oscillation peak is measured and called P_{cr} and is measured in seconds. When a PID controller is used the Ziegler-Nichols tuning method has a premade table which then allows the right values to be set for the controller shown in table 6.5. (Jenkins, H.E., 2014).

Table 6.5. Ziegler-Nichols tuning table (Jenkins, H.E., 2014).

Type of controller	K_p	K_i	K_d
P	$0.5 \times K_{cr}$	0	0
PI	$0.45 \times K_{cr}$	$\frac{1}{1.2} P_{cr}$	0
PID	$0.6 \times K_{cr}$	$0.45 \times P_{cr}$	$0.125 \times P_{cr}$

From the table above, it is easy to choose the right values for the PID controller used in this work as soon as the state where the steady state oscillation starts to occur is found. In this work the K_d causes the noise of the system to amplify which could lead to the system oscillating significantly and in order to maximize the performance of the system, the K_d part of the controller was set to zero. This method is used to find the initial PI controller values of an unknown system and will give response that yields a 25% overshoot and satisfactory setting time and after this is done the fine tuning of the controller can be done as described previously. (Jenkins, H.E., 2014).

7 MODEL CONTROL INTERFACE AND TESTING PREPARATIONS

The model was tested in the university computer by simply running the two software at the same time and by doing so the errors of the model and mistakes made in the code could be found out and corrected while observing the performance of the model. It was not possible to equip the computer with joysticks as the Mevea model provided by Mantsinen was highly complicated and would require real machine control system to work properly nevertheless the control of the system was done using the Mevea I/O control interface to tests simple movement as for more complicated movement would require the simulator environment with joysticks and other CAN bus-controlled instruments which is shown in figure 7.1.

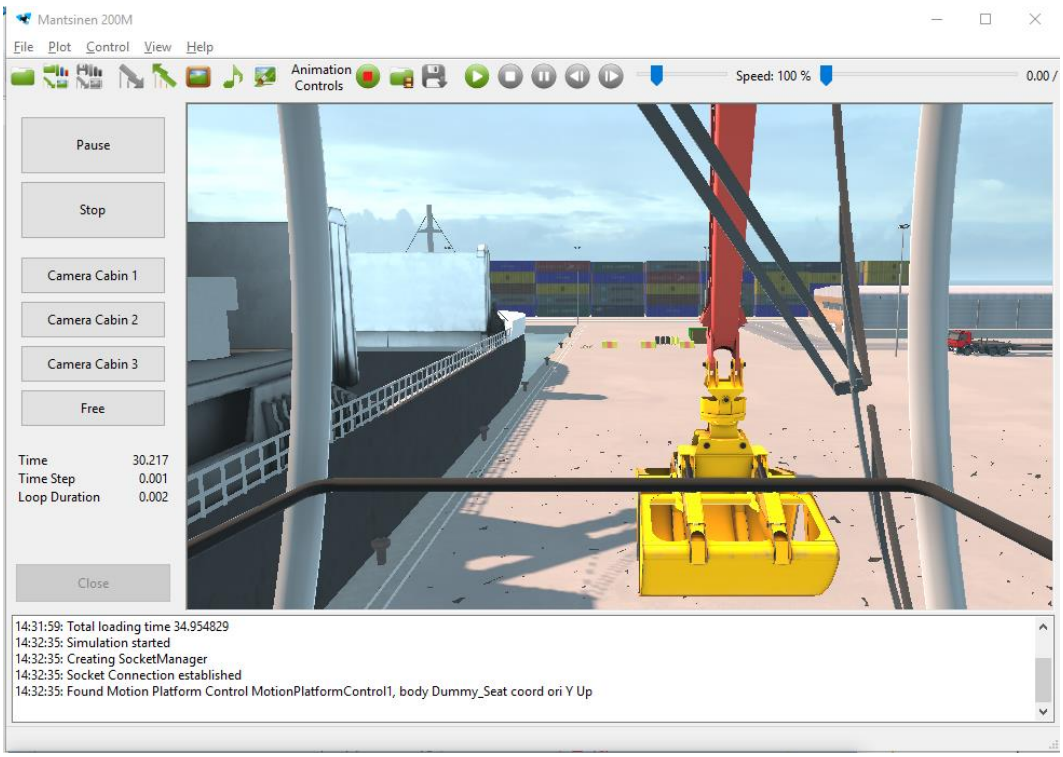

Figure 7.1. Mevea Solver simulation interface

The I/O fault control can only make step inputs as the system directly goes to the value inserted which does not represent the real-world control of these type of machines as the operator would linear increase the force input of the stick to move the machines arms. As a result of this the Simulink model was modified to have a slider so that the linear input of machine operator was possible simulate in the model.

Figure 7.2 below displays the relation of all the signals used in this work. Left side of the figure has the input signals from Mevea to Simulink which in Mevea are named outputs and right side has the output signals from Simulink to Mevea which in Mevea are named input signals.

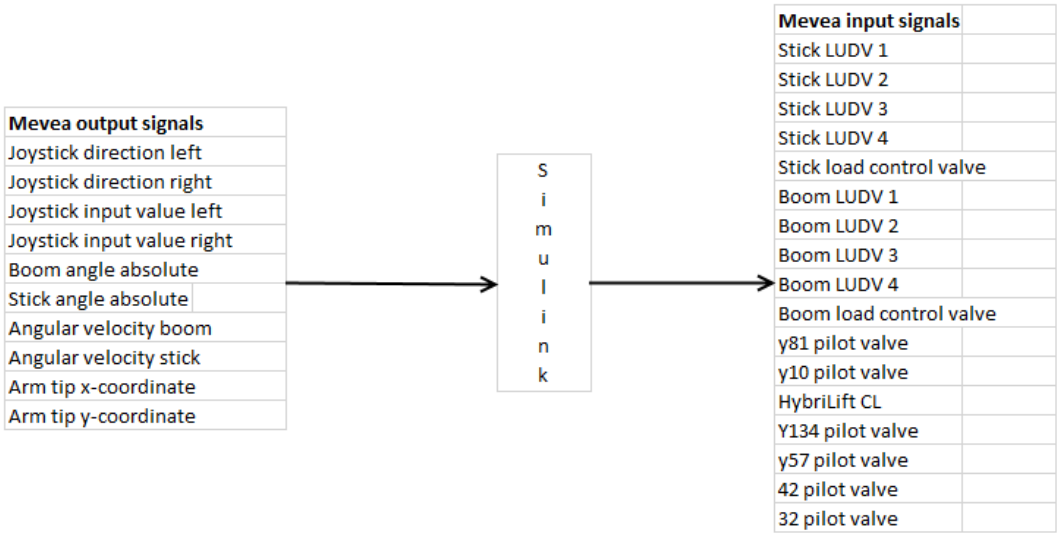

Figure 7.2. Mevea and Simulink signal relations

The original goal was to test the coordinate control system in a simulator provided by Mantsinen however due to ti me constraints that part of this work was not completed. The idea is to use the digital twin of the original machine to test the newly developed control system and to avoid possible damages or other costs that a real-world machine implementation would cause. Digital twin is virtual copy of any real-word application that can be produced accurately in virtual space and by doing so the possible problems in the design can be solved before real-world implementation. In the simulator test the fuel consumption and time required to complete the same task of the coordinate control system would be compared against Mantsinens' own control system.

8 RESULTS

The open loop system was first constructed to tests that the complex relation between Mevea and Simulink would work as intended and that the mathematical equations would yield correct results. This was the control method suggested by thesis supervisor Professor Handroos however Mantsinen requested that the system should be done with closed-loop feedback so the development of the open loop model was stopped after initial results were obtained and focus was turned to the closed loop system, which was then modeled and tested the same way as the open loop one and results of both of those tests are shown below.

All of the tests were done by applying the joystick to one direction and then measuring the changes in the tip position. In a perfect system, when given a x-direction control signal the y-coordinate of the tip should remain in the same position and by comparing these values of the two different systems and all of the four different joystick inputs can be concluded which method is satisfactory for this machine and for reference the machine was operated with Mantsinen control system to see how the tip position would change with the Mantsinen control system. The positive direction in x-direction is when the tip is moving further away from the cabin and negative when its moving closer to the cabin and the positive y-direction is when the arm is going upwards and negative when its going downwards. The y-direction zero level is at height of the swing link so the y-axis has negative values when it is under the swing link and positive when it is over the swing link.

8.1 Open loop results

For open loop system all the input signals were given as step functions where the input of the system is suddenly increased to the maximum value of the input joystick. There are velocity plots for the development of the velocity calculation performed by the code created for Simulink and position plots for the change of position during the simulation period. The simulation was completed in set where the simulation time for each control direction was limited to 20 seconds and a total of 100 seconds was simulated. Each of the given input signals is divided to its own category to see which of the input directions had desired performance.

8.1.1 Positive Y-direction

The first input given was to drive the tip in positive y-direction with maximum joystick input force from 5 seconds to 25 seconds in the simulation which can be seen in figure 8.1, where solid line represents boom actuator velocity and dashed line stick actuator velocity in meters per second. The calculated velocity of the x- and y- directions slowly decreases during time and in figure 8.2 are the results to the tip head coordinate changes where the x-axis has the time and y-axis has the position in meters and x-coordinate is solid line and y-coordinate is dotted line. Seen from the figure 8.2 below the tip x-value changes from 15.49 meters to 17.57 meters and y-value from -3.27 to -1.52 meters.

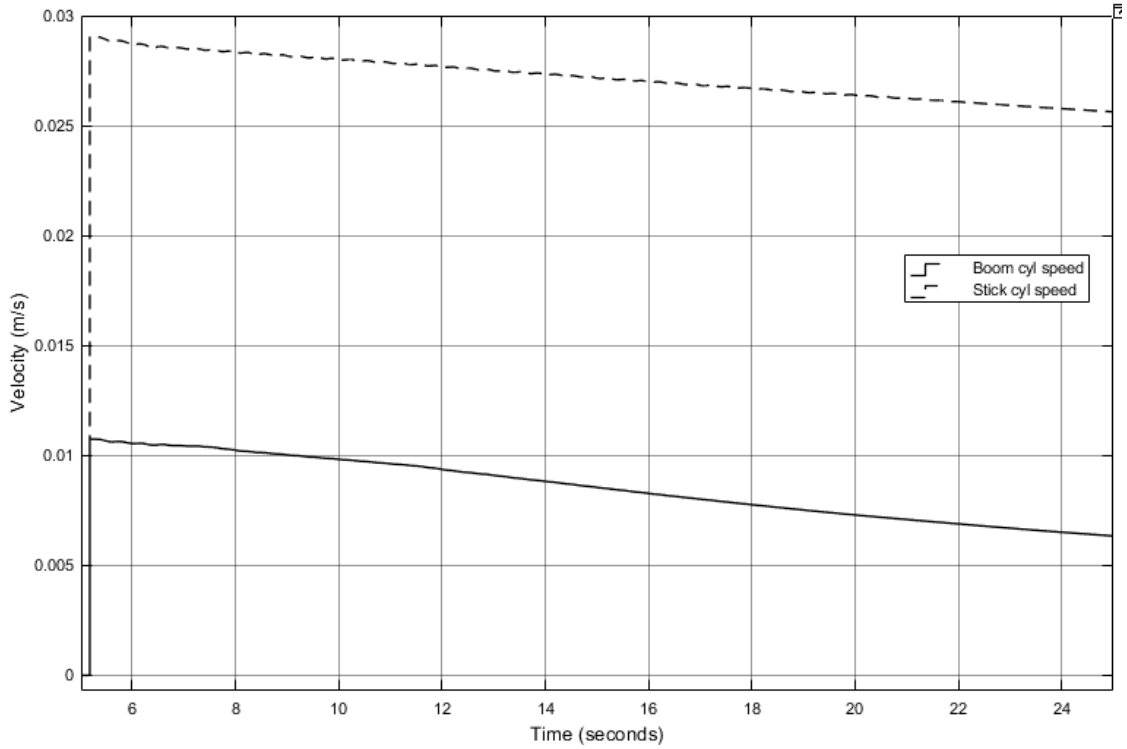

Figure 8.1. Calculated velocities of the tip in positive y-direction

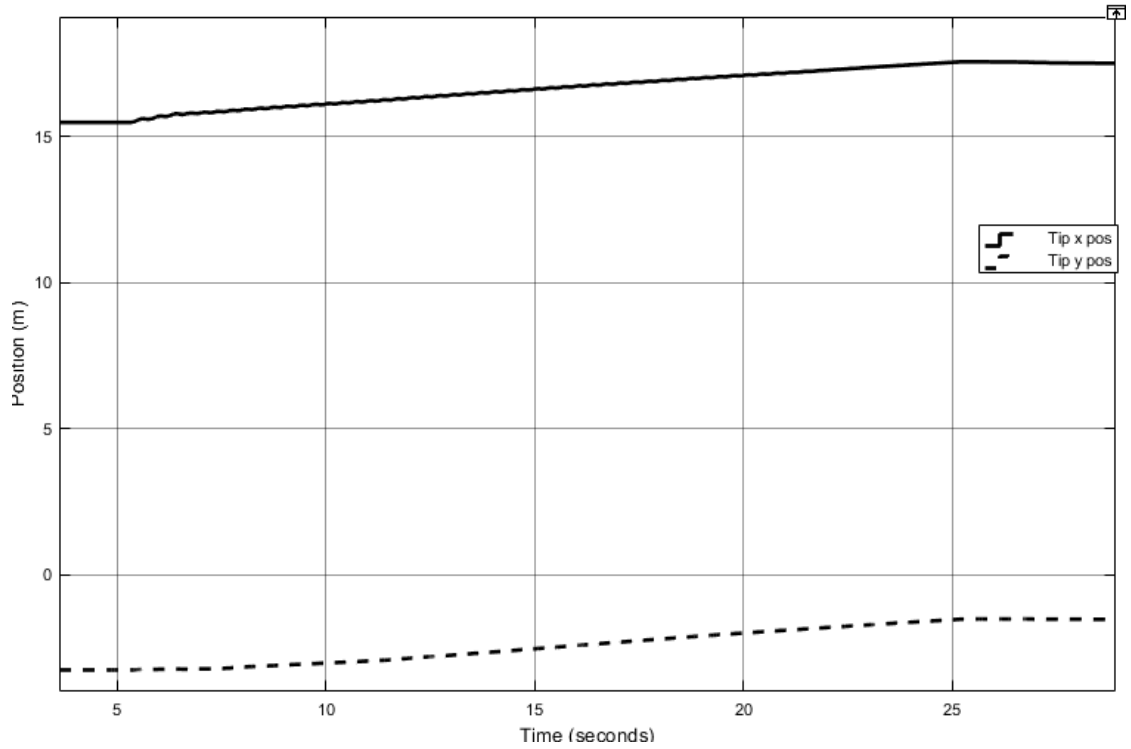

Figure 8.2. Tip position change with y-direction positive input

8.1.2 Positive X-direction

The second input was given in the positive x-direction with maximum joystick input and simulation time from 30 to 50 seconds. The same line properties are used for the figures 8.3 and 8.4 as before which can be seen in figure 8.3, the calculated velocity of the x- and y-directions slowly decreases during time after the given step input. Seen from the figure 8.4 below the tip x-value changes from 17.51 meters to 20.77 meters and y-value from -1.54 to -0.21 meters.

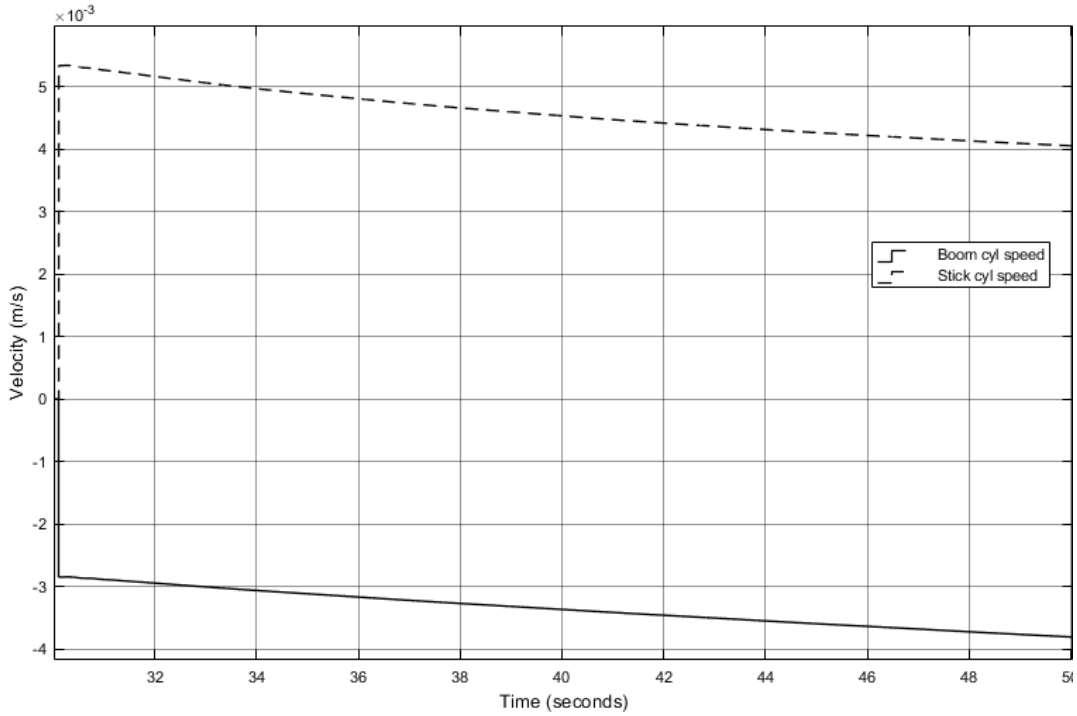

Figure 8.3. Calculated velocities of the tip in positive x-direction

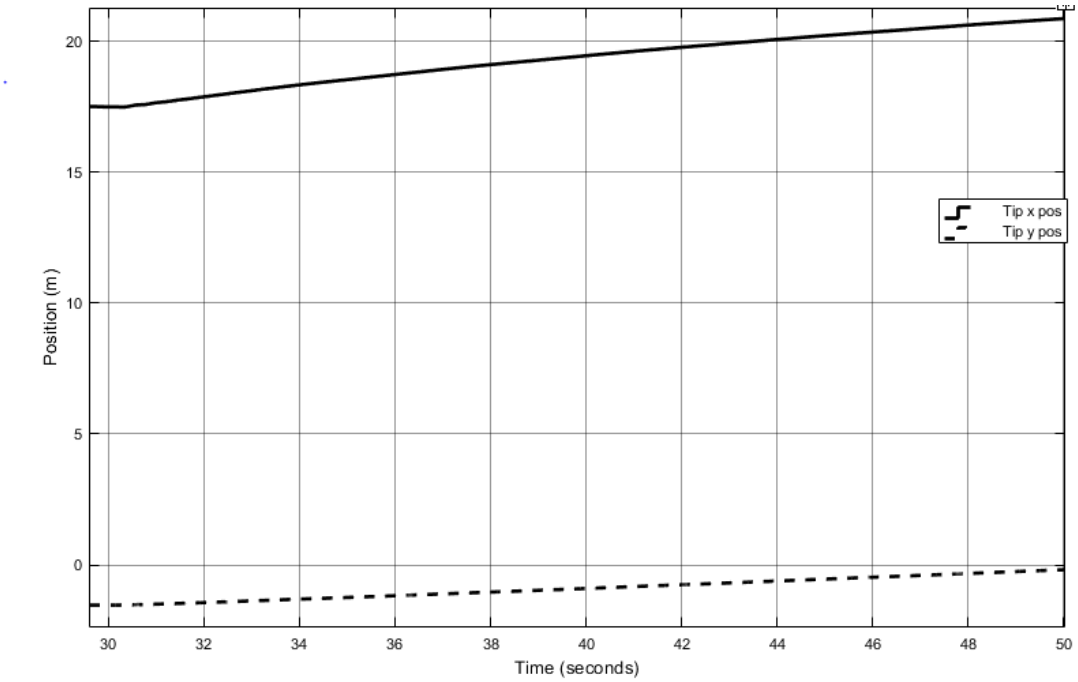

Figure 8.4. Tip position change with x-direction positive input

8.1.3 Negative X-direction

The third input was given in the negative x-direction with maximum joystick input and simulation time from 55 to 75 seconds. The same line properties are used for the figures 8.5 and 8.6 as before which can be seen in figure 8.5 where the calculated velocity of y- direction slowly decreases during the time after the given step input however less than in the two previous cases and the x-direction velocity increases to further negative. Seen from the figure 8.6 below the tip x-value changes from 20.90 meters to 20.29 meters and y-value from -0.17 to -0.50 meters.

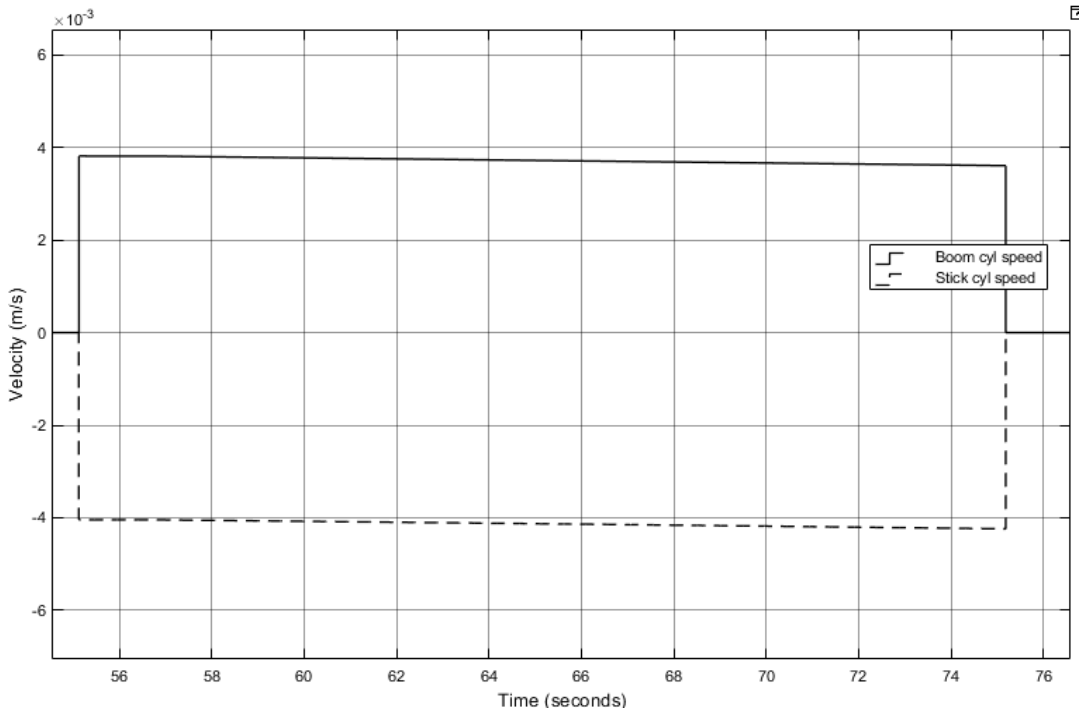

Figure 8.5. Calculated velocities of the tip in negative x-direction

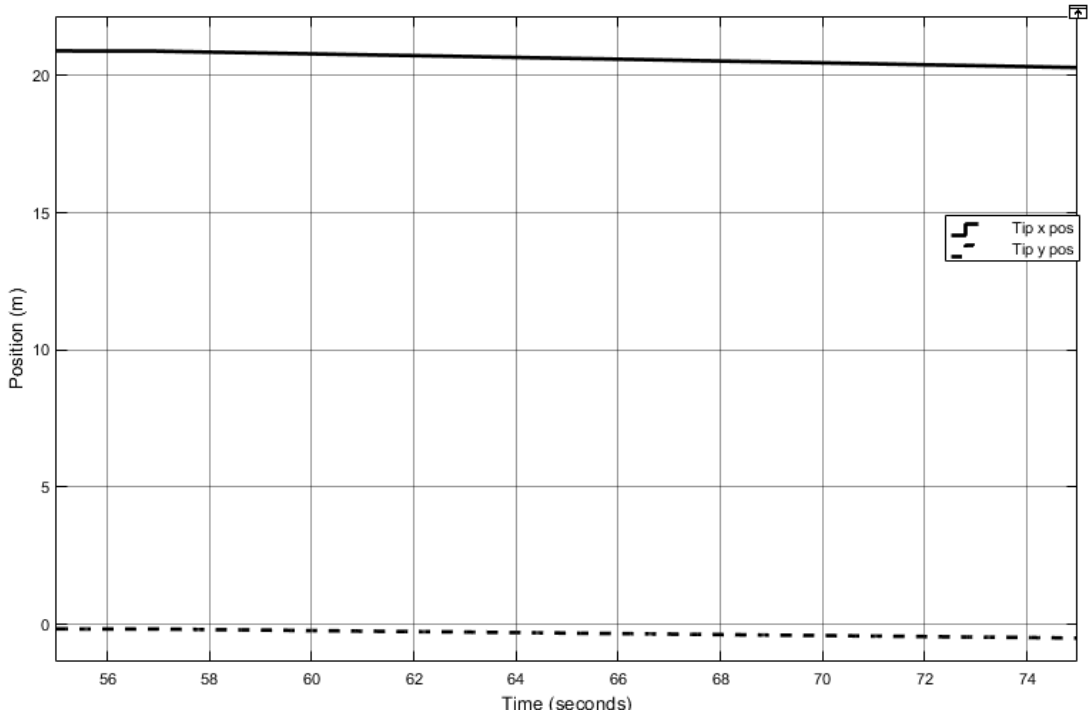

Figure 8.6. Tip position change with x-direction negative input

8.1.4 Negative Y-direction

The last input was given in the negative x-direction with maximum joystick input and simulation time from 80 to 100 seconds. The same line properties are used for the figures 8.7 and 8.8 as before which can be seen in figure 8.7 where the calculated velocity of the x- and y- directions slowly increases to the negative direction during time after the given step input. Seen from the figure 8.8 below the tip x-value changes from 20.28 meters to 16.13 meters and y-value from -0.51 to -1.74 meters.

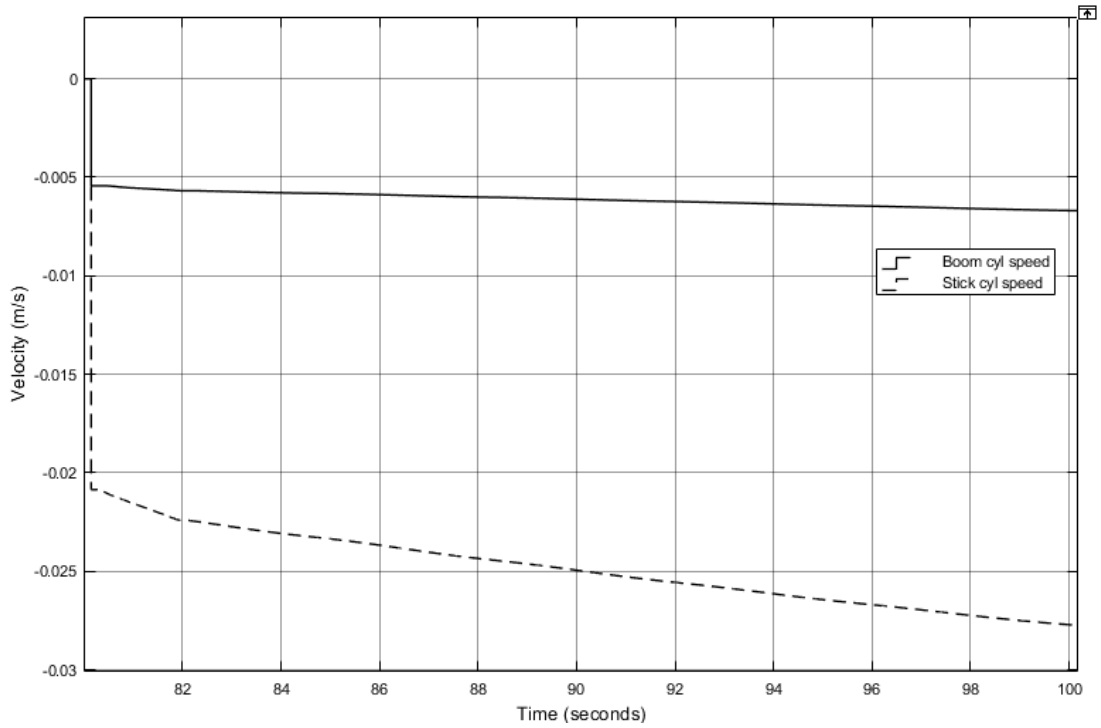

Figure 8.7. Calculated velocities of the tip in negative y-direction

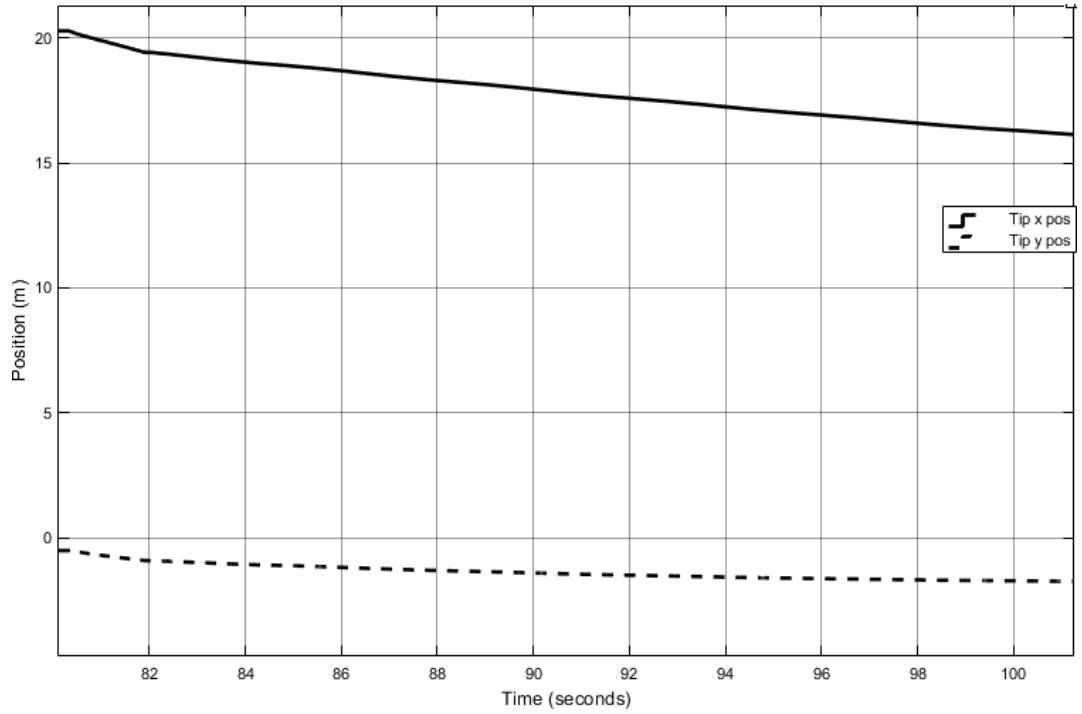

Figure 8.8. Tip position change with y-direction negative input

8.2 Closed loop results

The tests were done for the closed loop system using both the right and left to control the machine to see how well the controller would perform and how much the position changes would. Closed loop system was developed later and more effort was used to tune it however, step input is not a valid input method for closed loop system as it increases the chances of oscillations because of the rapid changes in the valve spool control values as a solution a slider was inserted to control the input signal force manually.

In both joysticks test the machine is operated for 20 seconds in which the arm is moved to one direction with the control input however he machine still has minor initial movement in the first ten seconds which is why the start of the simulation time is delayed slightly. The stick calculated values were amplified by 400 and calculated boom values for 800 in order to improve the controller performance and the feedback references were amplified by 4 and 8 respectively. The value of the K_p was set to 25 for boom link controller and 20 for swing link controller during these tests while K_i is set to one.

8.2.1 Positive Y-direction

The first input given was to drive the tip in positive y-direction with maximum joystick input force from 10 seconds to 30 seconds in the simulation. Seen from the figure 8.9 below, where the solid line is the x-coordinate and dotted line the y-coordinate of the tip, the tip x-value changes from 15.50 meters to 16.06 meters and y-value from -3.27 to -1.65 meters.

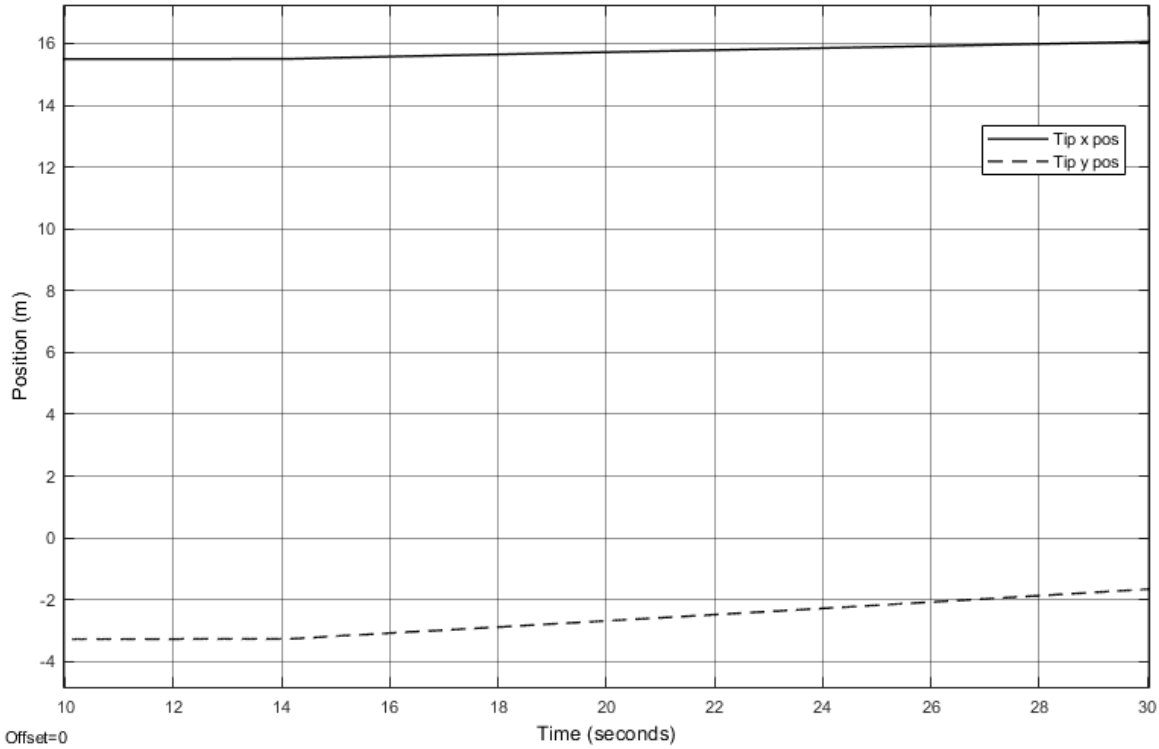

Figure 8.9. Tip position change with y-direction positive input

In figure 8.10 and 8.12 are the angular velocities of the two links and the solid line is the calculated value and dotted line the sensors feedback value. As can be seen that the boom link has small over shoot of roughly 10% of the requested speed after 2 seconds of simulation however towards the end of the time the two velocities catch each other. Figures 8.11 and 8.13 have the valve control signals and their change over the course of the time simulation. The legend of each figure shows the meaning of each line. Notable difference is the thickest line which represents the load control valve. As seen below the control signals are similar to the peaks in the reference velocity however with lower peaks. The controller can be seen reacting immediately to change in control signal however takes some time before the actuator movement has caused the manipulator arm to move. In figure 8.13 the stick control values for the three actuators are positive values described in table 6.2 however cause no movement in the manipulator and the angular velocity of the stick stays positive due to the movement of the first link.

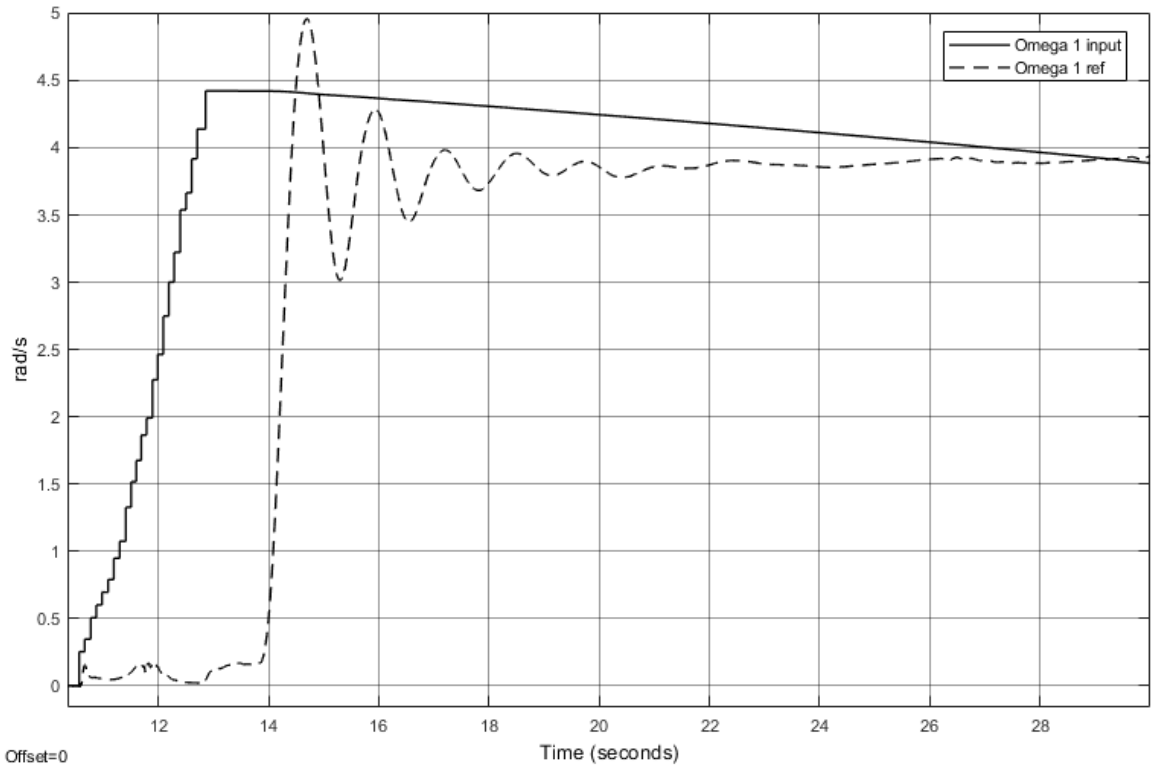

Figure 8.10. First link calculated angular velocity and reference angular velocity

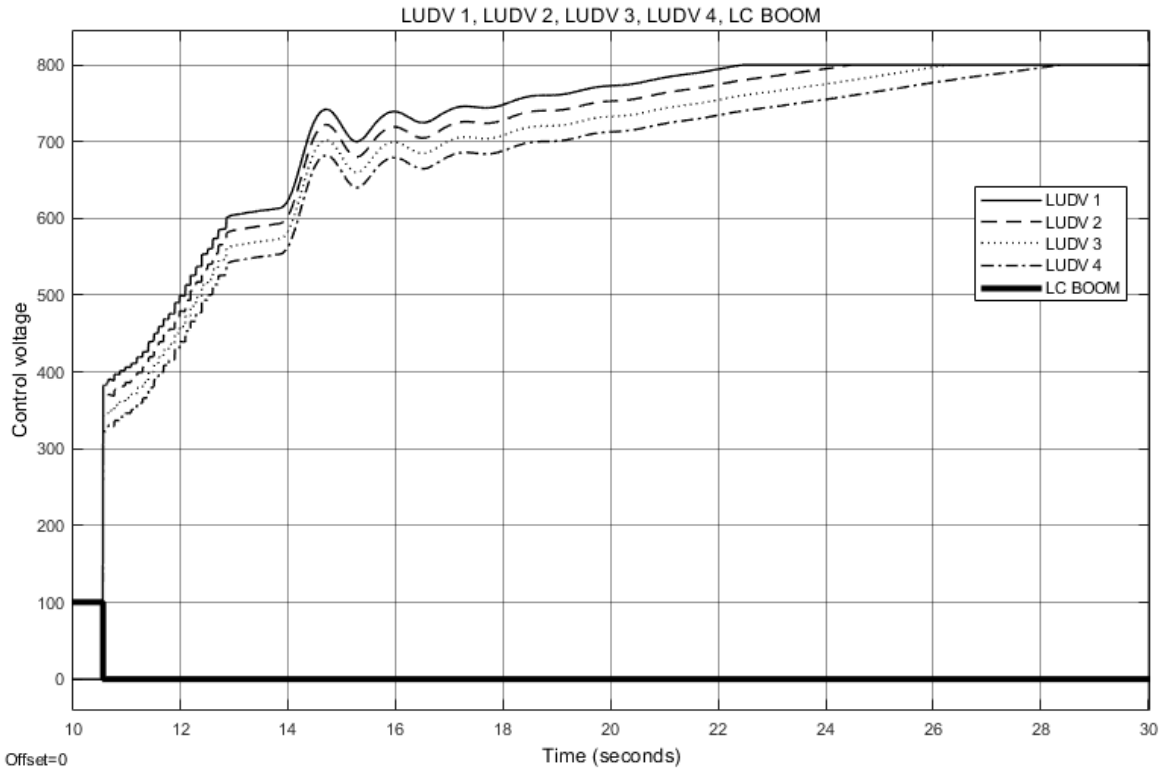

Figure 8.11. Valve control signals of first link valves

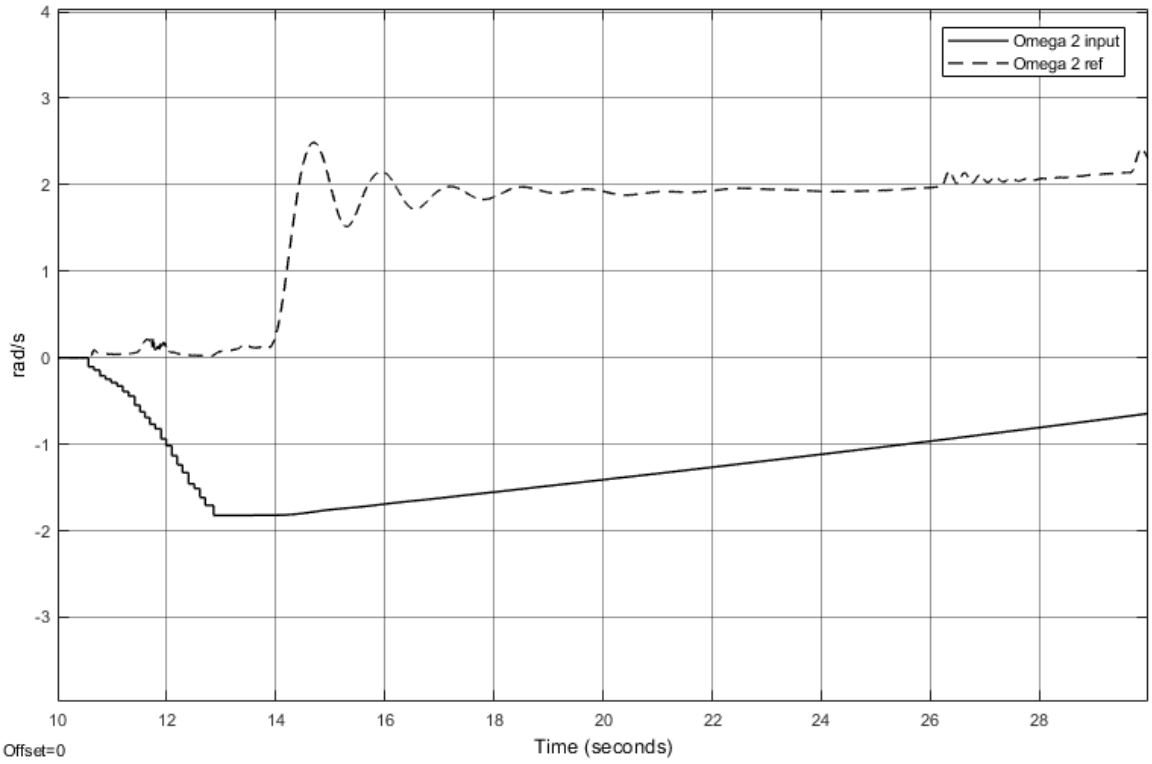

Figure 8.12. Second link calculated angular velocity and reference angular velocity

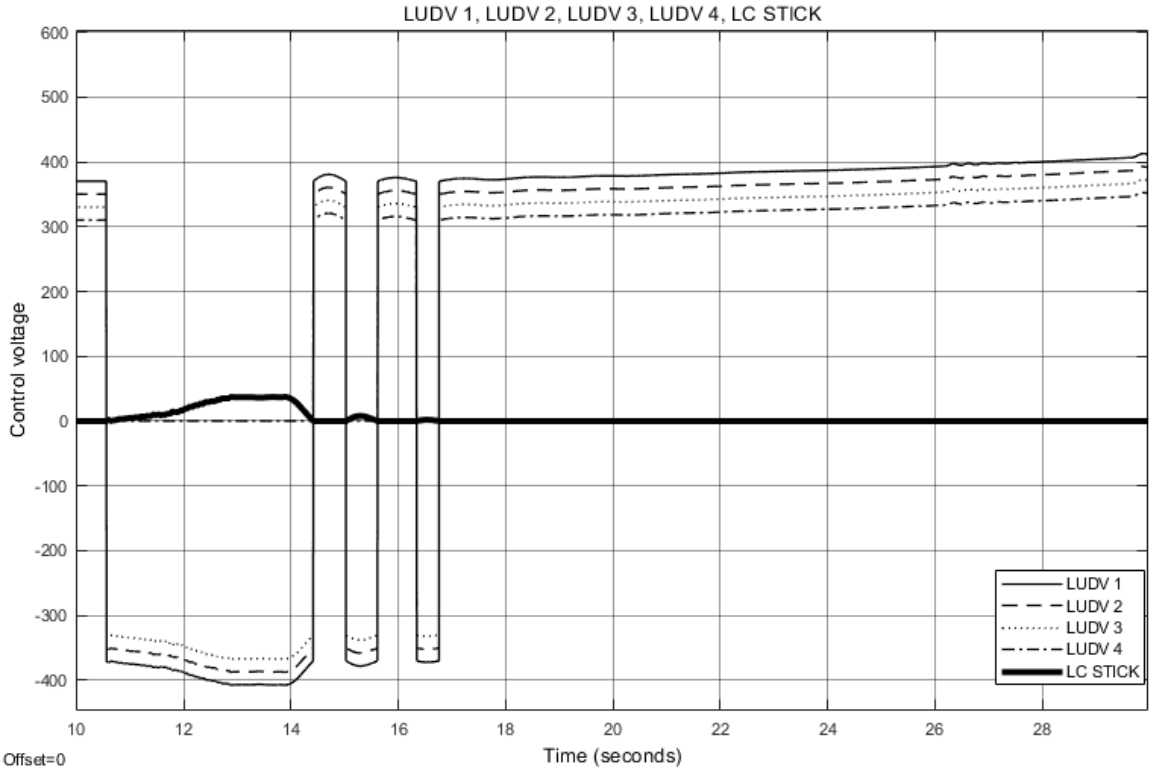

Figure 8.13. Valve control signals of second link valves

8.2.2 Negative Y-direction

The second input given was to drive the tip in negative y-direction with maximum joystick input force from 40 seconds to 60 seconds in the simulation. Seen from the figure 8.14 below, where the solid line is the x-coordinate and dotted line the y-coordinate of the tip, the tip x-value changes from 16.27 meters to 14.01 meters and y-value from -0.87 to -3.24 meters.

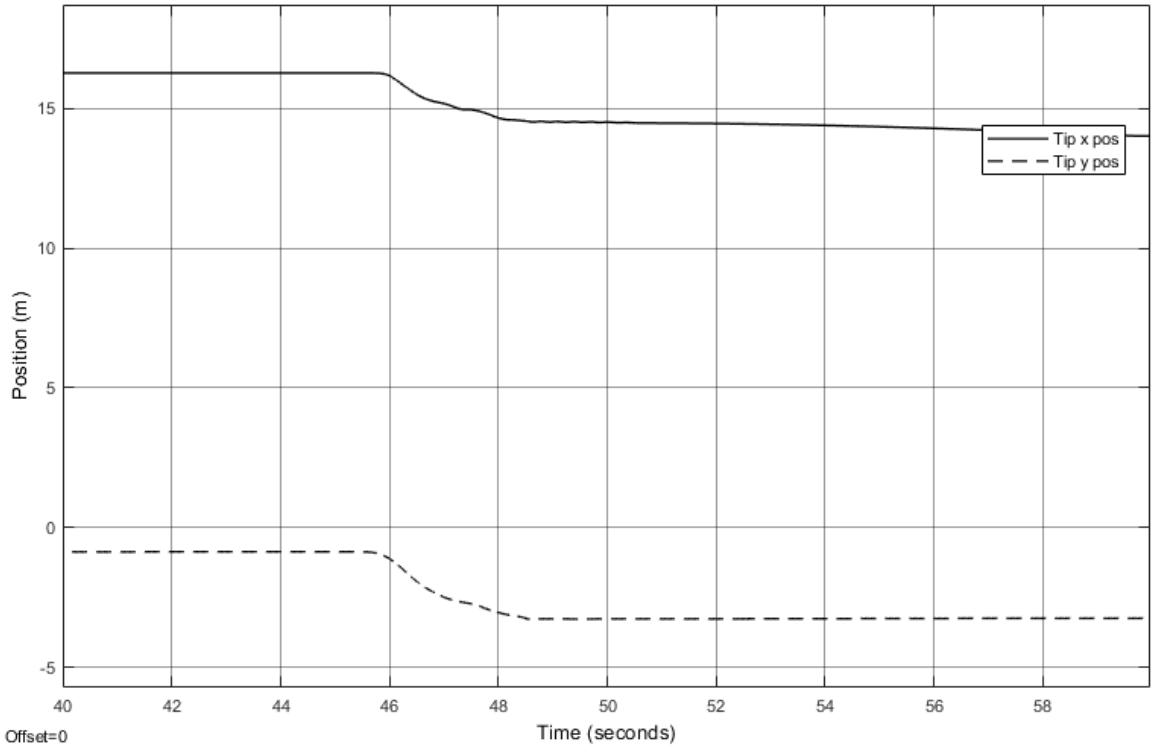

Figure 8.14. Tip position change with y-direction negative input

In figure 8.15 and 8.17 are the angular velocities of the two links and the solid line is the calculated value and dotted line the sensors feedback value. As can be seen that the boom link has no reaction to the initial negative velocity input however at 45.4 seconds in to the simulation the angular velocity jumps to extreme values and stabilizes over the next 4 seconds in which the tool has hit the ground and the velocity signal stops at 0. The calculated and occurring second link signals stay the same until the peak occurs. Figures 8.16 and 8.18 have the valve control signals and their change over the course of the time simulation. Notable difference is the thickest line which represents the load control valve. In figure 8.15 there is short amount of time where the system purely oscillates from 48 to 50 seconds which is caused by the bucket reaching the ground. The tip still moves in x-direction after touching

the ground. The same oscillation is also shown in the valve control voltage plot in figure 8.16.

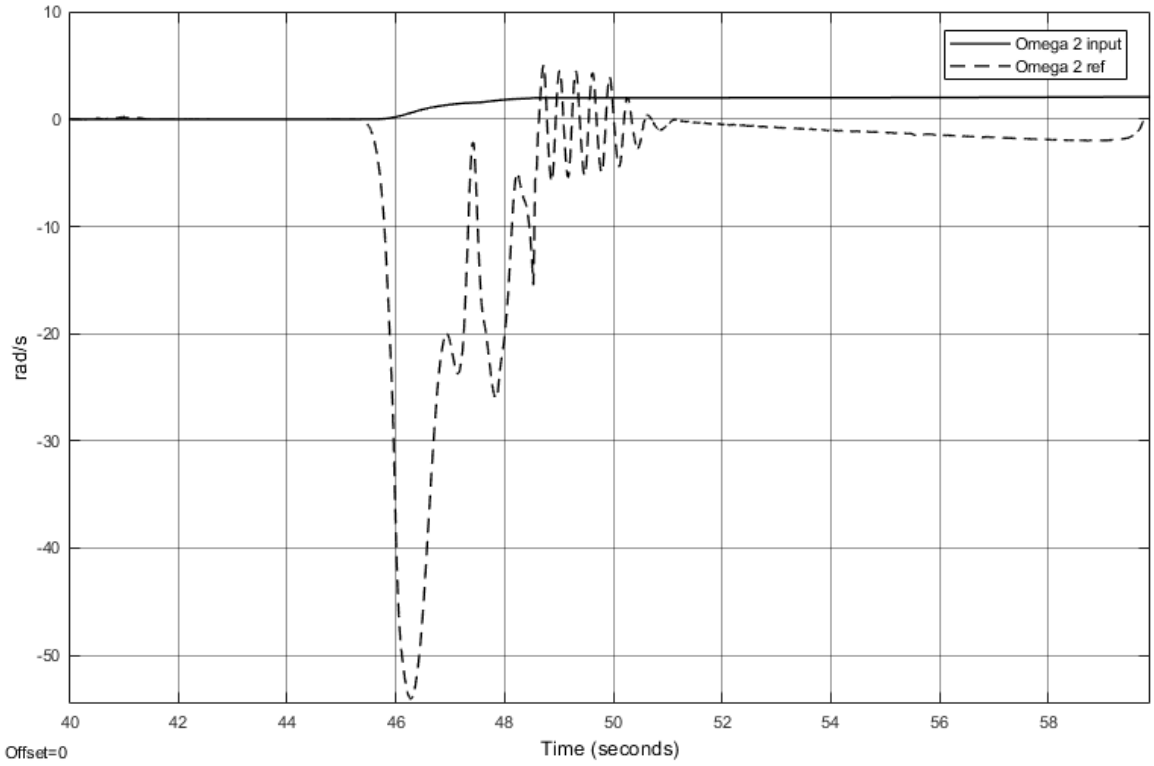

Figure 8.15. Second link calculated angular velocity and reference angular velocity

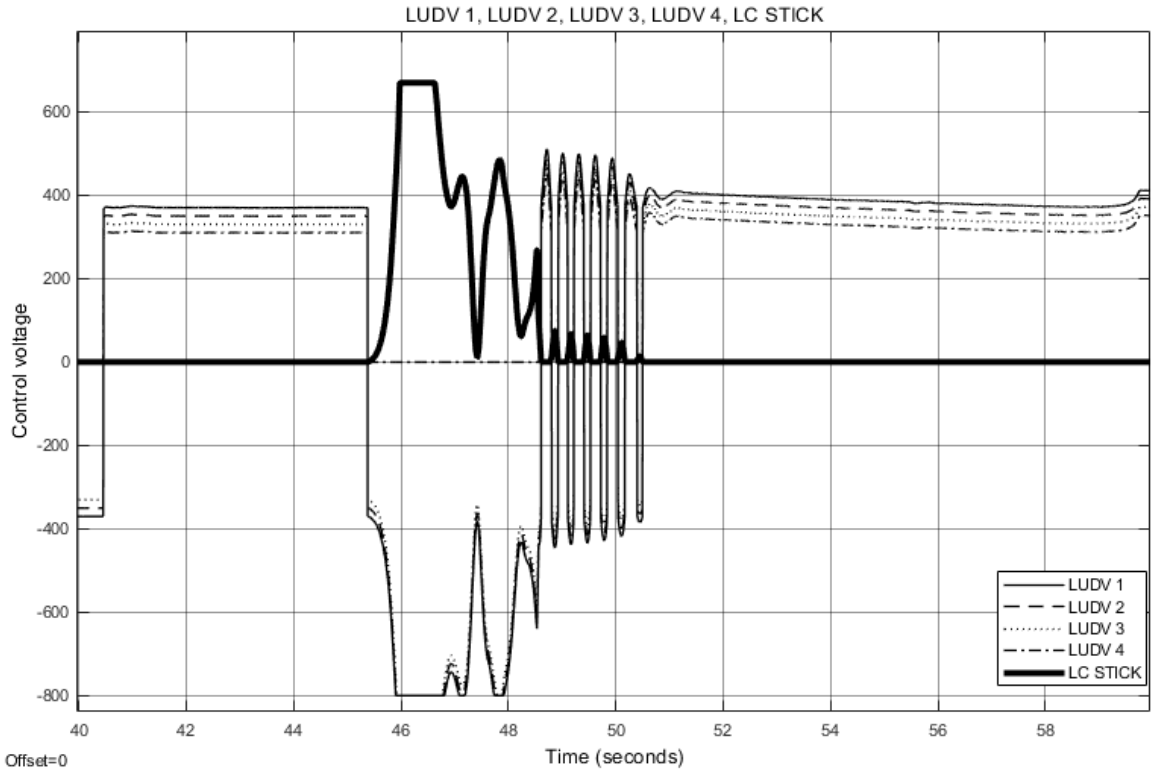

Figure 8.16. Valve control signals of second link valves

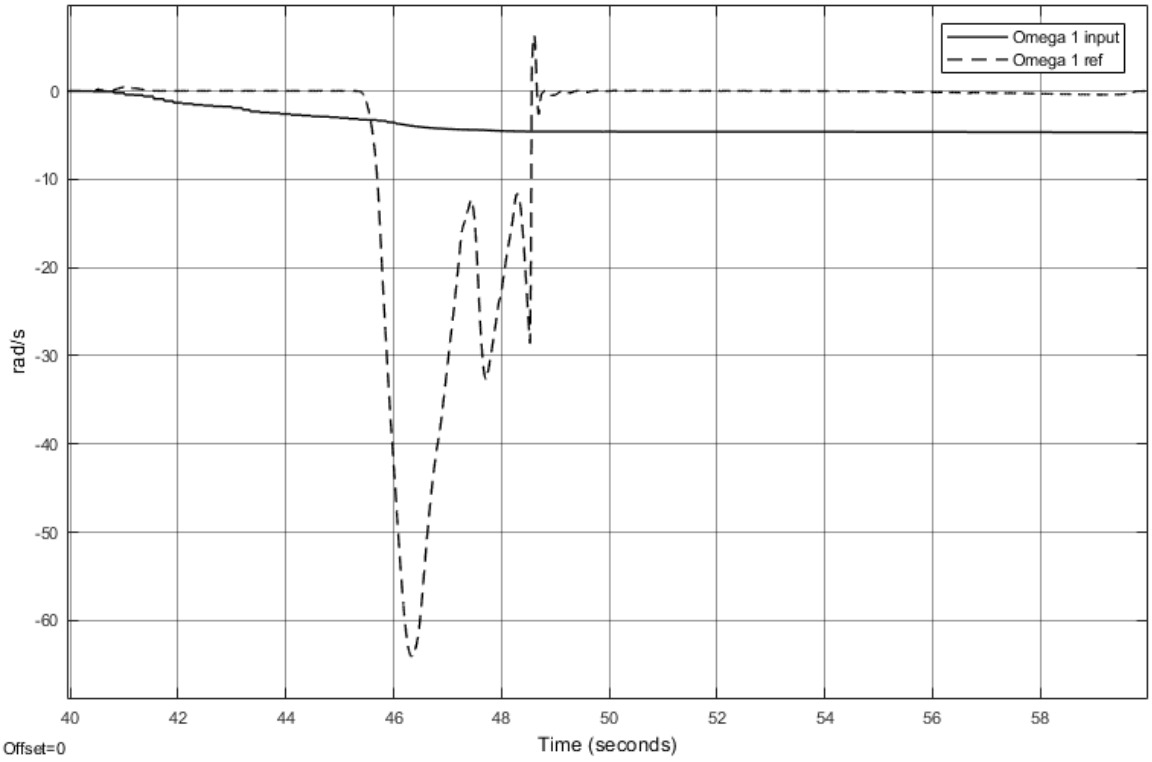

Figure 8.17. First link calculated angular velocity and reference angular velocity

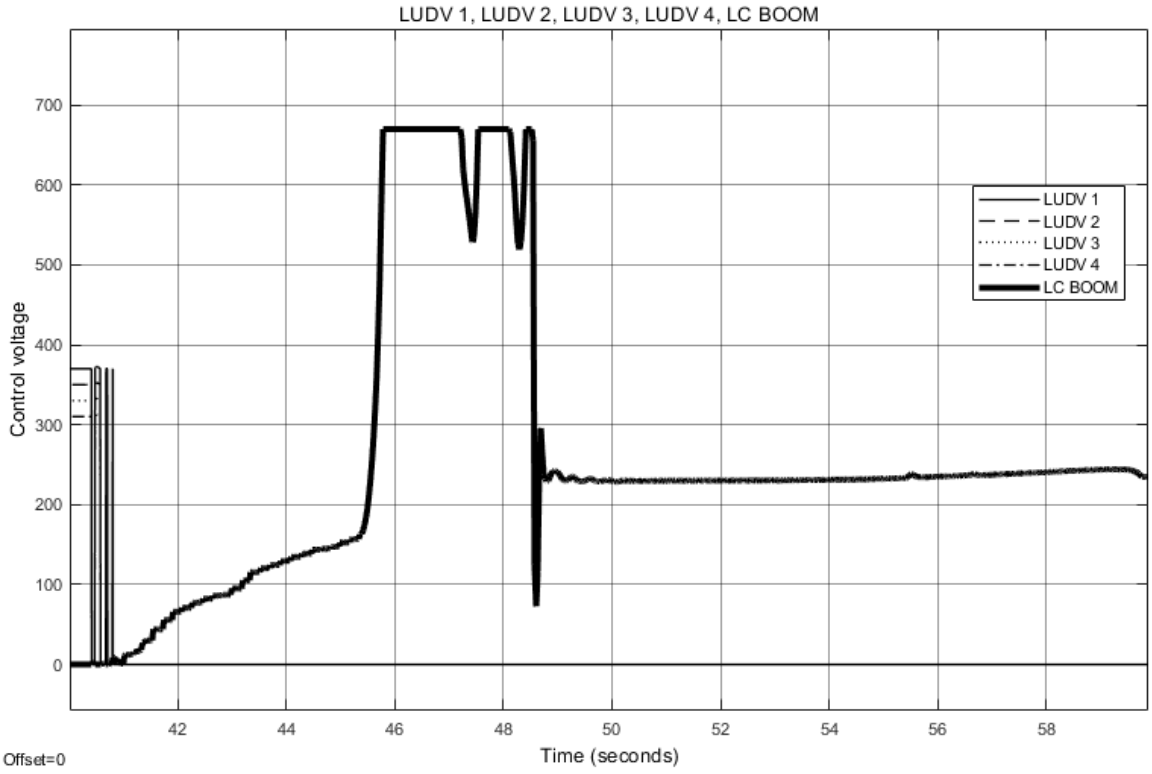

Figure 8.18. Valve control signals of first link valves

8.2.3 Positive X-direction

The third input given was to drive the tip in positive x-direction with maximum joystick input force from 40 seconds to 60 seconds in the simulation. Seen from the figure 8.19 below, where the solid line is the x-coordinate and dotted line the y-coordinate of the tip, the tip x-value changes from 16.20 meters to 18.23 meters and y-value from -1.08 to -0.64 meters before the time of 54.7 seconds where the system has an unexpected reaction dropping the tip to the ground after which the manipulator is still able to move to x-direction however stuck in the y-direction as the system is still giving negative y-direction control.

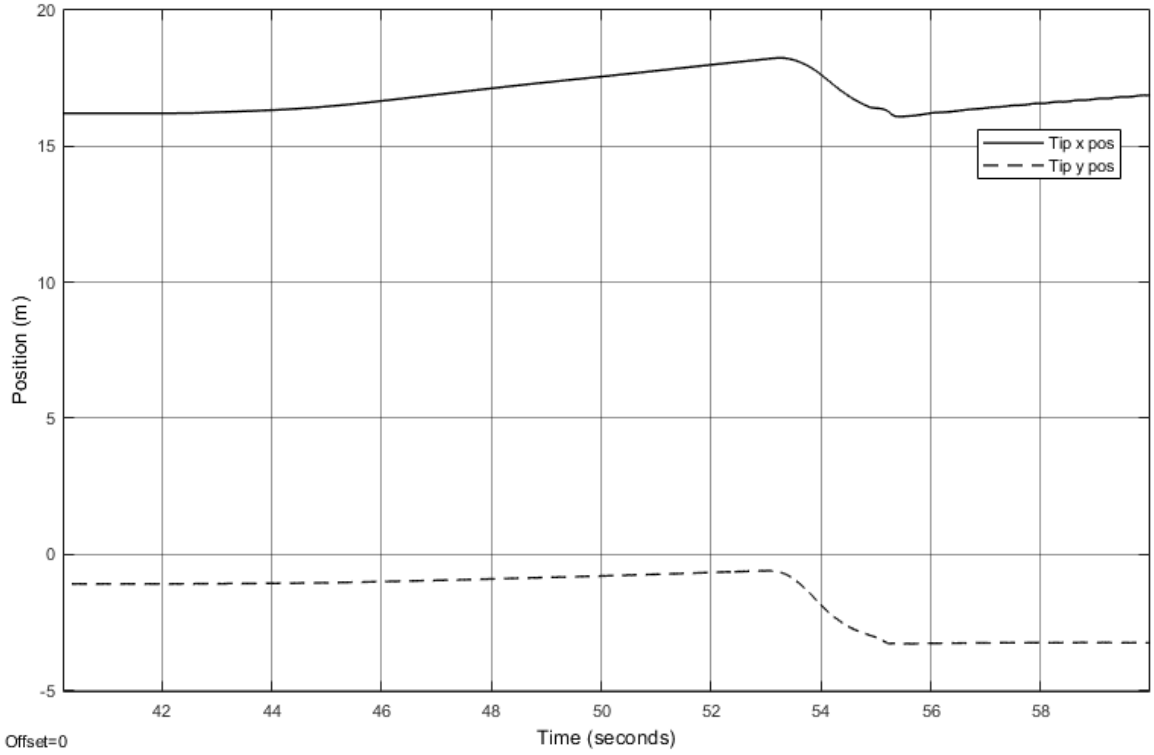

Figure 8.19. Tip position change with x-direction positive input

The drop that occurred during the simulation was unusual and required further investigation. The system was simulated for another 30 seconds as shown in figure 8.20 and the same behavior can be seen occurring regularly. The load control valve of the boom has a steady signal increase shown in figure 8.22 until the previously mentioned time point where the signal jumps to a point where the boom is allowed to fall down freely and the control of the

system is lost. Figure 8.20 shows that when the simulation is continued the effect occurs again at roughly 86 seconds.

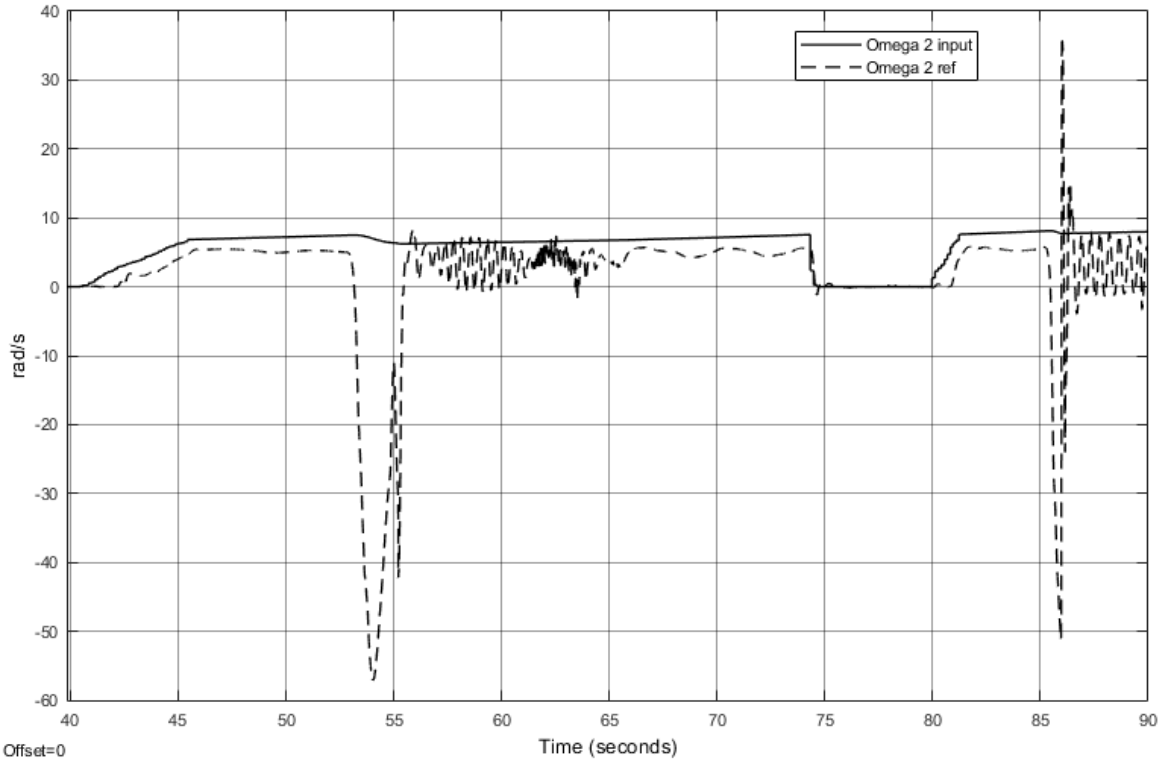

Figure 8.20. Loss of control occurs twice during simulation. First at 54.7 second and again at 86 seconds.

Figure 8.21 shows that the angular velocity input for the boom link was negative however based on the sensor data the system had little to no reaction to this nevertheless the load control valve was opened and linearly increased in the control values as seen in figure 8.22. Figure 8.23 shows the angular velocities of the stick link which follow the input signals however suffer from the major peak as explained before and start to oscillate towards the end of the simulation. The peak negative values also drive the valve control signals to be negative as shown in figure 8.24 which otherwise are not reaching the maximum values nevertheless the input is highest for that direction.

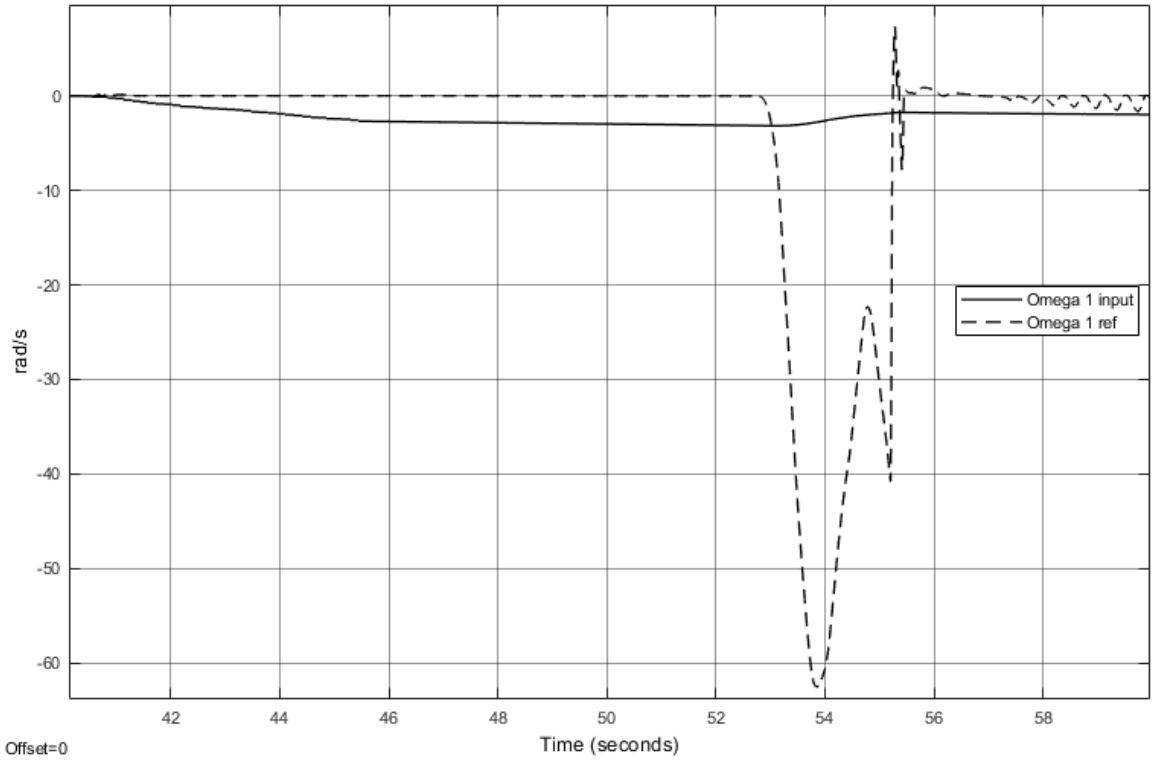

Figure 8.21. First link calculated angular velocity and reference angular velocity

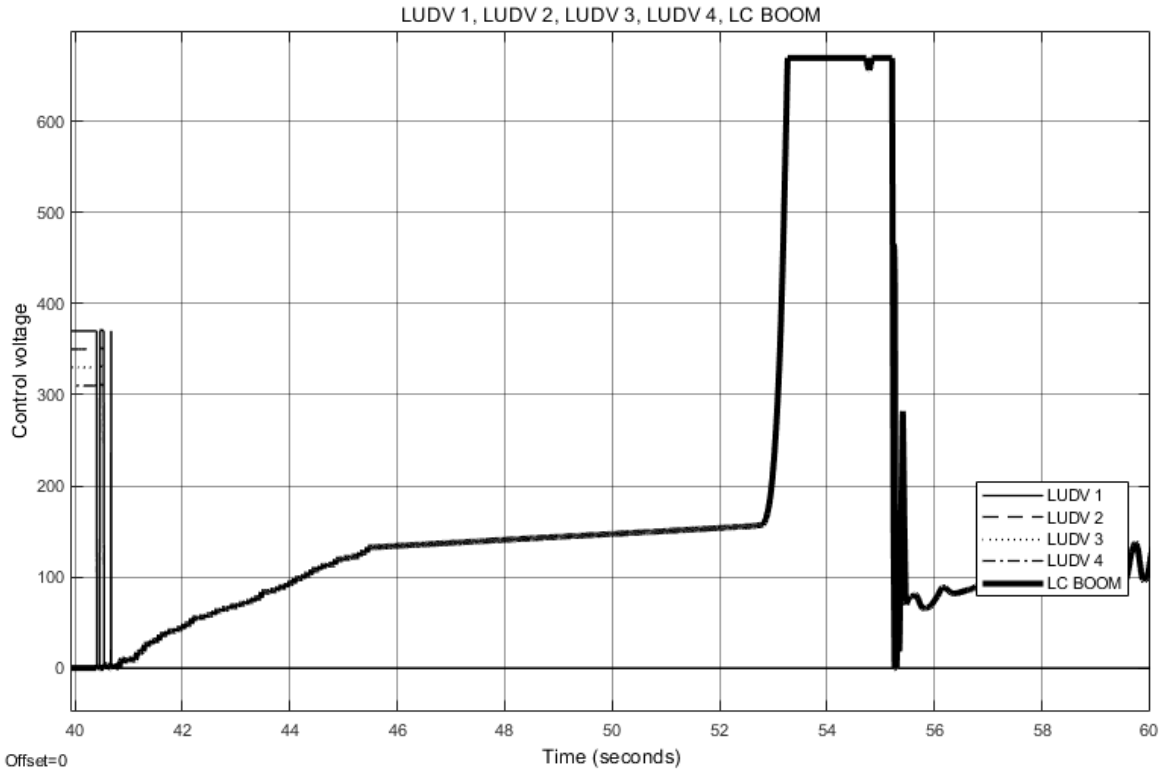

Figure 8.22. Valve control signals of first link valves

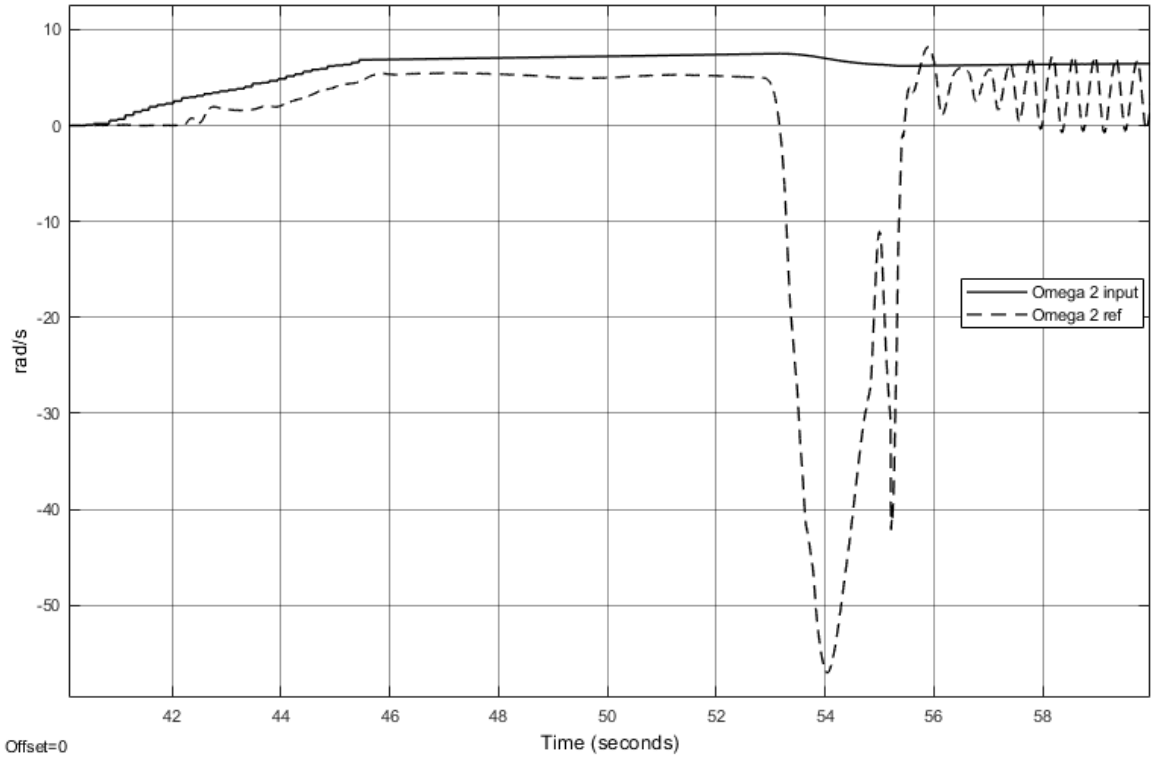

Figure 8.23. Second link calculated angular velocity and reference angular velocity

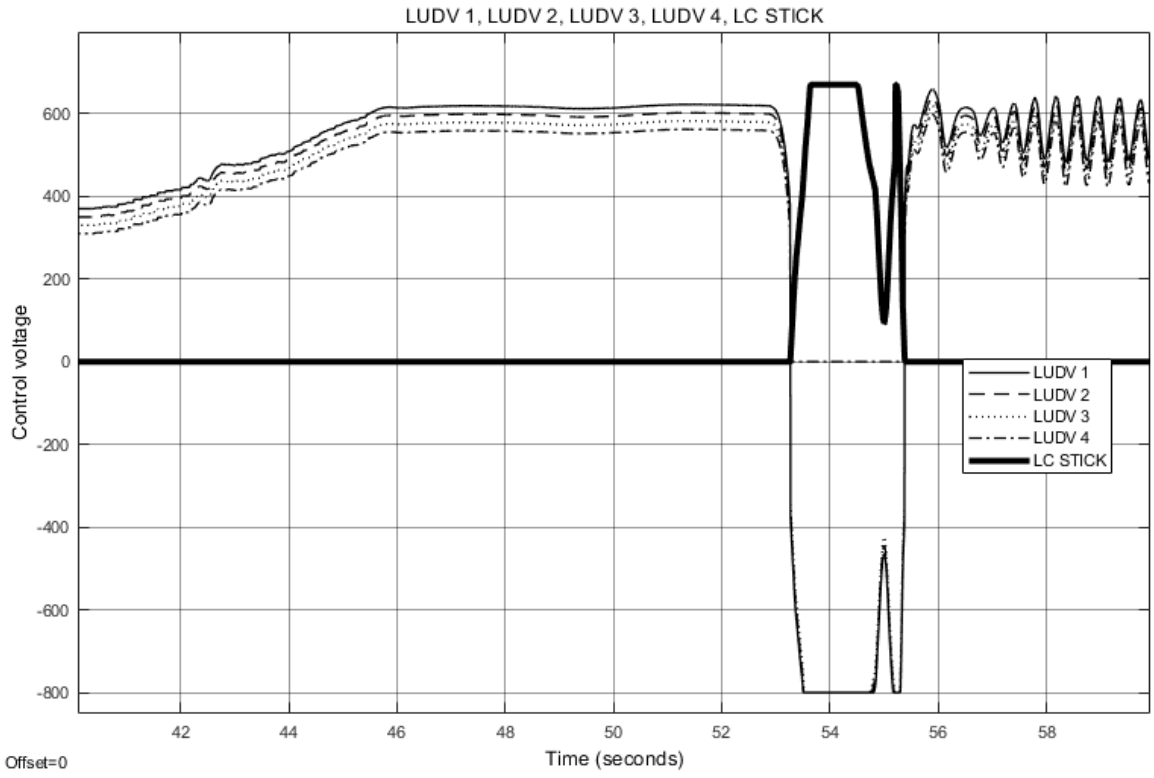

Figure 8.24. Valve control signals of second link valves

8.2.4 Negative X-direction

The last input given was to drive the tip in negative x-direction with maximum joystick input force from 20 seconds to 40 seconds in the simulation. Seen from the figure 8.25 below, where the solid line is the x-coordinate and dotted line the y-coordinate of the tip, the tip x-value changes from 16.27 meters to 8.24 meters and y-value from -0.13 to 0.98. This last direction has by far the largest displacement in the tip positions compared to any other tests done.

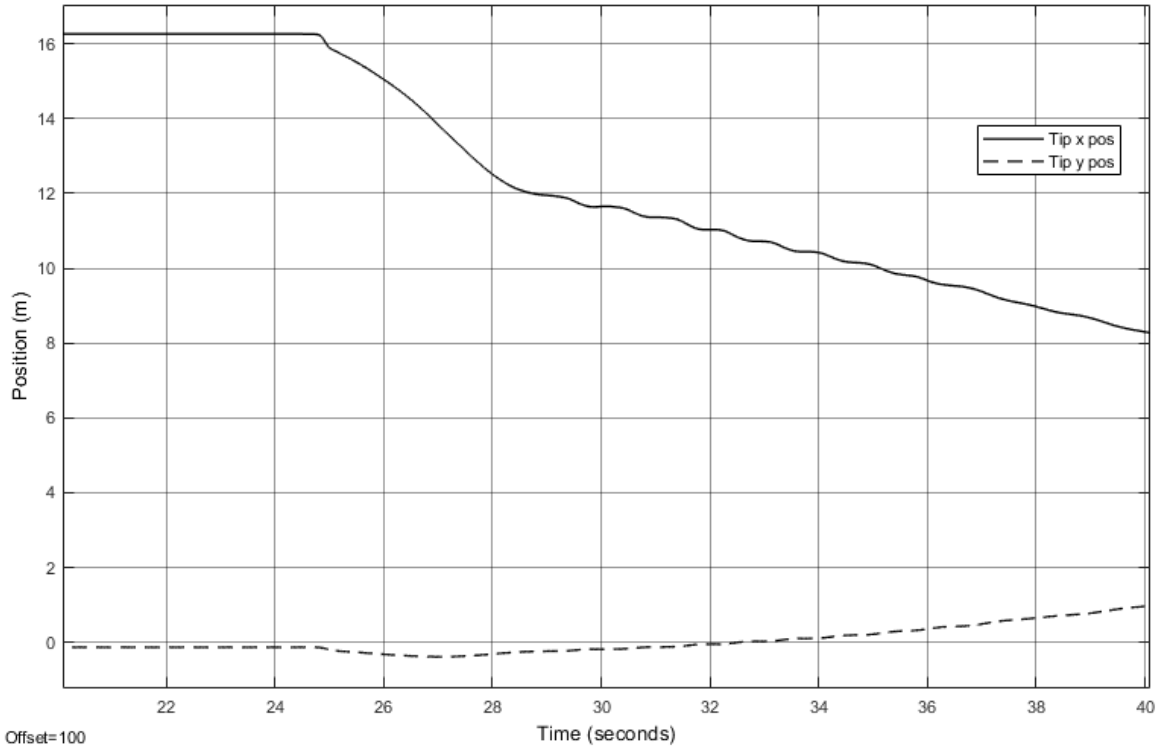

Figure 8.25. Tip position change with x-direction negative input

Figure 8.26 shows the boom link velocities and the feedback signals are not reaching the input values until at 24.6 seconds there is a massive overshoot in the boom velocity signal from the sensors which causes the system to also undershoot as counter reaction. The boom valve signals also show the same symptoms and are displayed in figure 8.27. The second link feedback values are oscillating throughout the simulation time while trying to follow the input signal. This causes the manipulator tip to move remarkably during the simulation and the control signal is overshooting the desired values as shown in figure 8.28. The same

reaction can be seen in the valve control signals in figure 8.29 where the signals are at maximum values for a large part of the simulation.

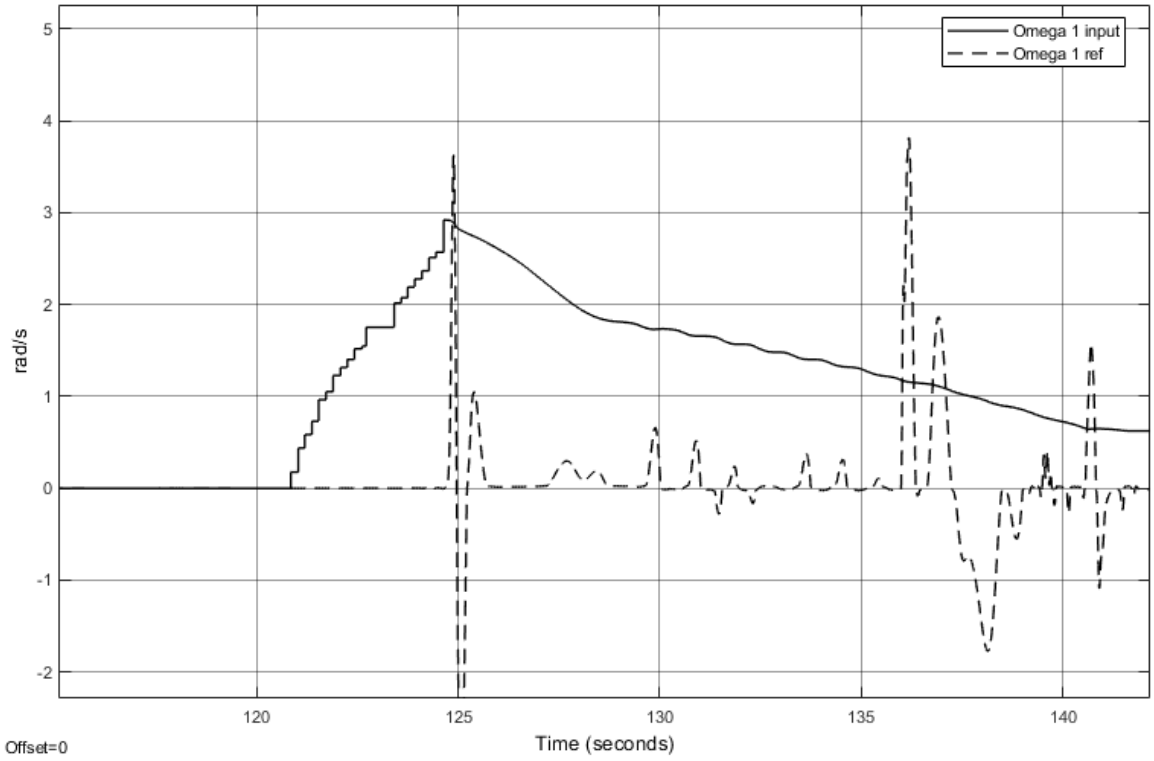

Figure 8.26. First link calculated angular velocity and reference angular velocity

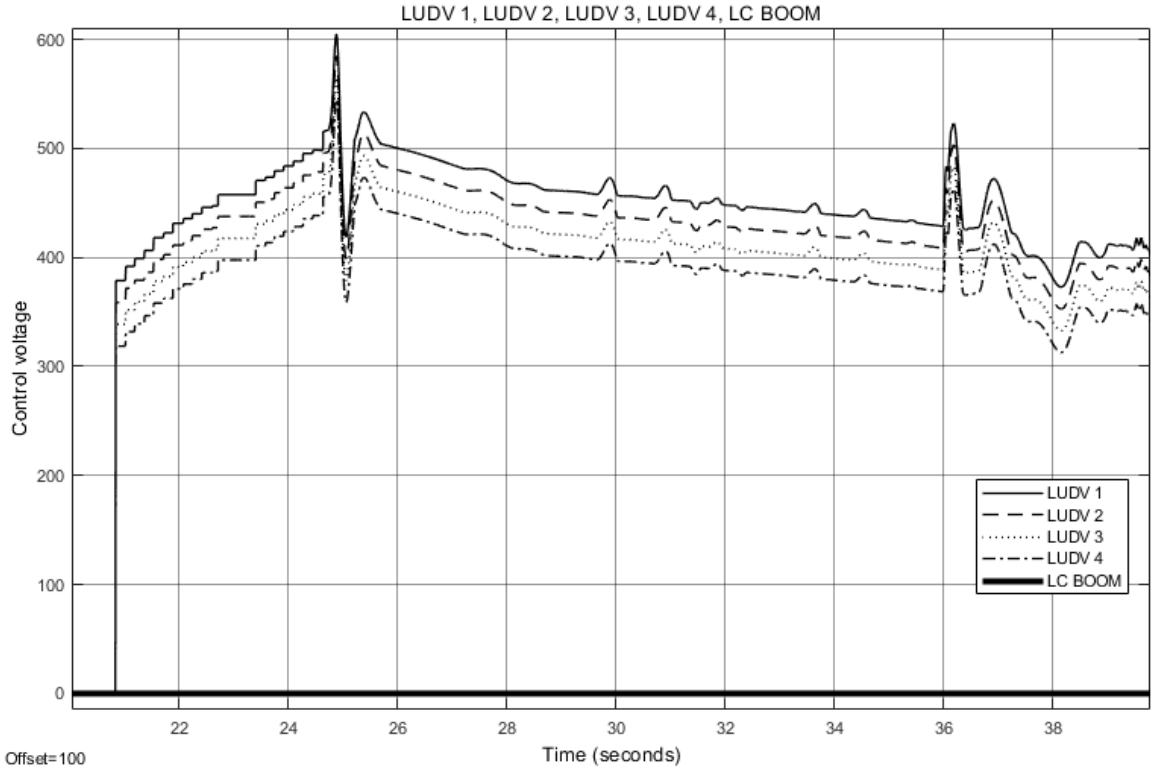

Figure 8.27. Valve control signals of first link valves

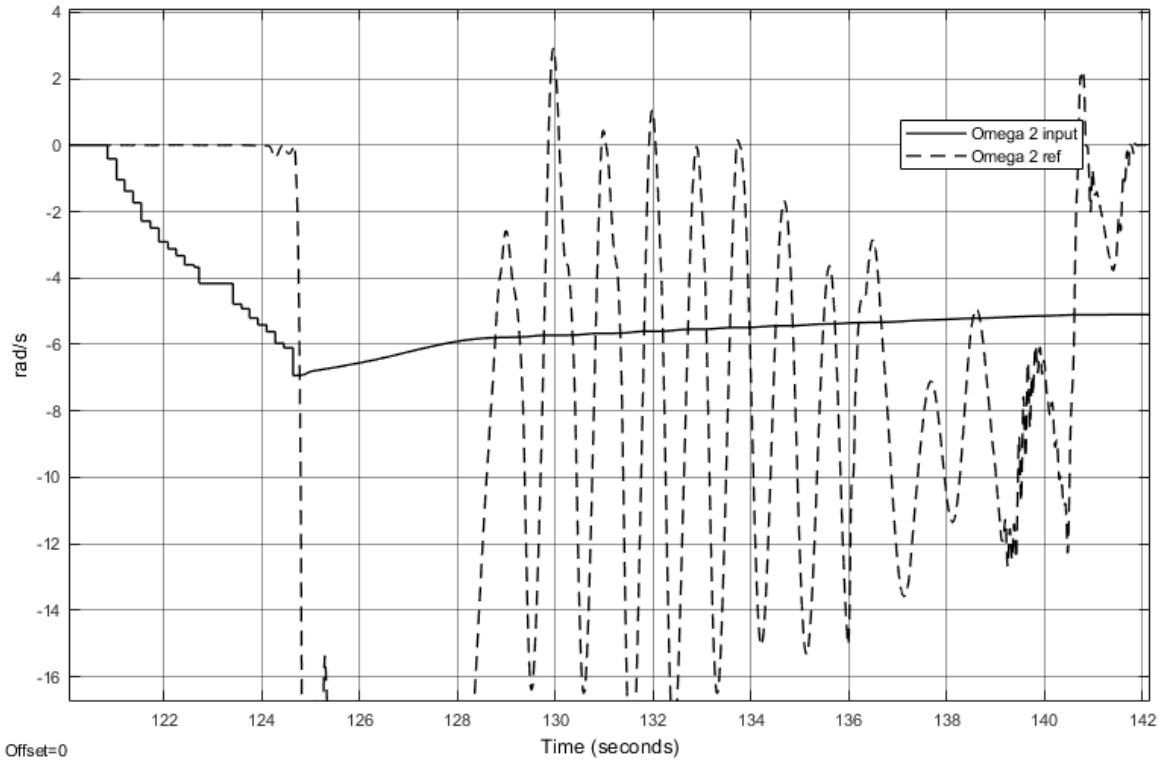

Figure 8.28. Second link calculated angular velocity and reference angular velocity

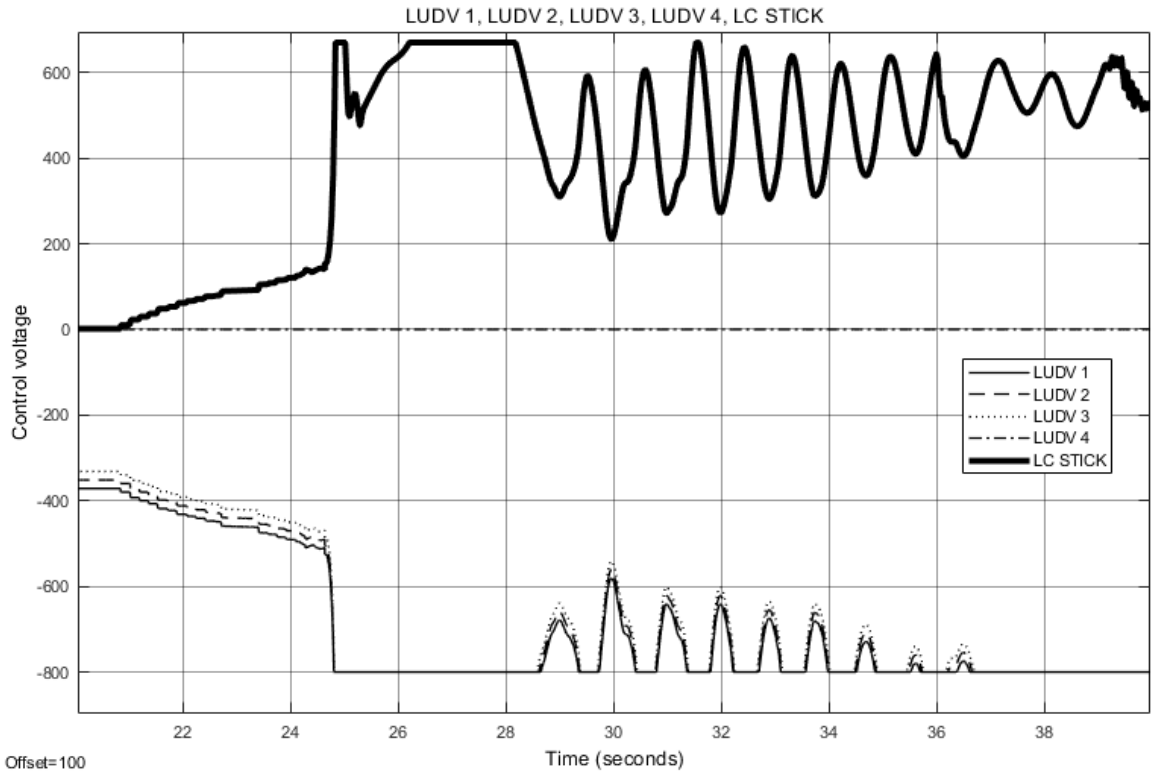

Figure 8.29. Valve control signals of second link valves,

8.3 Mantsinen control system

The Mantsinen control system was tested the same way as the two developed control systems and tests performed were merely done to obtain benchmark results of how much the tip position change with the Mantsinen control method. Each of the four directions were driven with maximum input of 250 given as a step input for the machine for 20 seconds and the results are shown in the figures 8.30 to 8.33 where the solid line in the figures shows the y-coordinate change and dotted line the x-coordinate change.

Figure 8.30 below shows that when the swing link is driven into positive direction, the tip x-value changes from 16.17 meters to 20.78 meters and y-value from -1.1 to 0.63.

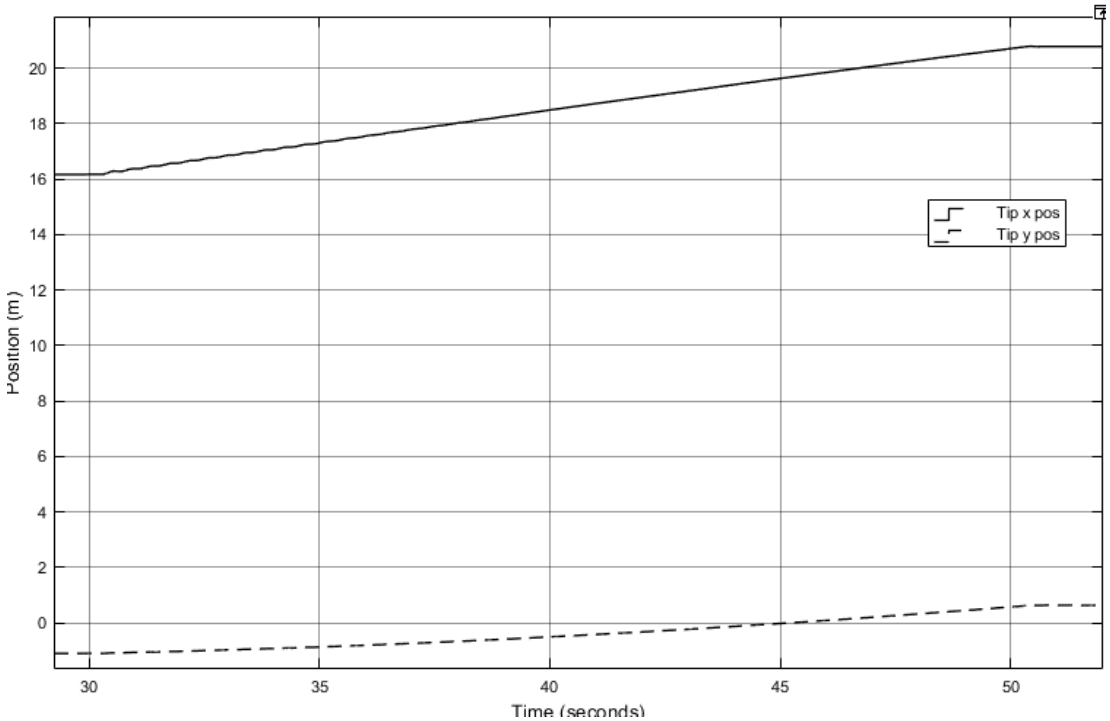

Figure 8.30. Mantsinen control system driven in positive x-direction

Figure 8.31 below shows that when the swing link is driven into negative direction, the tip x-value changes from 20.48 meters to 9.642 meters and y-value from -1.76 to -1.42.

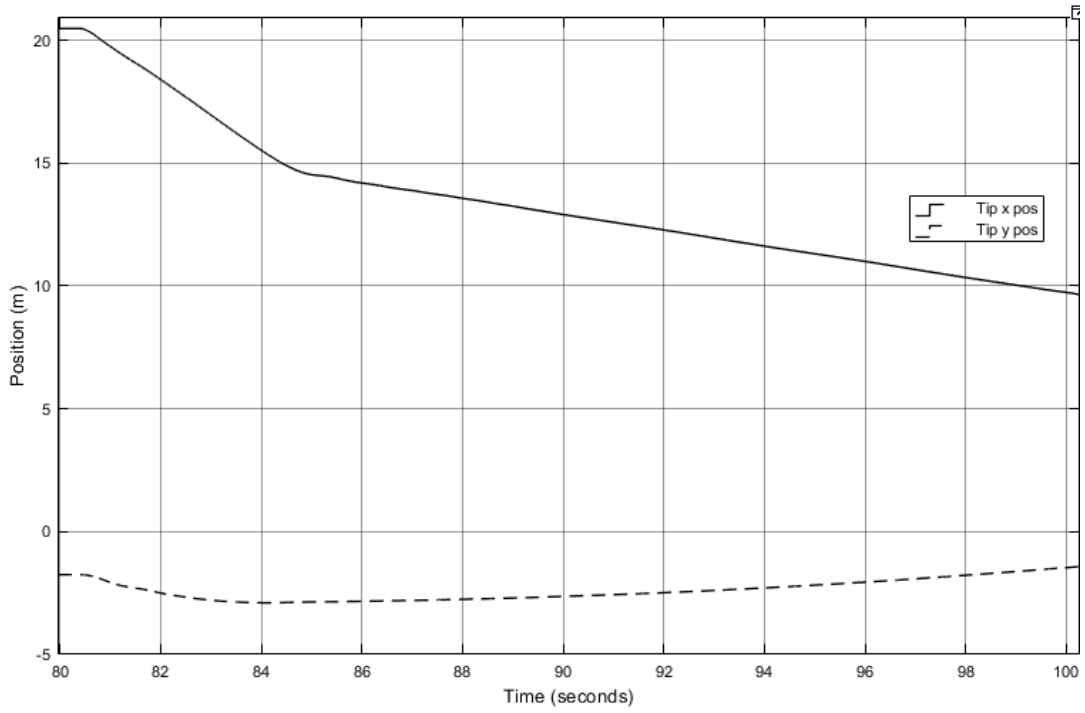

Figure 8.31. Mantsinen control system driven in negative x-direction

Figure 8.32 shows that when the boom link is driven into positive direction, the tip x-value changes from 15.5 meters to 16.17 meters and y-value from -3.27 to -1.10.

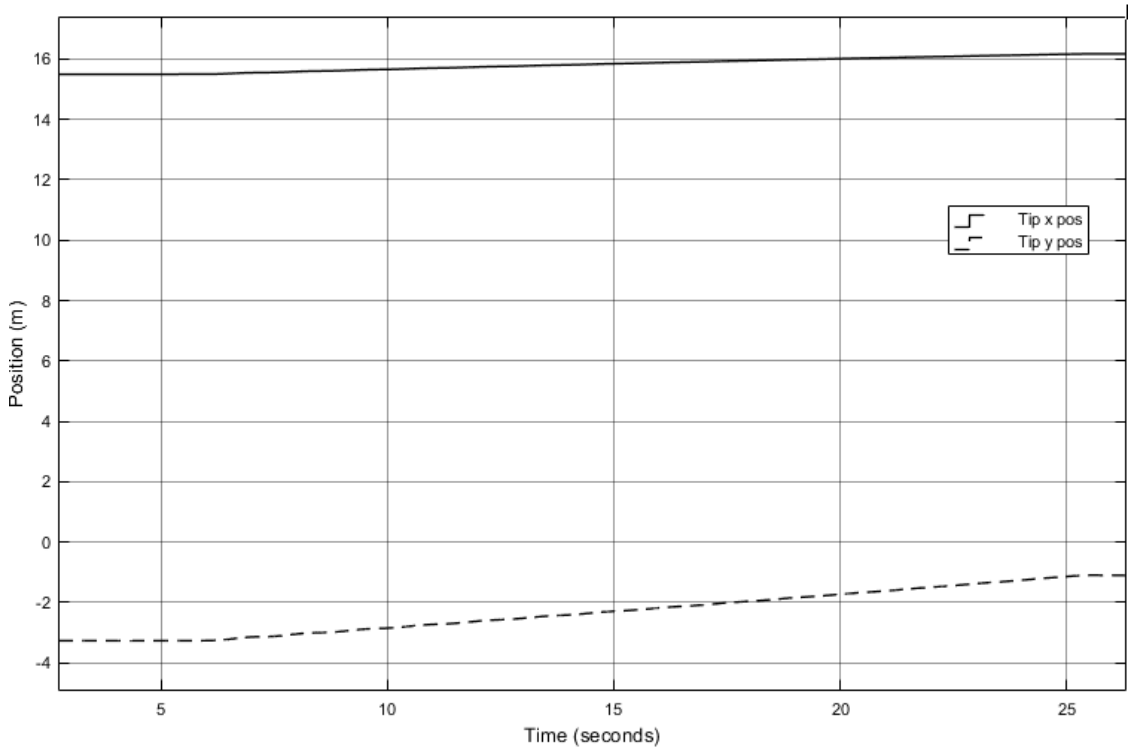

Figure 8.32. Mantsinen control system driven in positive y-direction

Figure 8.33 shows that when the boom link is driven into negative direction, the tip x-value changes from 20.78 meters to 20.09 meters and y-value from 0.63 to -3.28. At roughly 58.4 seconds in the simulation the bucket hits the ground and all movement stops.

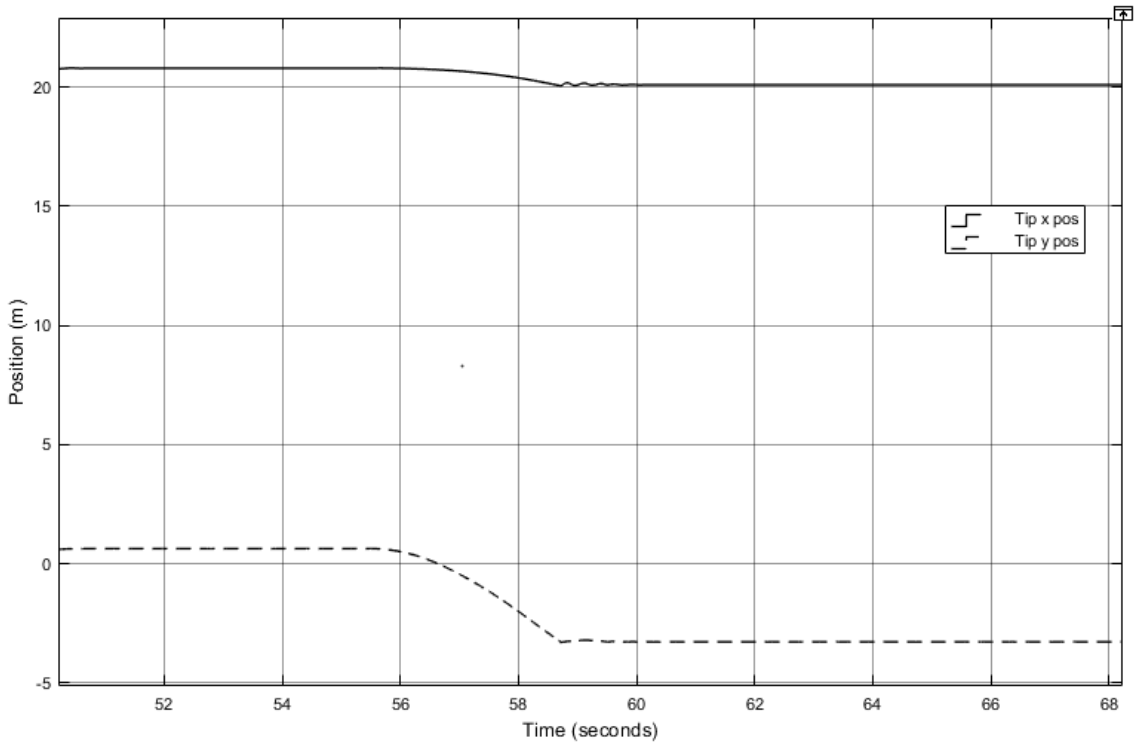

Figure 8.33. Mantsinen control system driven in negative y-direction

8.4 Result comparison

This chapter gathers the previously shown results of the manipulator control tests and shows in one simplified form a comparison between the open and closed loop control system results and makes a comparison which of them performed better in the specific tasks. The data of the test is shown in the table 8.1 below where the right side shows the operating direction and which coordinate is in question and on the top level there is the indication which system is being used and the values shown are changes in tip position. In the ideal situation when driven into x- or y-direction the other coordinate should stay in the same position. The values shown in table are the coordinate changes in the defined coordinate direction.

Table 8.1. Changes in coordinate values when driving the machine into specified directions. Values shown are in meters.

Parameter		Open loop	Closed loop	Mantsinen
Error	X	2,08	0.57	0.67
Positive	Y	1,75	1.62	2.17
Error	X	-4.15	-2.26	0.69
Negative	Y	-1.23	-2.37	-2.65
Positive	X	3,26	2.03	4.61
Error	Y	1,33	0.44	0.47
Negative	X	-0.51	-8.03	-10.84
Error	Y	-0.33	0.85	0.34

When comparing the errors between the boom tip control, it is easy to notice that the positive Y closed loop system has smaller error in x direction than open loop while the same occurs also in negative y direction. In the x-direction the closed loop system has also smaller error than the open loop system which then can be concluded that the closed loop system is more accurate than the open loop system which was to be expected. The closed loop system has similar performance to the Mantsinen control system however it has greater inaccuracy than the Mantsinen control system.

9 DISCUSSION

The open loop system is more complicated than the closed loop system and requires more calculations to obtain the correct values for the input signals. Less time was spent in fine tuning this control method which shows that it has some unlock potential still in it. In order to maximize the effectiveness of the open loop system the mathematical side should be double checked and all the kinematics should be verified. The current model has a system which checks the given direction of the actuator speed and uses the maximum actuator speed values to set the valve control percentages however, this system could be improved by running the calculations with all the possible values of the material handler so that the real maximum and minimum values for each actuator speed could be found in each situation and then based on the input signal, those values could be used to create the actuator control voltages. As can be seen in table 8.1, control in negative x-direction yielded barely any movement on the tip whereas the negative y-direction had much bigger impact on the tip position.

What is also notable is that the velocity directions in X-direction are the same for both open and closed loop system however with the Y-direction the case is not the same. In open system positive Y-direction yields both control signals as positive however with closed system the stick signal starts as negative however continues change towards positive and increase steadily until simulation is stopped. Same occurs in the negative Y-directions as in open system both are negative however in closed system the stick signal is positive. This is probably due to error in the code where the angle sensors data from stick is negative when coming in from Mevea and there is error in the sign change in the code. This error does compromise the results of the Y-direction slightly.

With the obtained results shown in previous chapter it is clear that the closed loop system has a better performance however suffers from some unexpected signal changes that hurt the performance of the system. These are caused when the Jacobian matrix gives a negative y-direction signal. As the machine operating principle is described previously the y-direction downwards control is done with only load control valve which allows gravity to pull down the manipulator arm and charge the HybriLift hybrid hydraulic battery. This design is likely causing the issues as the controllers K_i component reacts to the error between the desired

velocity and the occurring velocity which causes the controller values to spike up at certain moment in time. Other possibility is that there is commination problem with the two software and a bit or two is lost however the first some seems more plausible. With the stick link the negative direction control has 3 of the 4 control valves operating plus the load control valve which then gives a better response to negative velocity guides. Accuracy for some of the test done on the closed loop system were decent as the movement of the other coordinate that was not controlled, stayed close to the original tip position values.

During the work, the goals were slightly changed however nevertheless results of machine accuracy were obtained and these results can be reproduced easily. Developing a satisfactory coordinate system takes time and patience as can be seen when the coordinate control system results are compared with the Mantsinen control values. Mantsinen has achieved high accuracy by their own control system and improving from that is a challenge and as previously mentioned machine technical specifications may cause problems.

10 CONCLUSION

The goals and background of the work was set and a literature review was conducted on the importance of the driver and the different methods to implement manipulator control that would lead to full or semi-automation of the process. In this work a two different coordinate control system were created using the mathematical equations shown in chapter 3 and the principle idea of each control system was shown in chapter 5 and customized to work with the machine properties.

It was found out that the closed loop system works better than the open loop system which was to be expected however both control systems need more optimization to reach their full potential. Some characteristics of the material handler were limitations to obtain better results and some suggestions are given below on how to further develop this research project.

As described in the discussion part, the load control valve causes issues with the control of the system and due to the design choice of keeping the control as simple as possible there was not realistic chances to obtain the controller tuning to match the desired accuracy and the open loop system suffered from this same design principle. In order to improve the results obtained, another controller should be introduced to the boom link load control valve without the K_i component to see if it would perform better and re-tune the two other controllers. More experimenting with the amplification is necessary and to have the code running in a simulator to examine how well it would perform with real joysticks as input devices. It is recommended that the simulator tests would be performed with a someone from Mantsinen who truly understands all the complex functions of the machine as it has a complex design.

LIST OF REFERENCES

Bureau of Labor Statistics, U.S. Department of Labor. [2018] Occupational Outlook Handbook, Material Moving Machine Operators. [Webpage]. [Accessed 12.06.2018]. Available at: https://www.bls.gov/ooh/transportation-and-material-moving/material-moving-machine-operators.htm

Craig, J. J., 2005. Introduction to robotics: mechanics and control (Vol. 3). Upper Saddle River: Pearson Prentice Hall. 408 p.

Haga, M., Hiroshi, W. and Fujishima, K., 2001. Digging control system for hydraulic excavator. Mechatronics, 11(6), pp.665-676.

Jazar, R.N., 2010. Theory of applied robotics: kinematics, dynamics, and control. Springer Science & Business Media. 883 p.

Jenkins, H.E. 2014. Tuning for PID Controllers. Lecture notes. EGR 386 Feedback Control. Mercer University. [Accessed 25.8.2018]. Available at: http://faculty.mercer.edu/jenkins_he/documents/TuningforPIDControllers.pdf.

Karpenko, M. and Sepehri, N., 2010. On quantitative feedback design for robust position control of hydraulic actuators. Control Engineering Practice, *18*(3), pp.289-299.

Kim, J., Lee, S.S., Seo, J. and Kamat, V.R., 2018. Modular data communication methods for a robotic excavator. Automation in Construction, 90, pp.166-177.

Kim, S., Park, J., Kang, S., Kim, P.Y. and Kim, H.J., 2018. A Robust Control Approach for Hydraulic Excavators Using μ-synthesis. International Journal of Control, Automation and Systems, pp.1-14.

Koivumäki, J. and Mattila, J., 2017. Stability-guaranteed impedance control of hydraulic robotic manipulators. IEEE/ASME Transactions on Mechatronics, 22(2), pp.601-612.

Lee, C.S., Bae, J. and Hong, D., 2013. Contour control for leveling work with robotic excavator. International Journal of Precision Engineering and Manufacturing, 14(12), pp.2055-2060.

Lindroos, O., Ringdahl, O., La Hera, P., Hohnloser, P. and Hellström, T.H., 2015. Estimating the Position of the Harvester Head–a Key Step towards the Precision Forestry of the Future?. Croatian Journal of Forest Engineering: Journal for Theory and Application of Forestry Engineering, 36(2), pp.147-164.

Manner, J., Gelin, O., Mörk, A. and Englund, M., 2017. Forwarder crane's boom tip control system and beginner-level operators. Silva Fennica, 51(2).

Mantsinen Group Ltd Oy. 2018. Mantsinen 200. [Webpage]. [Accessed 12.06.2018]. Available at: http://www.mantsinen.com/files/file/Mantsinen_200_ENG.pdf.

MathWorks. 2018. [Webpage]. [Accessed 16.8.2018]. Available at: https://se.mathworks.com/matlabcentral/fileexchange/58257-unified-tuning-of-pid-load-frequency-controller-for-multi-area-power-systems-via-imc.

Mevea Ltd. 2018. Software for real-time simulation. [Webpage]. [Accessed 6.8.2018]. Available at: https://mevea.com/solutions/software/.

Mu, B. 1996. System Modelling, Identification and Coordinated Control Design for an Articulated Forestry Machine (Doctoral dissertation, McGill University).

Patel, B.P. and Prajapati, J.M., 2013. Kinematics of mini hydraulic backhoe excavator–part II. International Journal of Mechanisms and Robotic Systems, 1(4), pp.261-282.

Purfürst, F.T. 2010. Learning curves of harvester operators. Croatian Journal of Forest Engineering: Journal for Theory and Application of Forestry Engineering, 31(2), pp.89-97.

Rabie, M.G., 2009. Fluid power engineering (Vol. 28). New York, NY, USA: McGraw-Hill.

Rudolfsen, M.H., Aune, T.N., Auklend, O., Aarland, L.T. and Ruderman, M., 2017, July. Identification and control design for path tracking of hydraulic loader crane. In *Advanced* Intelligent Mechatronics (AIM), 2017 IEEE International Conference on (pp. 565-570). IEEE.

SFS-ISO 10968. 2017. Earth-moving machinery. Operator's controls. Helsinki: Suomen Standardisoimisliitto SFS ry. 18 p.

Shen, W., Jiang, J., Su, X. and Karimi, H.R., 2015. Control strategy analysis of the hydraulic hybrid excavator. Journal of the Franklin Institute, 352(2), pp.541-561.

Wang, T., Wang, Q. and Lin, T., 2013. Improvement of boom control performance for hybrid hydraulic excavator with potential energy recovery. Automation in Construction, 30, pp.161-169.

Westerberg, S., 2014. Semi-automating forestry machines: Motion planning, system integration, and human-machine interaction (Doctoral dissertation, Umeå Universitet).
Wonohadidjojo, D.M., Kothapalli, G. and Hassan, M.Y., 2013. Position control of electro-hydraulic actuator system using fuzzy logic controller optimized by particle swarm optimization. International Journal of Automation and Computing, 10(3), pp.181-193.

Yao, J., Jiao, Z. and Ma, D., 2015. A practical nonlinear adaptive control of hydraulic servomechanisms with periodic-like disturbances. IEEE/ASME Transactions on Mechatronics, 20(6), pp.2752-2760.

Ye, Y., Yin, C.B., Gong, Y. and Zhou, J.J., 2017. Position control of nonlinear hydraulic system using an improved PSO based PID controller. Mechanical Systems and Signal Processing, 83, pp.241-259.

Yoon, J. and Manurung, A., 2010. Development of an intuitive user interface for a hydraulic backhoe. Automation in Construction, 19(6), pp.779-790.

Åström, K.J. and Hägglund, T., 1995. PID controllers: theory, design, and tuning (Vol. 2). Research Triangle Park, NC: Instrument society of America.

Figures A.3.1 to A.3.2 show the open and closed loop models in Simulink and their structural differences

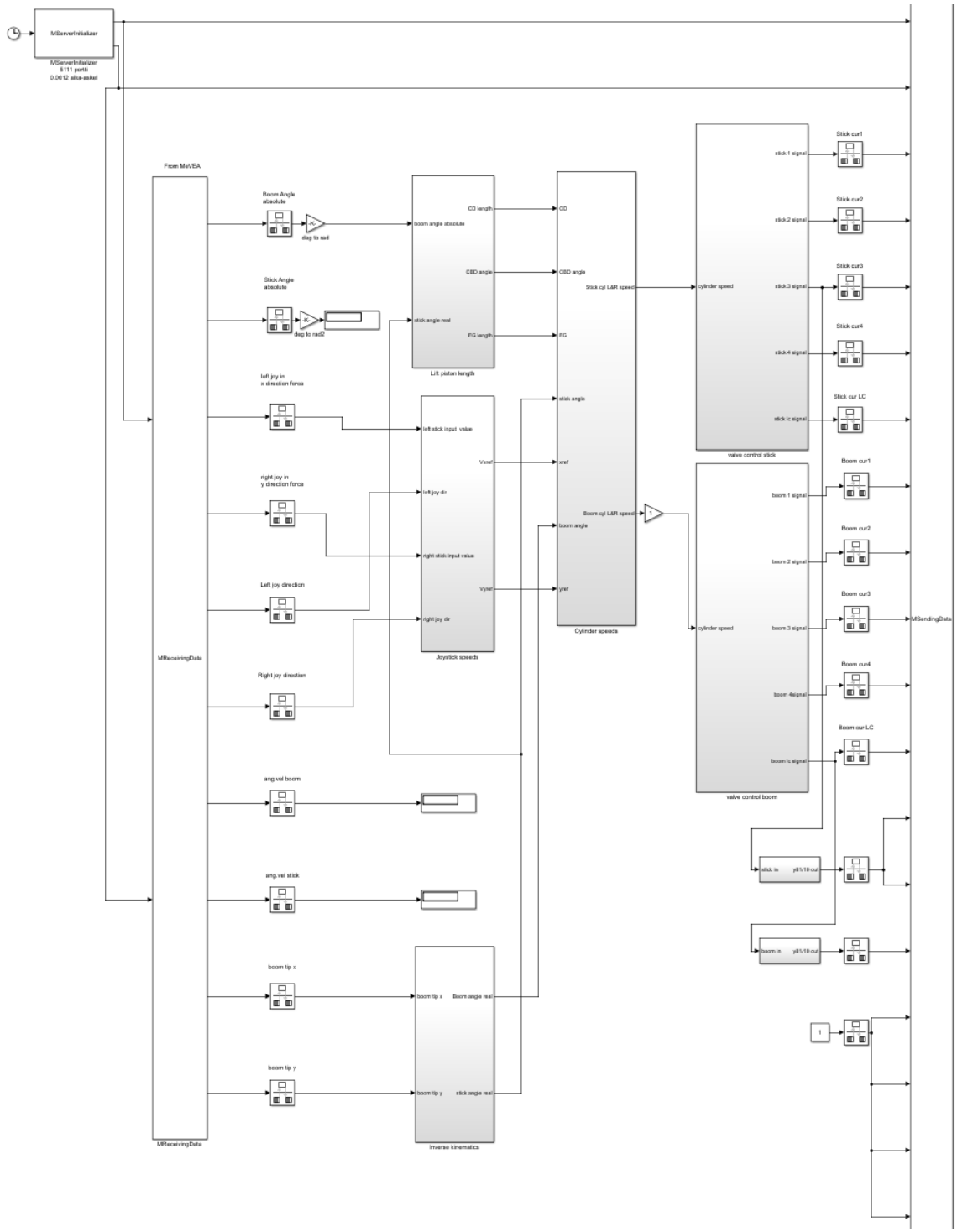

Figure A.1.1. Open loop Simulink model complete view

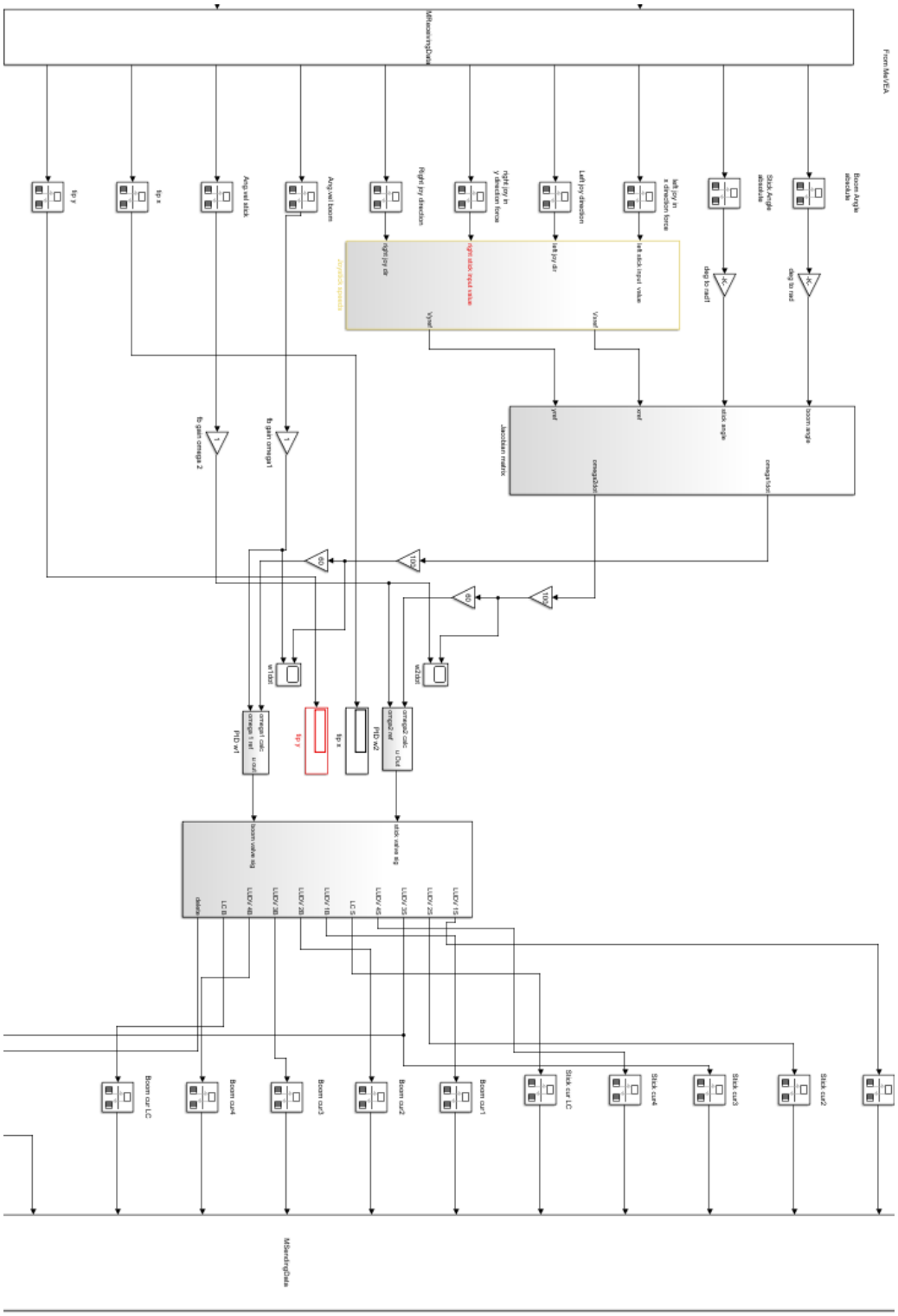

Figure A.1.2. Closed loop Simulink model complete view

```
close all
clear
clc

syms t1 t2 a1 a2 a3 dd2 w1dot w2dot w3dot w4dot xref yref;

d2=2.309;
L2=15.506;
L3=12;
L1=1.4;

%forward kinematics

A01=[cos(t1) -sin(t1) 0; sin(t1) cos(t1) 0; 0 0 1];
A12=[cos(t2) -sin(t2) a2; sin(t2) cos(t2) 0; 0 0 1];
A23=[0 0 a3; 0 0 0; 0 0 1];

%P0D=(A01*A12*A23)*P4D=A03*P3D
P3D=[a1 dd2 1];
A03=A01*A12*A23;
P0D=A03*transpose(P3D);
P0Dn=[a2*cos(t1)+a3*cos(t1+t2); a2*sin(t1)+a3*sin(t1+t2); 1];
x=P0Dn(1,1)+a1;
y=P0Dn(2,1)+dd2;
z=P0Dn(3,1);

AP=[x;
    y;
    z];

%velocity
v33=[a2*sin(t1)*w1dot;
    a2*cos(t2)*w1dot+a3*(w1dot+w2dot);
    0];
v03=[-a2*sin(t1)*w1dot-a3*sin(t1+t2)*(w1dot+w2dot);
    a2*cos(t1)*w1dot+a3*cos(t1+t2)*(w1dot+w2dot);
    0];


%jacobian
J0nn=[-a2*sin(t1)-a3*sin(t1+t2) -a3*sin(t1+t2);
      a2*cos(t1)+a3*cos(t1+t2) a3*cos(t1+t2)];


J0nn2=[-a2*sin(t1)-a3*sin(t1+t2)-a1 -a3*sin(t1+t2);
      a2*cos(t1)+a3*cos(t1+t2)+dd2 a3*cos(t1+t2)];


Vref=[xref;
      yref];

omegadot=(J0nn^-1)*Vref;
omegadot2=(J0nn2^-1)*Vref;
```

```
%trigonometry
c=15.506;
a=12;
b=15.36;


T1=acos((-a^2+b^2+c^2)/(2*b*c));
T2=acos((-b^2+a^2+c^2)/(2*a*c));
T3=acos((-c^2+a^2+b^2)/(2*a*b));

%lifting piston

by=2.309;
bx=1.4;
cx=2.68;
cy=0.835;

bcx=cx-bx;
bcy=by-cy;
bc=sqrt(bcx^2+bcy^2);

E1=40*(pi/180);
E3=T1-E1;
E6=(pi/2)-E1;
E5=acos((-bcx^2+bcy^2+bc^2)/(2*bcy*bc));
E4=(pi/2)-E3-E5;
E4T1=E4+T1;

dx=4.774;
dy=1.082;
bd=sqrt(dx^2+dy^2);
cd=sqrt(bc^2+bd^2-2*bc*bd*cosd(E4T1));

E9=asind(bc*sind(E4T1)/cd);
E7=180-E4T1-E9;
E8=180-E4-E7;

bl=(bc*sind(E7))/sind(E8);

%T1dot=cddot/bl;

%jib

ex=11.82;
ey=1.548;
hx=1.2;
hy=0;

hj=hx;
ez=sqrt(ex^2+ey^2);
ej=c-ez;
E10=180-T2;
he=sqrt(ej^2+hj^2-2*ej*hj*cosd(E10));
E12=asind(sind(E10)*hj/he);
E11=180-E12-E10;
jk=ej*sind(E12);
```

```
%T2Cdot=hedot/jk;

fx=11.517;
fy=0.599;
gx=1.192;
gy=0.138;

fz=sqrt(fx^2+fy^2);
fj=c-fz;
gz=sqrt(gx^2+gy^2);
jg=gz;
fg=sqrt(jg^2+fj^2-2*fj*jg*cosd(T2));
E13=asind(jg*sind(T2)/fg);
jn=fj*sind(E13);

%T2LRdot=fgdot/jn;

boomab=0.1883;
boomba=-2.598;
stickab=0.1474;
stickba=-0.7958;

%valve guidance values
v1=370;
v2=350;
v3=330;
v4=310;
bs1=430;
bs2=450;
bs3=470;
bs4=490;
```